

final report

(NASA-CF-161286) SPACE FABRICATION
DEMONSTRATION SYSTEM, TECHNICAL VOLUME
Final Report (Grumman Aerospace Corp.)
117 p HC A06/MF A01

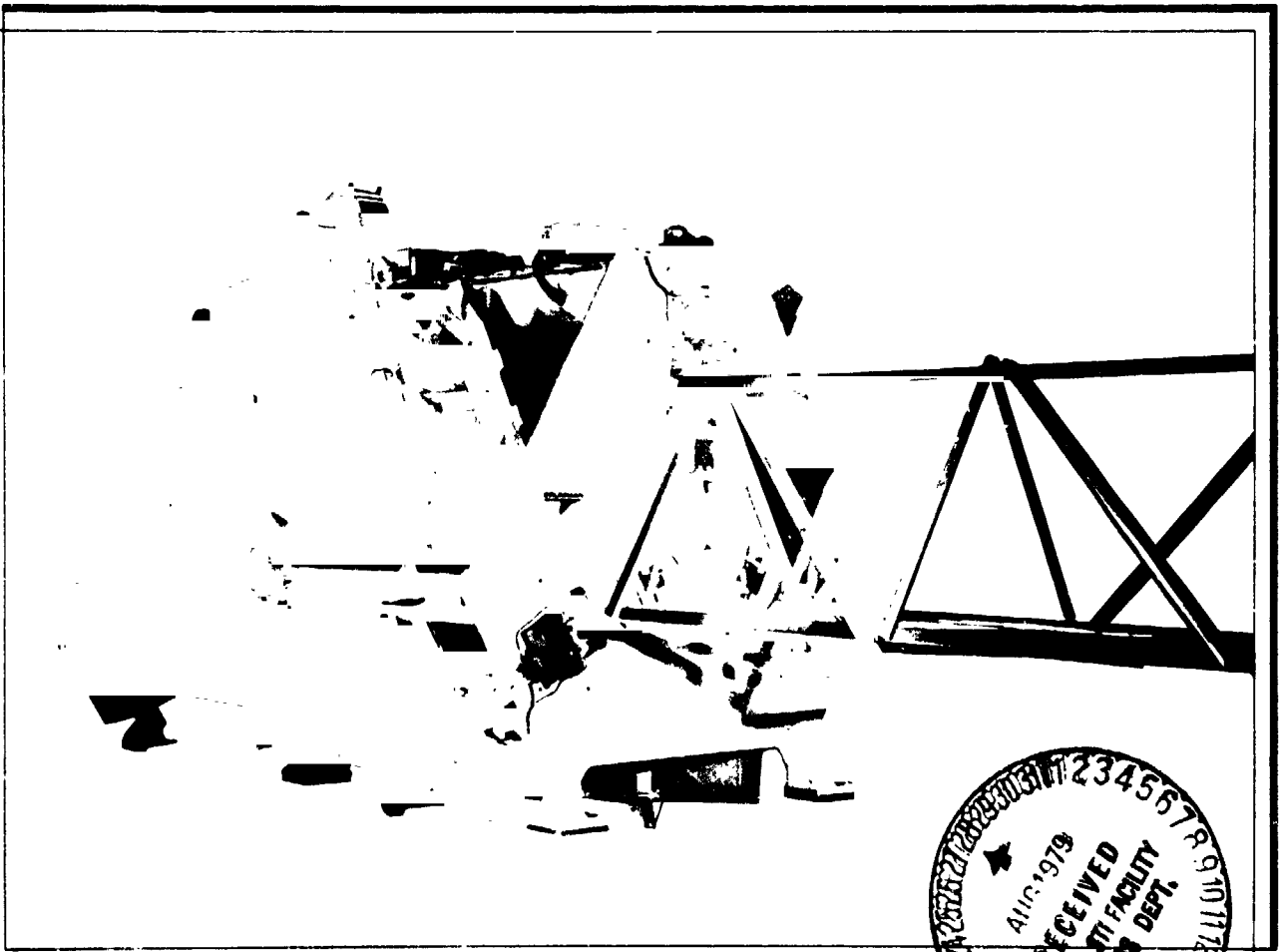
N79-29213

CSCL 22A

Unclas
G3/15 31722

SPACE FABRICATION DEMONSTRATION SYSTEM

technical volume



GRUMMAN AEROSPACE CORPORATION

final report

SPACE FABRICATION DEMONSTRATION SYSTEM

technical volume

prepared for
National Aeronautics and Space Administration
Marshall Space Flight Center
Huntsville, Alabama

Under Contract No. NAS 8-32472
(Contracting Officer Representative: Erich E. Engler)

prepared by
Grumman Aerospace Corporation
Bethpage, New York 11714

NSS-SFDS-RP013

MARCH 15, 1979

FOREWORD

This report was prepared by Grumman Aerospace Corporation in fulfillment of NASA Contract NAS 8-32472, Space Fabrication Demonstration System (SFDS) Ground Demonstration Program, Paragraph 3 of the Statement of Work. The SFDS program successfully developed and demonstrated a machine capable of automatically fabricating 1-m deep aluminum beams. This report documents the effort, i.e. analysis of the beam required and design, fabrication, and verification of the Automatic Beam Builder (ABB).

Major contributors to the successful NASA/Grumman team development effort and to this final report included:

Erich E. Engler	- NASA Contracting Officer Representative
Walter Muench	- Grumman Program Manager
John Huber	} Design & Fabrication of ABB
Warren Marx	
Richard Romaneck	
Hank Morfin	- Test & Flight Demonstration Program Plan
Al Weyhreter	- Quality Assurance

CONTENTS

<u>Section</u>		<u>Page</u>
	FOREWORD	ii
1	INTRODUCTION & SUMMARY	1-1
	1.1 Introduction	1-1
	1.2 Summary	1-2
	1.2.1 Structural Beam	1-2
	1.2.2 Automatic Beam Builder	1-2
2	BEAM DESIGN	2-1
	2.1 Introduction	2-1
	2.1.1 Task Objectives & Scope	2-1
	2.1.2 Summary	2-2
	2.2 Requirements & Data	2-2
	2.2.1 Satellite Solar Power System	2-2
	2.2.2 Orbiter Payload Bay	2-4
	2.3 Design Conditions	2-5
	2.3.1 SSPS Operations	2-5
	2.3.2 Orbiter Payload Bay Operation	2-19
	2.4 Material Properties	2-23
	2.5 1-m x 40-m Beam Design Data	2-24
	2.5.1 Design Detail	2-24
	2.5.2 Beam Section Properties	2-26
	2.5.3 Torsional Stiffness (Non-Buckled State)	2-26
	2.5.4 Static Load Analysis	2-26
	2.5.5 Torsion at End Attachments	2-28
	2.5.6 Summary Design Loads	2-28
	2.5.7 Thermal Analysis	2-29
	2.5.8 Thermal Stresses	2-37
	2.5.9 Deflection	2-39

CONTENTS (contd)

Section	Page
2.6 Beam Failure Modes	2-39
2.6.1 Beam Cap	2-40
2.6.2 Diagonal Brace	2-42
2.6.3 40-m Beam	2-42
2.6.4 Combined Thermal & Mechanical Loading Conditions ...	2-44
2.6.5 References	2-44
3 SPACE FABRICATION DEMONSTRATION SYSTEM	3-1
3.1 Overall Configuration Characteristics	3-1
3.1.1 General Arrangement	3-1
3.1.2 Operation	3-3
3.1.3 Mass Distribution	3-4
3.1.4 Power Requirements	3-4
3.2 Machine Structure	3-6
3.2.1 Base Mounting Stand	3-6
3.2.2 External Support Structure	3-6
3.2.3 Internal Support Structure	3-8
3.3 Cap Member Roll Forming Subsystem	3-8
3.3.1 Feed Roller & Guides	3-8
3.3.2 Roll Form Tooling	3-8
3.3.3 Roll Form Equipment	3-14
3.4 Brace Member Storage Dispensing Subsystem	3-16
3.4.1 Brace Storage & Dispenser - Design Approach	3-16
3.4.2 Equipment Design	3-16
3.4.3 Fabrication Method	3-19
3.5 Brace Clampup & Attachment Subsystem	3-19
3.5.1 Design Approach	3-19
3.5.2 Welding Equipment	3-22
3.6 Beam Cutoff	3-24

CONTENTS (contd)

Section	Page
3.7 Controls	3-25
3.7.1 Rolling Mill Control	3-26
3.7.2 Controlling Bay Length	3-26
3.7.3 Fastening Cycle	3-26
4 TESTING	4-1
4.1 Component Tests	4-1
4.1.1 Ultrasonic Spotwelding	4-1
4.1.2 Static & Fatigue Characteristics of Spotwelded 2024-T3 Aluminum Joints	4-3
4.1.3 Six Spotweld Attachment Component Tests	4-6
4.2 Quality Assurance	4-10
4.2.1 Beam Bulder	4-10
4.2.2 Beam	4-11
4.3 Structural Tests	4-14
4.3.1 Compression Test of 0.56-m (22-in.) Cap Specimens	4-16
4.3.2 Compression Test of Two 1.22-m (48-in.) Cap Specimens	4-17
4.3.3 Compression Test of 1.5-m (59 in.) Cap Specimens	4-17
4.3.4 Test of 1-m x 6-m (4-Bay) Beam, Hand Assembled	4-17
4.3.5 Test of 1-m x 6-m (4-Bay) Beam Fabricated by Beam Bulder	4-26
4.3.6 Test of 1-m x 4.5-m (3-Bay) Beam, Hand Fabricated . .	4-28
5 CONCLUSIONS & RECOMMENDATIONS	5-1
5.1 Conclusions	5-1
5.2 Recommodations	5-1

ILLUSTRATIONS

<u>Fig.</u>		<u>Page</u>
1-1	Typical Large Space Structures	1-1
1-2	Automatic Beam Builder Ground Demonstration Machine	1-2
2-1	SSPS Structural Arrangement	2-3
2-2	Isometric View of One-Bay SSPS	2-4
2-3	Stationkeeping Maneuver	2-5
2-4	SSPS Math Model Geometry	2-7
2-5	Math Model	2-8
2-6	SSPS Solar Array Upper Structure NASTRAN Model Output Data	2-10
2-7	Biaxially Pretensioned Solar Reflectors & Solar Array (Typical)	2-11
2-8	Solar Reflection Natural Frequency versus Perimeter Preload	2-12
2-9	Average Temperature of Major Members during Eclipse, GEO	2-14
2-10	Solar Reflector Support System Schematic	2-15
2-11	Design Loading Condition 20-m x 493-m Beam	2-15
2-12	Maximum Moment versus Co for 20-m x 493-m (Continuous Beam).	2-16
2-13	Design Loading Condition for 1-m x 40-m Beam	2-17
2-14	Maximum Moment versus Initial Deflection (1-m x 40-m Beam Pin Ended)	2-18
2-15	Modes & Frequencies (1-m x 40-m Beam)	2-20
2-16	Fundamental Frequency versus Beam Length	2-21
2-17	Beam Model Node & Member Designations	2-22
2-18	Tip Acceleration versus Time	2-23
2-19	Orbiter Acceleration versus Time	2-24
2-20	Tip Deflection versus Time (Step Input 0 to 4 sec)	2-25
2-21	1-m Beam Design	2-27
2-22	1-m Beam Cap to Batten Attachment (2024-T3 Aluminum Alloy)	2-28
2-23	Beam Cross Section	2-29
2-24	Cap & Batten Cross Sections	2-30

ILLUSTRATIONS (contd)

Fig.		Page
2-25	Torsional Stiffness	2-31
2-26	1-m Beam Finite-Element Model	2-31
2-27	End Torsion versus Manufacturing Eccentricity in X-Y Plane (1-m x 40-m Beam)	2-33
2-28	1-m Beam Loading Conditions	2-34
2-29	Critical Cap Compression Load	2-34
2-30	Fabrication Orbiter Bay	2-34
2-31	Beam Orbital Orientation	2-35
2-32	Beam Temperature Response	2-36
2-33	Thermal Gradient at $\theta = 180^\circ$	2-36
2-34	Solar Blockage Geometry	2-37
2-35	Thermal Stress in 1 1/2-m Long Cap due to Gradient; Unrestrained Boundaries	2-38
2-36	Thermal Stress in 1 1/2-m Long Cap due to Gradient Fully Restrained in Rotation about Y & Z Axes	2-38
2-37	Deflection & Slope versus Temperature Differential (1-m x 40-m Beam).	2-40
2-38	Torsion-Flexure Buckling Load versus Effective Length Diagonal Brace	2-43
2-39	Buckling of Modes (1-m x 40-m Beam).	2-43
3-1	1-m Beam Design Configuration	3-2
3-2	Ground Demonstration Floor Plan & Facility Requirements	3-3
3-3	Ground Demonstration System Weight Distribution	3-4
3-4	Ground Demonstration System Estimated Average Power Requirements	3-4
3-5	Base Mounting Stand	3-6
3-6	Ground Demonstration Machine External Support Structure	3-7
3-7	Ground Demonstration Machine Internal Support Structure	3-9
3-8	Cap Roll Forming System	3-10
3-9	Internal Evaluation on Production Equipment	3-11

ILLUSTRATIONS (contd)

<u>Fig.</u>		<u>Page</u>
3-10	Seven-Station Roll Form Tests	3-12
3-11	Seven-Station Progressive Roll Form Steps	3-12
3-12	Cap Configuration	3-13
3-13	Index Hole Blanking Setup	3-13
3-14	Typical Rolling Mill Cross Section	3-14
3-15	Typical Section of Modified Mill Drive	3-15
3-16	Magazine/Dispensing Mechanism Fixture	3-17
3-17	Magazine & Helix Dispenses.	3-18
3-18	Brace Transporter Carriage.	3-18
3-19	Brace Roll Forming Sequence	3-19
3-20	Brace Clampup Attachment Subsystem	3-20
3-21	Weld Electrode Cam Mechanism.	3-21
3-22	Welding Process Schematic	3-22
3-23	Shear Assembly	3-24
3-24	Control System Block Diagram	3-25
3-25	Cap Member Feed Strip Length Encoder Setup.	3-27
3-26	Ten-Bay Beam.	3-27
4-1	Ultrasonic Spotwelding	4-2
4-2	Spotweld Evaluation Static & Fatigue Test Specimen Configurations	4-4
4-3	Spotweld Evaluation Fatigue Test Results	4-6
4-4	Spotweld Configuration No. 1: 8 Weld/Junct	4-7
4-5	Spotweld Configuration No. 2: 6 Weld/Junct, Maximum Spacing	4-7
4-6	Spotweld Configuration No. 3: 6 Weld/Junct, Minimum Spacing	4-8
4-7	Component Test Arrangement	4-8
4-8	Six Weld/Joint Test Specimen	4-9
4-9	Cap Member Dimensions Locations	4-14

ILLUSTRATIONS (contd)

<u>Fig.</u>		<u>Page</u>
4-10	Compression Test Specimen Comparison Failure Load Six or Eight Spotwelds per Brace	4-16
4-11	Compression Tests of SFDS Cap Elements	4-18
4-12	6-m Compression Test Specimen	4-19
4-13	Typical Instrumentation	4-20
4-14	Cap Stresses Bay No. 1 versus Developed Flat Pattern of Cap at 1300 Pounds	4-23
4-15	Cap Stresses Bay No. 1 versus Developed Flat Pattern of Cap at 930 Pounds	4-24
4-16	Stresses in Diagonals in Bay No. 1 at Limit Load	4-25
4-17	Stresses in Diagonal in Bay No. 1 at Ultimate Load	4-25
4-18	Stresses in Batten versus Developed Flat Pattern at Bottom of Bay No. 1	4-26

TABLES

<u>Table</u>		<u>Page</u>
2-1	SSPS Solar Array Upper Structure Member Loads from NASTRAN Model (1277 N Ultimate at End Tip)	2-9
2-2	Shuttle-Beam Mass Data	2-19
2-3	Vibration Modes (1-m x 40-m Beam)	2-20
2-4	Candidate Material Property Data	2-26
2-5	Summary of Static Finite-Element Model Analysis Results	2-32
3-1	SFDS Estimated Weight Breakdown by Subsystem	3-5
3-2	Rolling Drive Torque Values	3-14
3-3	Rolling Mill Roll Adjustment Settings	3-15
4-1	Spotweld Evaluation. Static Test Results	4-5
4-2	Spotweld Evaluation: Fatigue Test Results	4-5
4-3	Mechanical Properties of 2024-T3 0.016-in. Aluminum Sheet	4-12
4-4	Actual Chemical Analysis of 2024-T3 Aluminum Coil Sheet per QQA-250/4	4-12
4-5	Angular Measurements of Cap Member Manufactured by Beam Builder	4-13
4-6	Length Dimensions of Beams & Caps	4-14
4-7	Test Specimen Instrumentation	4-21
4-8	Test Log - Manually Assembled Beam	4-22
4-9	Test Log - Automatically Fabricated Beam	4-27

1 - INTRODUCTION & SUMMARY

1.1 INTRODUCTION

Large area, low density structures are a key technology developmental requirement for the future practical utilization of space. Figure 1-1 illustrates typical systems requiring these large structures. The lightweight 1-m beam which can be automatically fabricated in space has emerged as a viable, basic building block for construction of these large space structures, i.e., large reflector antennas, microwave radiometer antennas, radar astronomy telescopes, solar thermal power systems, photovoltaic solar power systems, microwave power transmission antennas, and a variety of other unmanned applications.

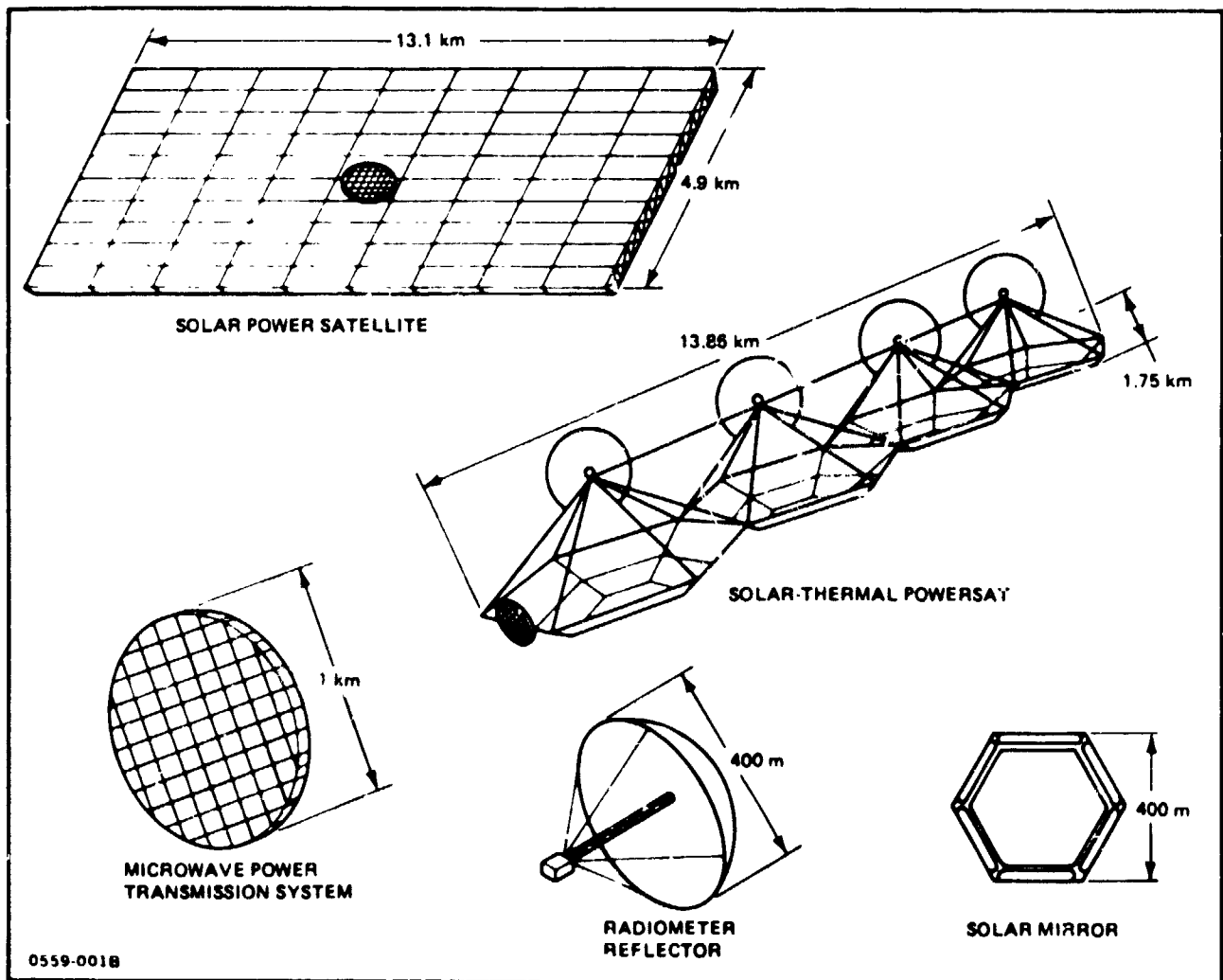


Fig. 1-1 Typical Large Space Structures

This report contains the results of analysis and tests conducted to define the basic 1-m beam configuration required and the design, fabrication and verification of the machine required to automatically produce these beams.

1.2 SUMMARY

1.2.1 Structural Beam

The structural 1-m beam developed for the selected baseline vehicle, the Grumman photovoltaic Satellite Solar Power System (SSPS), was designed for automatic fabrication by the ground demonstration beam builder. Three beams were built and structurally tested; the first two were hand assembled, the second was built in the beam builder without any manual operations. The planned tests simulated the middle bays of the 1-m x 40-m 26-bay beam under compression load only; the design condition was combined bending and axial load. All three beams were tested to design data derived from the SSPS requirements. Each test specimen carried loads that exceeded the ultimate design load of 1260 lb.

1.2.2 Automatic Beam Builder

Several design trades were conducted to define the forming, attachment and automatic control methods. The final Automatic Beam Builder (ABB) design selected is shown in Fig. 1-2 and is comprised of the following subsystems:

- Beam cap member forming is accomplished by three seven-station rolling mills which progressively form the longitudinal members of the beam from 162-mm wide x 0.4-mm thick flat stock. The flat stock is fed into the rolling mills from three reels. Each reel can hold 300 m of the flat aluminum stock and can be easily replaced by another when depleted
- Beam cross braces are prefabricated in a conventional manner and stored in magazines for dispensing at the proper time in the correct geometric position. They are made of the same aluminum flat stock as the cap members. Each magazine holds approximately 200 cross braces, enough to make 300 m of beam. As was the case with the aluminum feed reels, these can also be replaced with loaded magazines or alternately may be individually reloaded with prestacked bundles of 50 cross braces
- Fastening of the cross braces to the three caps is accomplished by a single mechanism at each fastening location. With the carriage mechanism holding a cross brace in place on the beam cap member, the clamp/wedge block moves into place and clamps the cross brace to the beam cap member, at which time the

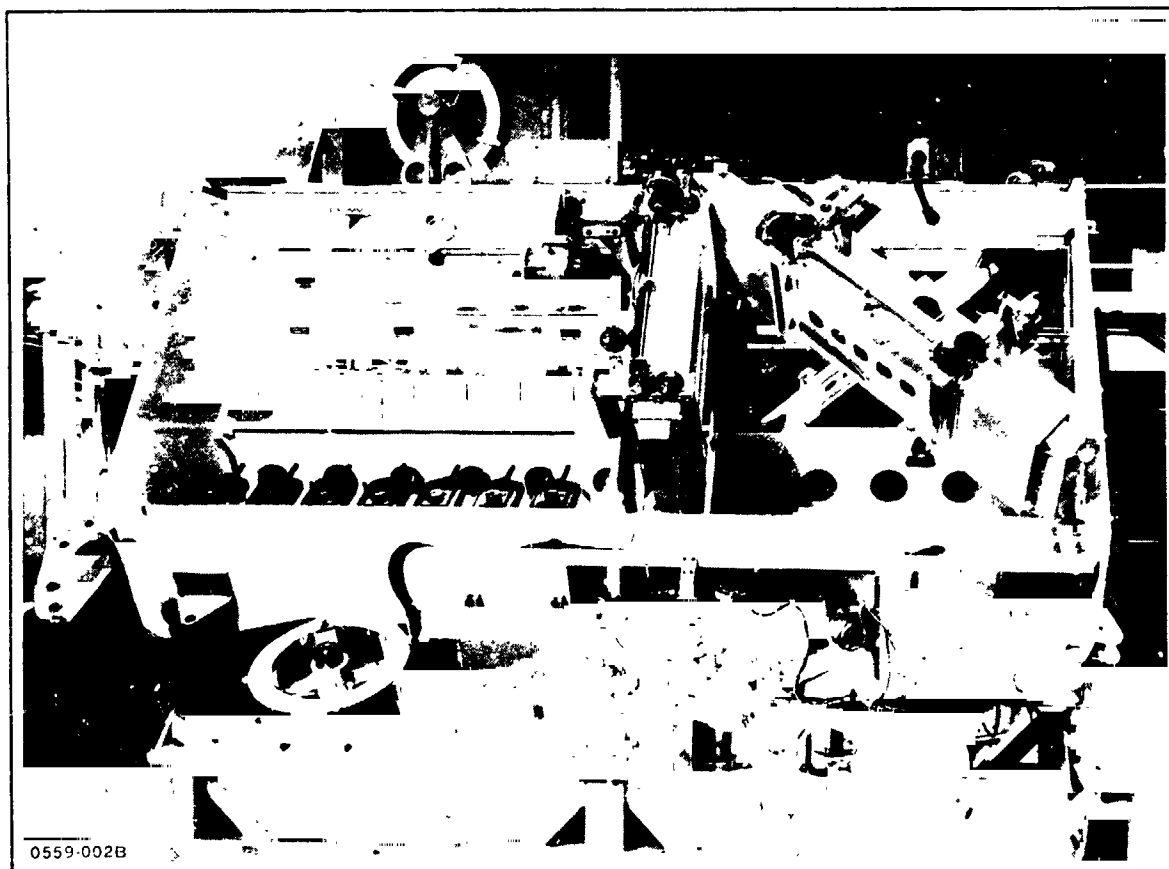


Fig. 1-2 Automatic Beam Builder Ground Demonstration Article

carriage mechanism releases the cross brace and retracts to its rest position, where it is ready to receive the next cross brace. Once the clamp/weld block is in position clamping the cross brace to the beam cap member, the series spotweld cycle begins with each pair of spotweld electrodes being activated individually until six spotwelds are accomplished at each end of each cross brace. All vertical cross braces are dispensed, clamped and welded in place before the same fastening sequence takes place for the diagonal cross braces

- Once the desired length of beam has been produced, beam cutoff is accomplished by three guillotines which cut through the three beam cap members
- Automatic control is accomplished by means of a simple, commercial-type computer which monitors all the operational functions of the ABB. Each function, from rolling the proper length of beam cap member to form one beam bay length, 1.5 m through cross brace dispensing and welding, length of beam produced and beam cutoff, is monitored and registered as completed

before the next function is permitted to take place. This monitoring is accomplished by encoders, tachometers, photoelectric sensors, and limit switches strategically placed throughout the machine.

The ABB achieved operational capability on May 3, 1978, and since then has automatically produced several hundred meters of 1-m beam section of various bay lengths.

2 - BEAM DESIGN

2.1 INTRODUCTION

This section contains a description of the design studies, analyses, and tests of the basic 1-m deep beam, which together with the development of the ground demonstration ABB, demonstrate the feasibility of on-orbit fabrication of large space structures. The design, construction and beam fabrication demonstration of the ABB is described in Section 3 of this final report.

Analytic studies presented in this report include structural criteria and requirements, load and environmental data, temperature histories, structural math models, and dynamic and structural analyses. Also included are tests and test results conducted to establish verification of concepts.

2.1.1 Task Objectives & Scope

The objectives of this phase of the Space Fabrication Demonstration System (SFDS) Program were to develop, design, and test an aluminum alloy structure which could be automatically fabricated in orbit from ground preprocessed basic strip material. A significant part of the preprocessing operations include the application of selected thermal coatings and position locating holes used to null out relative cap misalignment errors after fabrication of a bay. The primary manufacturing processes used to construct the basic 1-m x 40-m beam structure are: (1) roll forming of the three caps, (2) dispensing and positioning of the prefabricated battens and diagonals, (3) resistance series spot welding of braces to caps, and (4) shearing operation for beam cutoff. With the connection of a proper end attachment structure at each end, this structure becomes a building block for the construction of larger assemblies. The potential for beam builder modification to incorporate material thickness and other changes, such as adaptation of the beam builder to process and fabricate composite beams, makes the concept usable for a wide range of large space structures applications.

The space vehicle baselined to provide the design environments and requirements for the development of the lightweight structure and ground demonstration beam builder was the Satellite Solar Power System (SSPS) studied earlier at Grumman under various funded and in-house programs. An additional requirement placed on the concept included compatibility of beam and beam builder with Orbiter environments and geometric

constraints. Because it was designed and built as a low-cost ground demonstration article, the beam builder was not optimized as a lightweight flight article.

Structural design data was obtained from the stationkeeping maneuvers at geosynchronous orbit in the SSPS mission. Neither on-orbit SSPS construction nor orbital transfer was used to design the structure. Beam construction for the case where the beam builder was supported in the Orbiter payload bay at low earth orbit (LEO) was studied and is included.

Based on the design environments, a 1-m x 40-m beam was designed and hand fabricated from roll formed parts made by using final tooling from the beam builder. The objective was to use this specimen in structural test to establish an acceptable baseline load capability against which an automatically fabricated beam could be compared to satisfy test requirements.

2.1.2 Summary

The structural member developed for the selected baseline vehicle, the SSPS, was designed for automatic fabrication by the ground demonstration beam builder. Two beams were built and structurally tested; the first was hand assembled, the second was built in the beam builder without any manual operations. The planned tests simulated the four middle bays of the 1-m x 40-m, 26-bay beam under compression load only; the design condition was combined bending and axial load. For obvious reasons, a test of a 40-m member was not planned. Both beams were tested to design data derived from the SSPS requirements. Each test specimen carried loads that exceeded the ultimate design load.

2.2 REQUIREMENTS & DATA

2.2.1 Satellite Solar Power System

Design and analytic studies conducted in developing a basic structural member to be built in the automatic beam builder were based on the SSPS configuration (Fig. 2-1) (Ref. 2-1).

Some of the pertinent characteristics of SSPS include the following:

- Size: 13.1 km x 4.93 km
- Power: 5 GW
- Orbit: Geosynchronous
- Concentration Ratio: 2.0

- Operating Life: 30 yrs
- Structure Natural Frequency: 5.26 CPH bending
- Factor of Safety: 1.40.

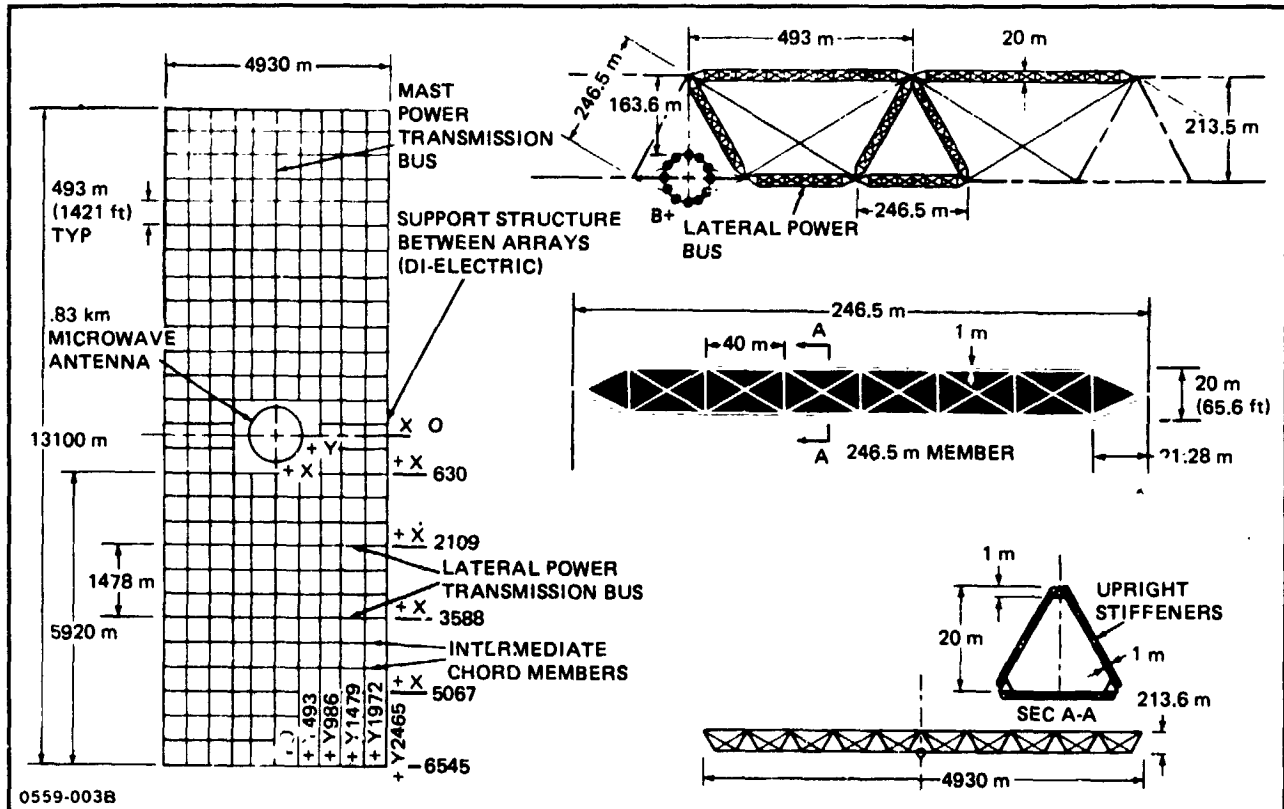


Fig. 2-1 SSPS Structural Arrangement

Solar array blankets and the solar reflectors are biaxially pretensioned in order to attain membrane frequencies well above the satellite structural frequency. Power is collected in the lateral power transmission buses and transferred to the central mast power bus. The central mast also provides the support for the microwave antenna which beams power to the ground rectenna in the form of microwave energy. As noted on Fig. 2-1, the structure between the two 5.92 x 4.93 km solar arrays is constructed from dielectric material inasmuch as the continuously earth pointing microwave antenna "looks" through the structural space frame; the dielectric material selected for this structure was S-glass.

The satellite primary structure consists of 20-m x 493-m beams in the X direction; in the Y direction both 20-m x 493-m and 20-m x 246-m beams are used. The vertical and diagonal members are also 20-m x 246-m beams; the entire system as shown forms a space framework with shear stiffness provided by preloaded tension cables. The entire satellite

structure is 213.5-m deep. The main power transmission bus, the central mast, is structurally integrated with the remainder of the solar array and acts as part of the primary structure. Figure 2-2 shows an isometric view of a 1479-m bay of the SSPS.

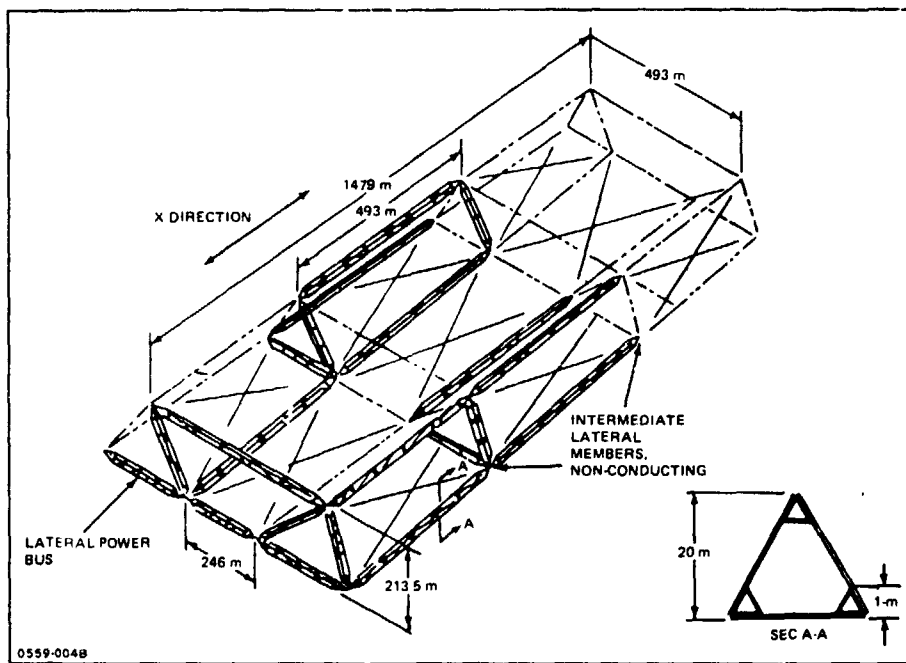


Fig. 2-2 Isometric View of One-Bay SSPS

The 20-m beams, as shown in the figure, consist of three 1-m deep beams each of which is 40-m long and is supported at the node points by 1-m battens. Shear stiffness is provided by pretensioned crossed cables.

The loads, temperatures, and other environments used in this study to design the structure were taken from the SSPS operational modes only; no attempt was made to design for the various environments experienced during construction, assembly of large modules, and transport to operational orbits. However, analyses were conducted under several related programs to evaluate the structural problems associated with construction and orbital transfer. Initial review of the preliminary study results indicated those design conditions were within the selected structure capability, although considerable additional work would have been required to evaluate these areas in greater detail.

2.2.2 Orbiter Payload Bay

The beam was also designed to satisfy the requirements and environments experienced during fabrication on orbit when the beam builder is mounted and operates in the payload bay. The requirements and environments were taken from NASA Report, "Payload Accommodations Document," NASA JSC 07700 Vol. XIV (Ref. 2-2).

2.3 DESIGN CONDITIONS

2.3.1 SSPS Operations

2.3.1.1 Stationkeeping Maneuver - Stationkeeping maneuver thruster loads required to nullify the perturbations in orbit eccentricity and altitude drift caused primarily by solar radiation pressure were evaluated and applied to the solar power satellite as represented in Fig. 2-3. This loading condition resulted in the maximum axial compression load case for the beam design.

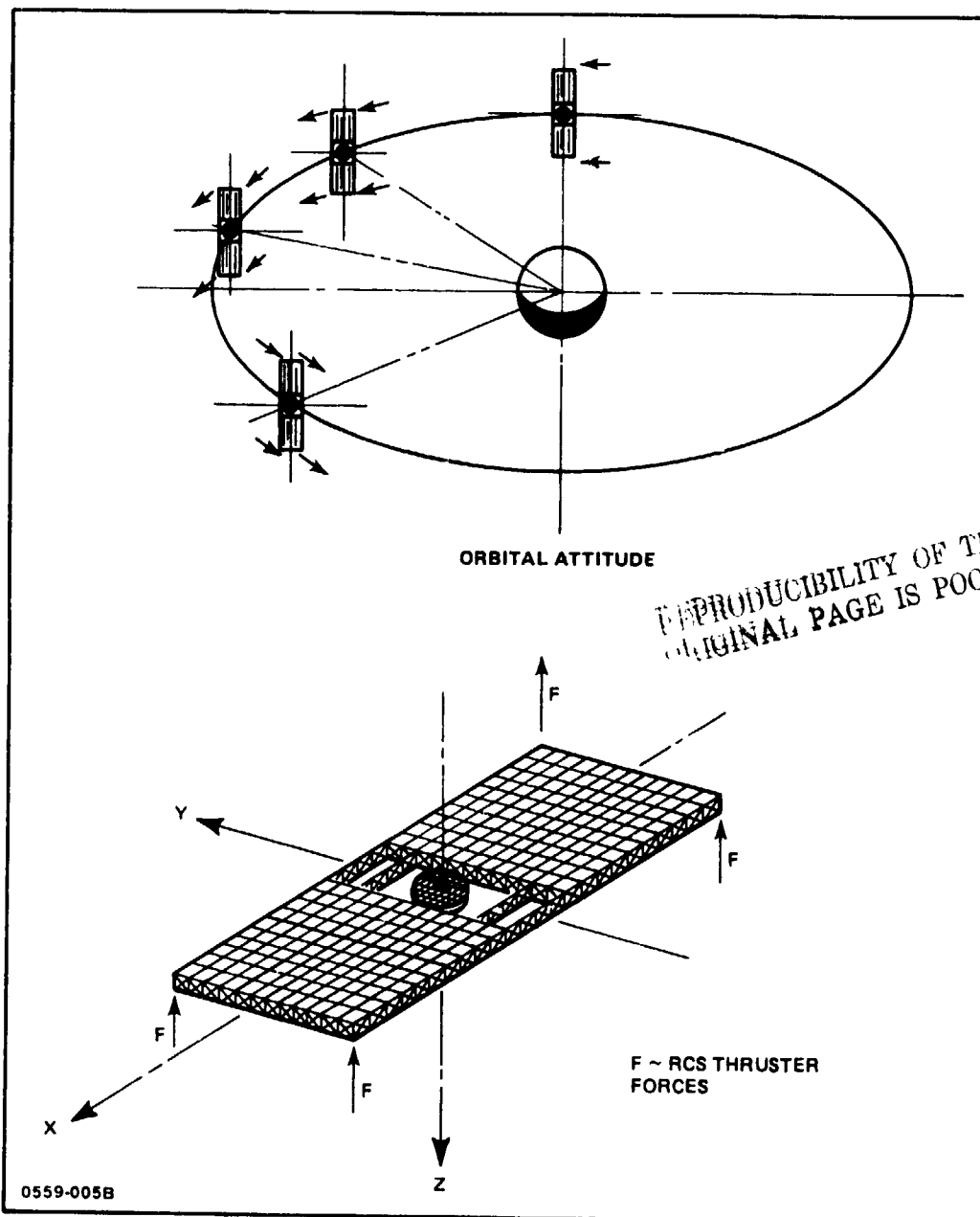


Fig. 2-3 Stationkeeping Maneuver

The stationkeeping load level given in Ref. 2-3 is 913 N (205.3 lb) for the total satellite divided equally between the four satellite tips 228 N (51.3 lb). The 228-N load was increased by a dynamic magnification factor of 2 and a safety factor of 1.4; in addition, the load was conservatively increased by an additional factor to give 1277 N (287 lb) at each tip. This load was used in the NASTRAN model results to obtain member loads.

2.3.1.2 SSPS Structural Math Model - The SSPS solar array structure was idealized into a finite-element system in order to obtain static and dynamic responses to external excitations; in this section the internal member loads caused by stationkeeping maneuvers were calculated. The math model geometry and computer graphic representation of the model are shown in Fig. 2-4 and 2-5, respectively. The 20-m deep members are the basic bar elements used in the model. The non-conducting members cross section areas used in the model were based on earlier calculations; updated calculations since the math model was formulated indicate some area increases which, however, should not effect the results significantly. The conducting structure cross section areas were based on power transmission requirements; this also applied to the central mast power conductor, the elements of which incorporate bending and torsional stiffness. Masses were lumped at the node points. The number of degrees of freedom (DOF) was reduced by assuming the antenna at the array centerline and assuming symmetry and antisymmetry. The following list summarizes the assumptions used in the finite-element model:

- Structure is symmetrical about antenna centerlines perpendicular and parallel to mast
- Analysis uses only half structure
- Antenna is included as rigid body, rigidly attached to flexible mast, and lies at center of structure
- Antenna has 6 DOF
- Mast is idealized as consisting of multiple beams having bending and torsional stiffness
- Mast moments of inertias are based on six current elements per polarity
- All other support structure is idealized as axial loaded struts
- Solar array elements lie in plane of blankets
- Total cross section area of non-conductive struts is 0.572 in.^2 (aluminum) and 1.91 in.^2 (dielectric)

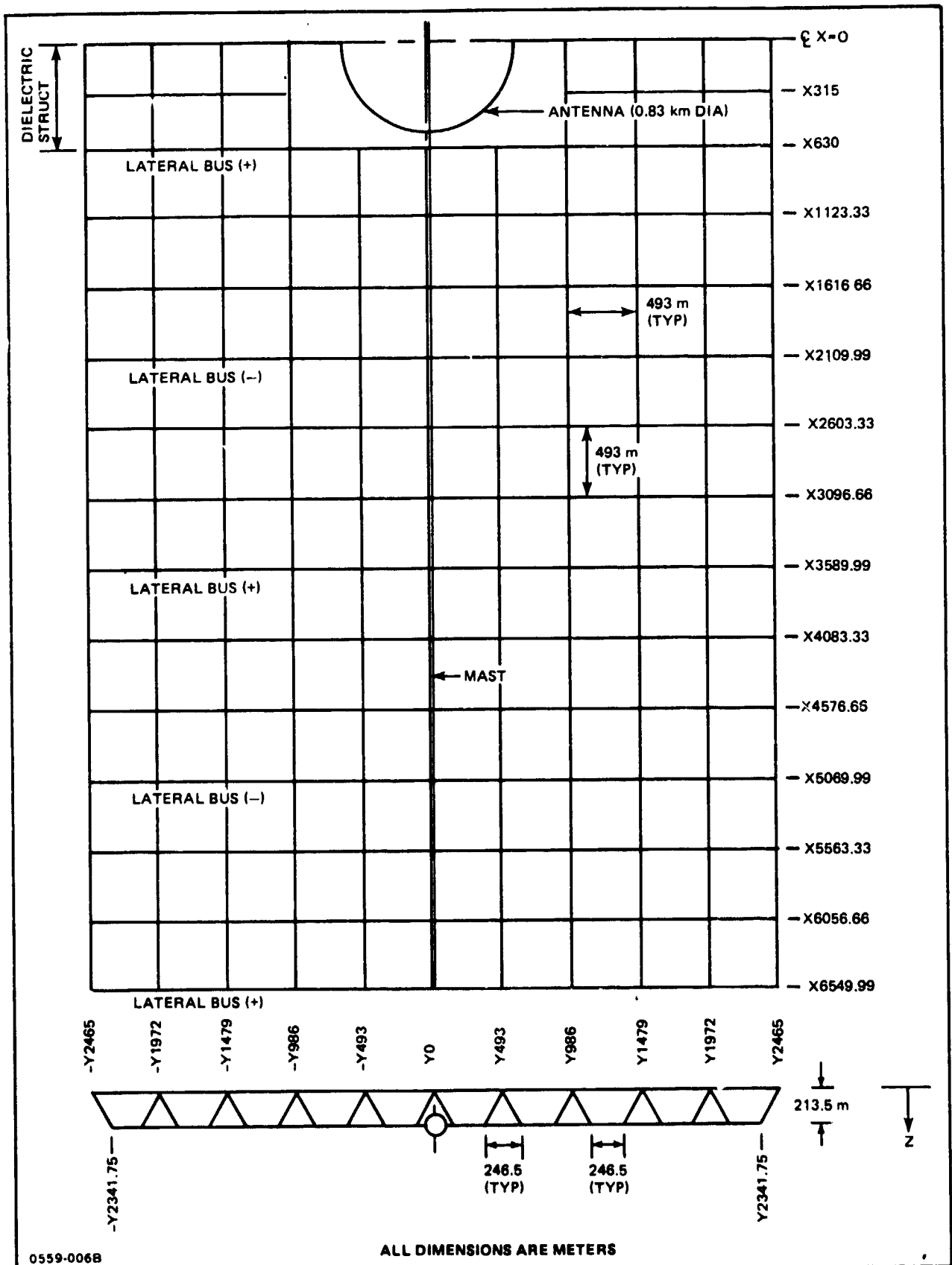
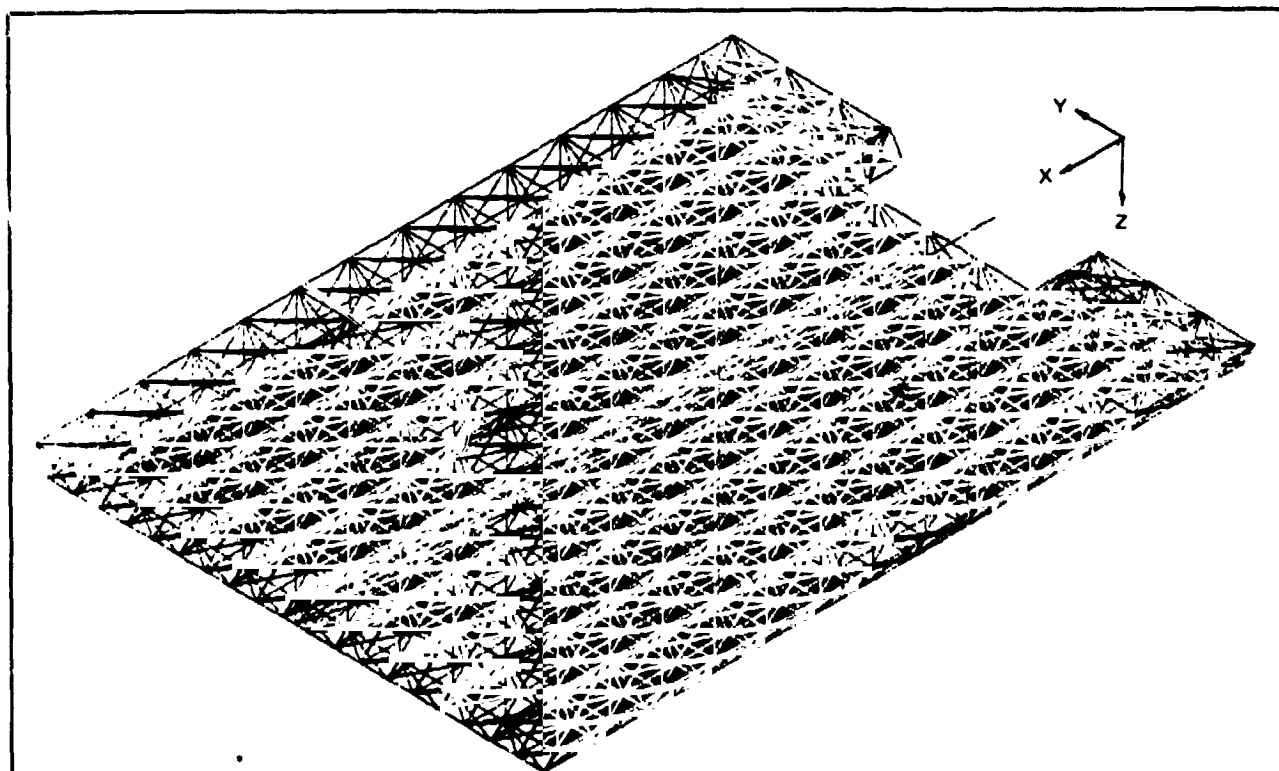


Fig. 2-4 SSPS Math Model Geometry

- Total cross section area of conductive struts is 1.674 in.^2 (+ Bus) and 3.35 in.^2 (- Bus)
- Tension-only wires replaced by single tension/compression struts cross section area are 0.0123 in.^2 (aluminum) and 0.0123 in.^2 (quartz)
- Model representing half-structure consists of 1127 members and 462 nodes
- Satellite weight is distributed as lumped masses at node points.



- HALF STRUCTURE CONSISTS OF 1127 MEMBERS & 462 NODES
- SATELLITE WEIGHT DISTRIBUTED AS LUMPED MASSES AT NODE POINTS
- TENSION-ONLY WIRES REPLACED BY TENSION/COMPRESSION STRUTS
- PROPERTIES (FULL STRUCTURE)

WT	=	$18.06 \times 10^6 \text{ kg}$	
		$(39.74 \times 10^6 \text{ lb})$	
X_{CG}	=	0	
Y_{CG}	=	0	
Z_{CG}	=	261.6 m (858.3 ft)	
I_x	=	$2.445 \times 10^{13} \text{ kg-m}^2$	$(1.803 \times 10^{13} \text{ slug-ft}^2)$
I_y	=	$1.883 \times 10^{14} \text{ kg-m}^2$	$(1.389 \times 10^{14} \text{ slug-ft}^2)$
I_z	=	$2.118 \times 10^{13} \text{ kg-m}^2$	$(1.5652 \times 10^{14} \text{ slug-ft}^2)$

0559-007B

Fig. 2-5 Math Model

2.3.1.3 Internal Member Loads - The internal member loads calculated using the NASTRAN model are summarized in Table 2-1, and the member designation are shown in Fig. 2-6. The compression loads for the satellite upper surface structure are shown in the table; for the case where the control forces are applied to induce compression forces on the lower surface, the individual members loads are lower inasmuch as there are a larger number of members on the bottom surface. The maximum loads 4942 N (1111 lb) occur in Bay 1 near the cutout for the microwave antenna. The dielectric structure was not designed at this time because it represents a smaller percentage of the overall manufacturing in space problem. However, this type of structure should be addressed eventually.

Table 2-1 SSPS Solar Array Upper Structure Member Loads from NASTRAN Model (1277 N Ultimate at Each Tip)

BAY 1				BAY 2			
MEMBER	MEMBER DESIGNATION	MEMBER LOAD		MEMBER	MEMBER DESIGNATION	MEMBER LOAD	
		(lbf)	(N)			(lbf)	(N)
1	42301	816	3629	12	42101	796	3541
2	42302	925	4114	13	42102	895	3981
3	42303	983	4376	14	42103	935	4159
4	42304	1111	4942	15	42104	1002	4457
5	42305	81	360	16	42105	234	1041
6	42306	131	583	17	42106	333	1481
7	42307	81	360	18	42107	234	1041
8	42308	1111	4942	19	42108	1002	4457
9	42309	983	4372	20	42109	935	4159
10	42310	925	4114	21	42110	895	3981
11	42311	816	3629	22	42111	796	3541

BAY 3				BAY 4			
MEMBER	MEMBER DESIGNATION	MEMBER LOAD		MEMBER	MEMBER DESIGNATION	MEMBER LOAD	
		(lbf)	(N)			(lbf)	(N)
23	41901	768	3416	34	41701	732	3256
24	41902	853	3794	35	41702	804	3576
25	41903	875	3892	36	41703	808	3594
26	41904	900	4003	37	41704	804	3576
27	41905	339	1508	38	41705	392	1744
28	41906	435	1935	39	41706	475	2113
29	41907	339	1508	40	41707	392	1744
30	41908	900	4003	41	41708	804	3576
31	41909	875	3892	42	41709	808	3594
32	41910	853	3794	43	41710	804	3576
33	41911	768	3416	44	41711	732	3256

0559-008B

REPRODUCIBILITY OF THE ORIGINAL PAGE IS POOR

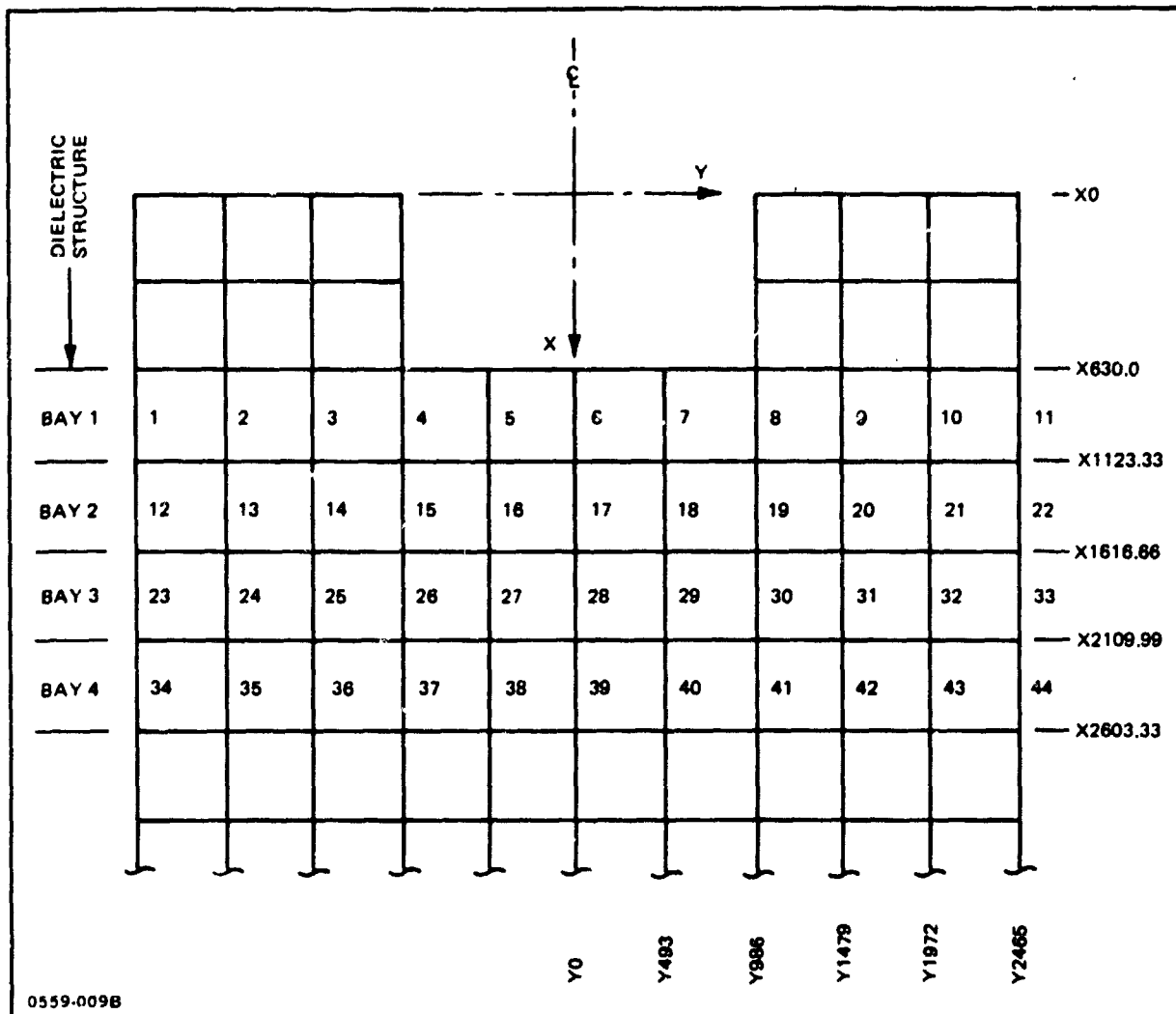


Fig. 2-6 SSPS Solar Array Upper Structure NASTRAN Model Output Data

The 4942-N load was used on the 20-m x 493-m beam to calculate the design load for the 1-m element.

2.3.1.4 Solar Reflector Pretension Load - In order to prevent dynamic coupling of the solar reflector membrane and the solar array structure, the reflector membrane (Fig. 2-7) is loaded biaxially by a system of preloaded springs to increase its natural frequency. Calculations of the satellite structural frequency show the first bending frequency is 5.26 CPH (Ref. 2-4), and it was assumed that the membrane frequency should be two to four times higher. The frequency separation must be maintained throughout the thermal excursions experienced at geosynchronous orbit as the satellite enters and leaves the earth's shadow.

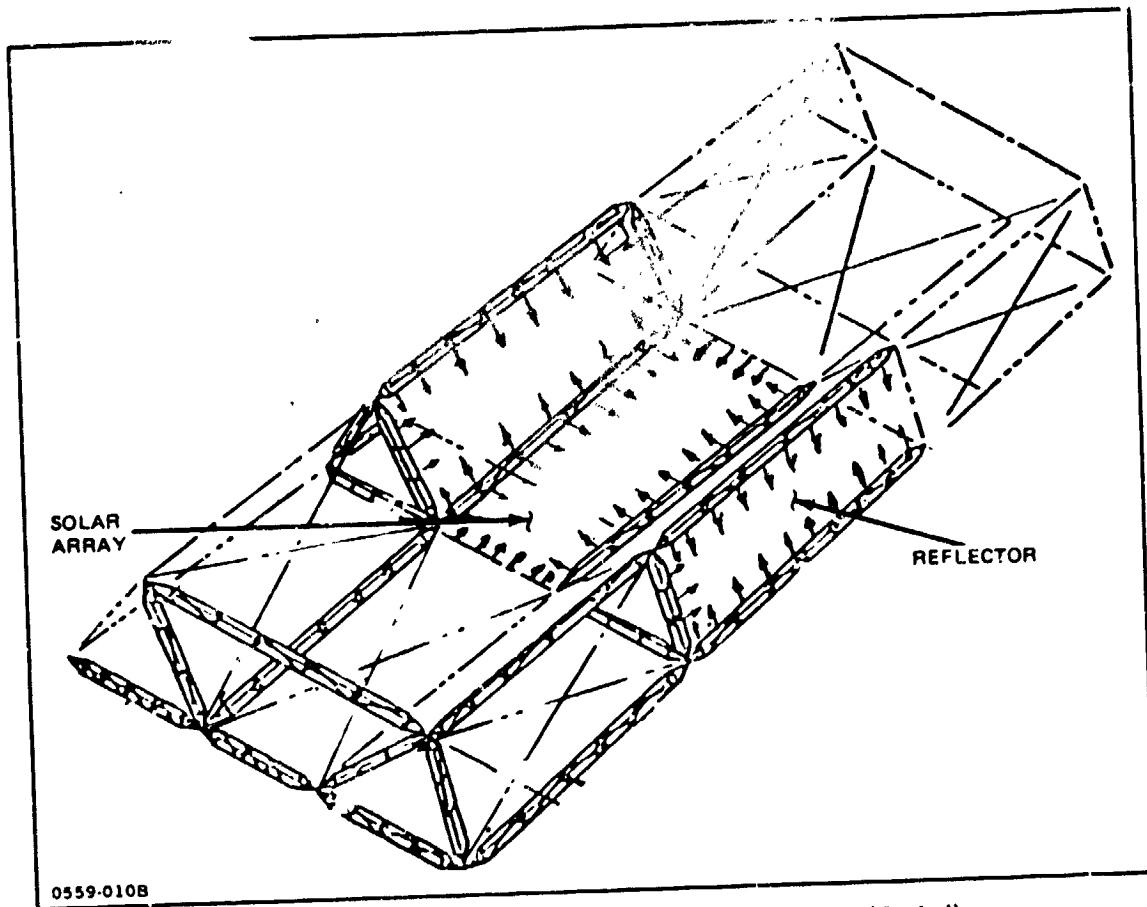


Fig. 2-7 Biaxially Pretensioned Solar Reflectors & Solar Array (Typical)

The heavier solar arrays will require a greater pretension load than the reflectors to maintain frequency separation. These loads can, however, be balanced by a series of connecting cables between bays without producing net loads on the supporting beams. The reflector loads were therefore considered critical.

2.3.1.4.1 Reflector Membrane Frequency - The natural frequency of a rectangular membrane with a tension force per unit length on the perimeter is given by:

$$\omega_n = \pi \sqrt{\frac{T}{\rho}} \left[\left(\frac{m}{a}\right)^2 + \left(\frac{n}{b}\right)^2 \right]^{1/2}$$

$$f_n = \frac{0.6124}{b} \sqrt{\frac{T}{\rho}}$$

Where

$$m = n = 1$$

a = 2b for given reflector configuration

$$a = 493 \text{ m}; b = 246 \text{ m}$$

REPRODUCIBILITY OF THE ORIGINAL PAGE IS POOR

T = tension force per unit dimension

ρ = mass per unit area = $1.321 \times 10^{-7} \frac{\text{lb-sec}^2}{\text{in.}^3}$

f_n = membrane natural frequency Hz

$$T = 33.04 f_n^2$$

The frequency equation for the 2:1 rectangular Kapton membrane was used to obtain the data plotted in Fig. 2-8. If a factor of four times the array structural frequency is assumed, the minimum reflector preload is $175 \times 10^{-3} \text{ N/m}$ ($1 \times 10^{-3} \text{ lb/in.}$). This load is modified in the following section to take into consideration the thermal excursions experienced on orbit.

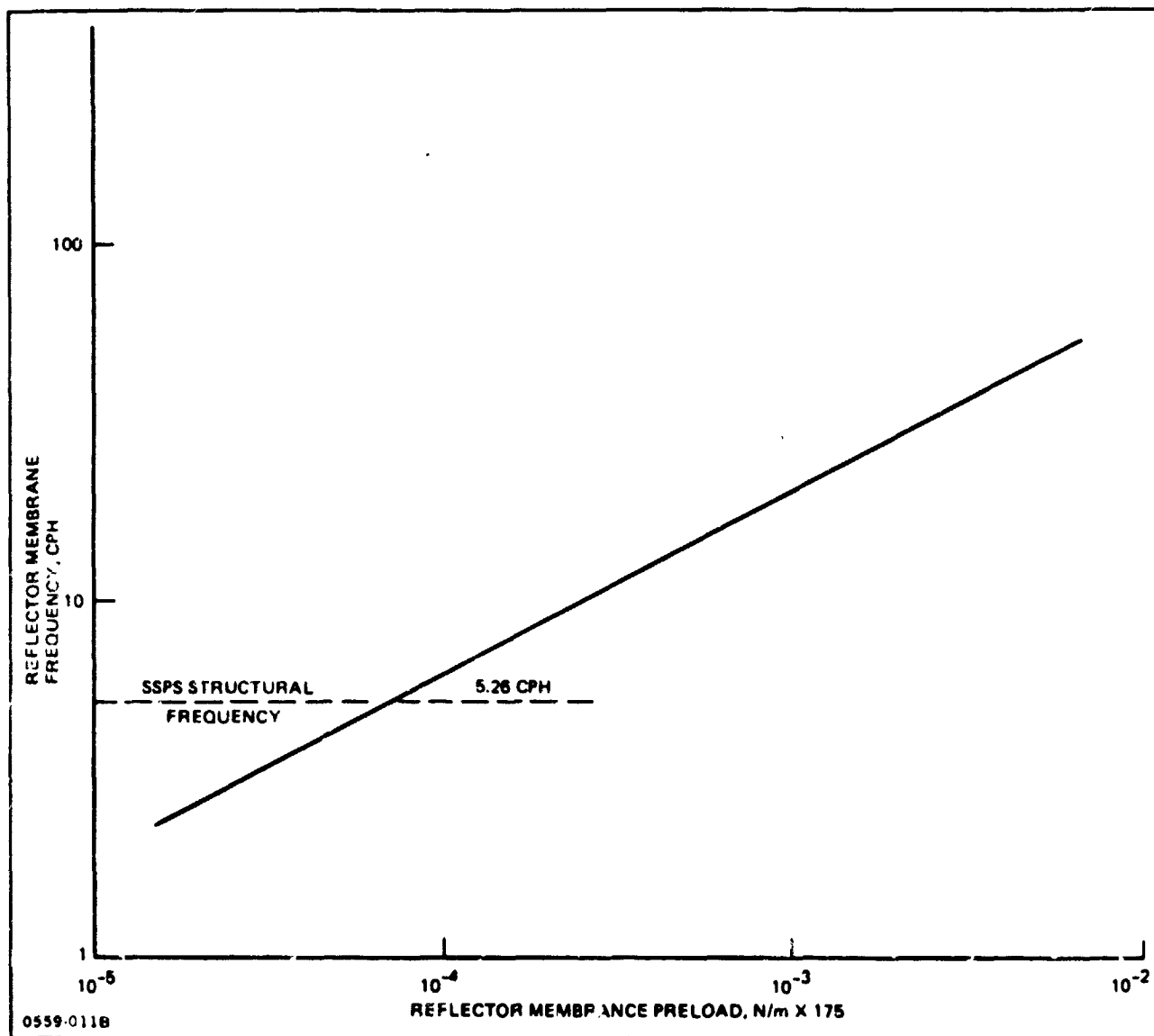


Fig. 2-8 Solar Reflector Natural Frequency versus Perimeter Preload

2.3.1.4.2 Reflector Temperature History - The time temperature history curve (Fig. 2-9) from Ref. 2-5 for the solar array is shown for the peak 72-min. eclipse period at geosynchronous orbit. The satellite is eclipsed daily during a 45-day period, twice each year at the time of the vernal and autumnal equinoxes. The time spent in the earth's shadow varies from nearly zero to a maximum of 72 min. The data plotted in Fig. 2-9 shows the very rapid temperature decrease of the 1 mil Kapton reflector compared to the supporting aluminum structure. When exiting the earth's shadow, the reflector temperature will increase at a much greater rate than the supporting aluminum structure.

Because the temperature variations and coefficients of thermal expansion for the structure and Kapton result in appreciably large relative dimensional changes (Fig. 2-10), the preload was modified to account for the thermal effect.

The relative dimensional change between the aluminum structure and the Kapton reflector is given by:

$$\Delta l = \alpha_{al} \Delta T_{al} l + \alpha_k \Delta T_k l$$

Where $\alpha_{al} = 12.5 \times 10^{-6} / ^\circ F$

$\alpha_k = 3.6 \times 10^{-5} / ^\circ F$ (average value for temperature range)

$\Delta T_{al} = 185^\circ F$	}	temperature change during the eclipse
$\Delta T_k = 370^\circ F$		

The relative dimension change in the X-axis direction between sunlight and eclipse is 2.7 m per edge; the springs, which must provide a minimum preload of 0.175 N/m, will increase the tension force depending on their spring rate. An initial evaluation showed that a series of springs with rates of 1.15 N/m would provide an perimeter tension force of 0.7 N/m (4×10^{-3} lb/in.); this load is applied to the beams together with axial forces due to the primary bending loads.

2.3.1.5 Design Loads 1-m x 40-m Beam - The critical loads on the 1-m x 40-m beam are a function of a combination of loads and temperatures applied to the 20-m x 493-m beam of which the 1-m beam is a basic element or cap. Figure 2-11 illustrates the external loading system; in addition the beam internal loads can be effected by initial manufacturing imperfections such as bowing along the length as shown in the figure. During power generation at geosynchronous orbit, at which time the upper surface is sun oriented, the thermal gradients are in a direction to relieve the lateral beam deflections caused by the reflector load on both the 1-m and 20-m beams. During eclipses, the stationkeeping maneuver will

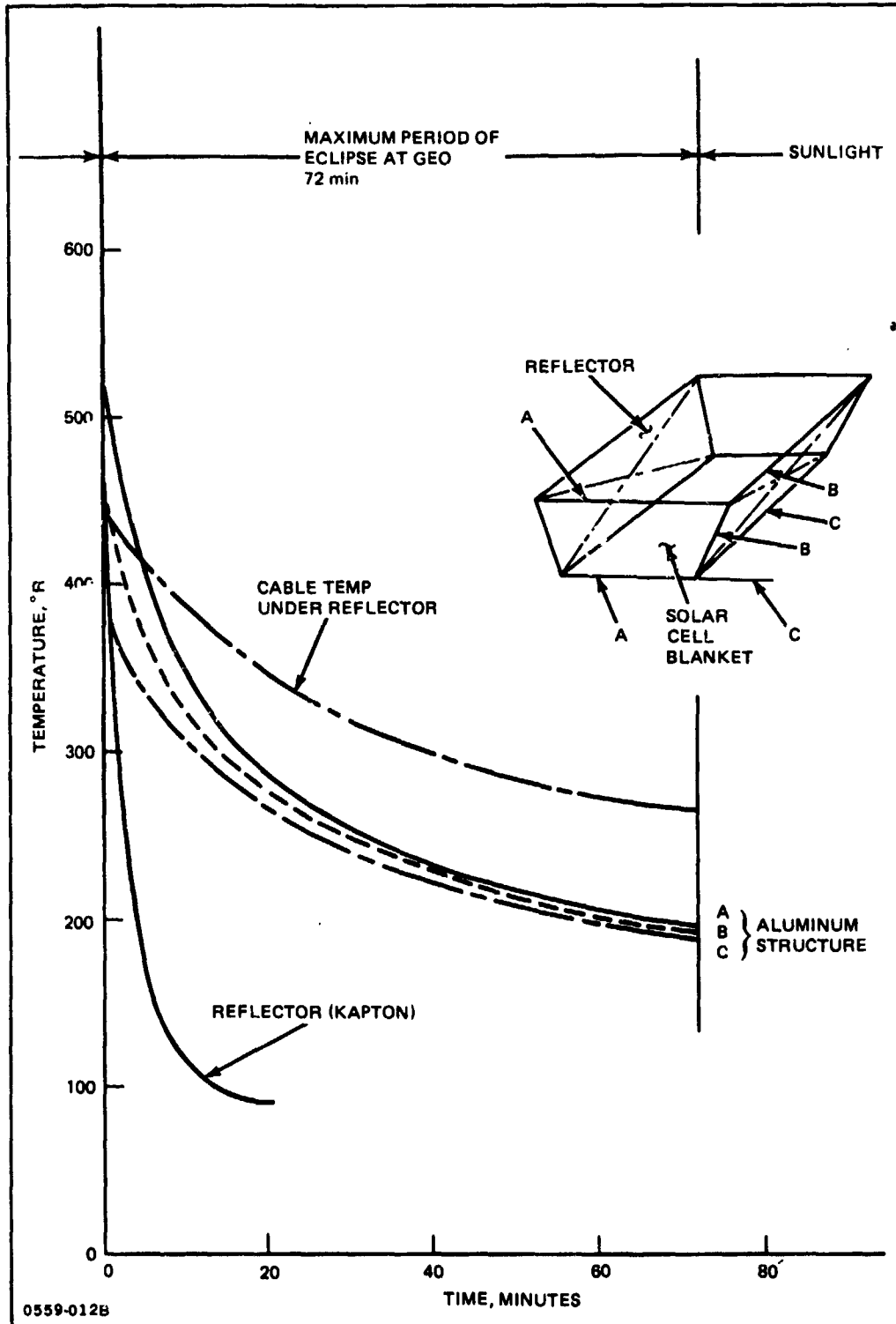


Fig. 2-9 Average Temperature of Major Members during Eclipse, GEO

not be programmed, thus eliminating the bending in the solar array caused by the maneuver. The maximum moment at the centerline of the 20-m x 493-m beam (assuming the beam is continuous) is given by:

$$M_{\max} = j^2 (\omega \pm 2 Pk) \left[\frac{u}{2} \operatorname{cosec} \frac{u}{2} - 1 \right]$$

$$j = \sqrt{\frac{EI}{P}}$$

$$u = \frac{L}{j}$$

$$k = \frac{4C_0}{L^2}$$

C_0 = initial bow at center

$$P = 794 \text{ lb (3530 N) limit}$$

$$W = 6.93 \times 10^{-3} \text{ lb/in. (1.21 N/m) limit}$$

$$j^2 = 1.469 \times 10^9 \text{ in. (3.73} \times 10^7 \text{ m)}$$

$$M_{\max} = 1.099 \times 10^5 \pm 262 C_0$$

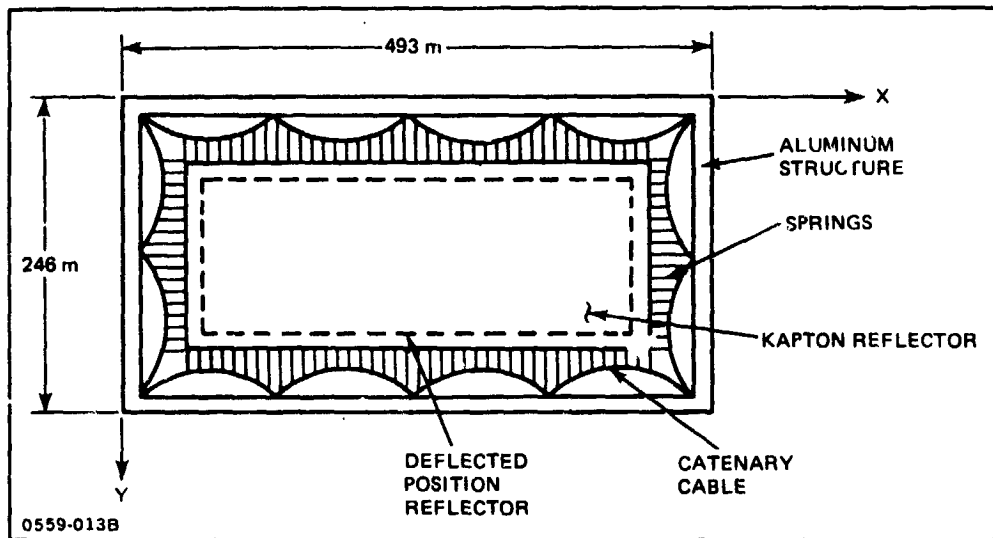


Fig. 2-10 Solar Reflector Support System (Schematic)

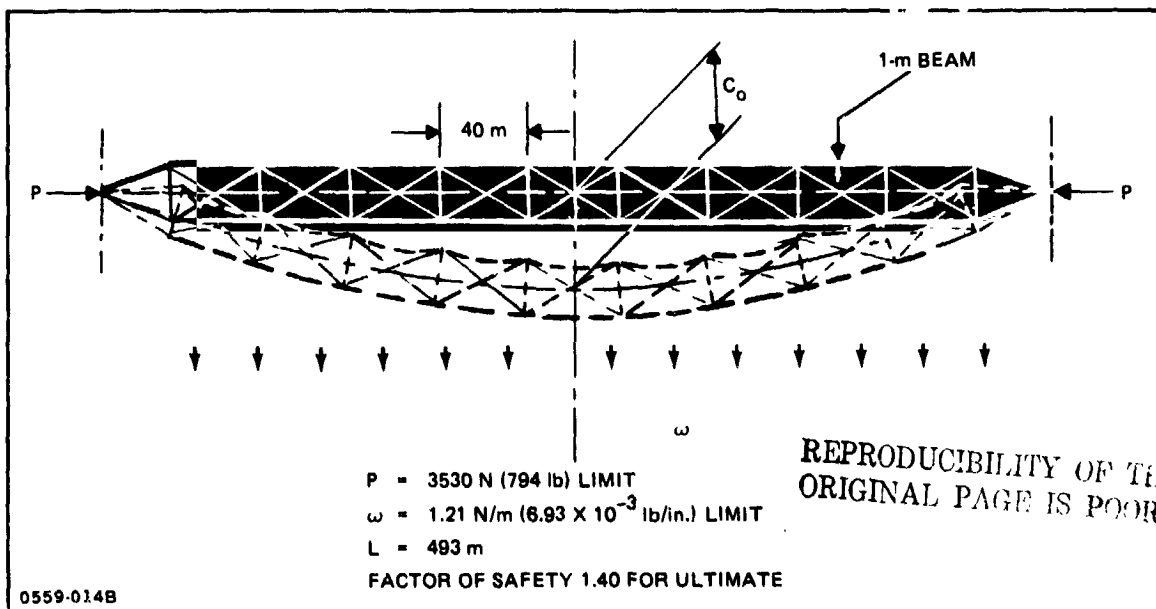


Fig. 2-11 Design Loading Condition 20-m x 493-m Beam

The curve of maximum moment versus C_0 is shown in Fig. 2-12; the moment used from this curve to calculate the incremental load on the 1-m x 40-m beam was 1.74×10^4 N·m (1.54×10^5 in.-lb) ultimate at $C_0 = 0$.

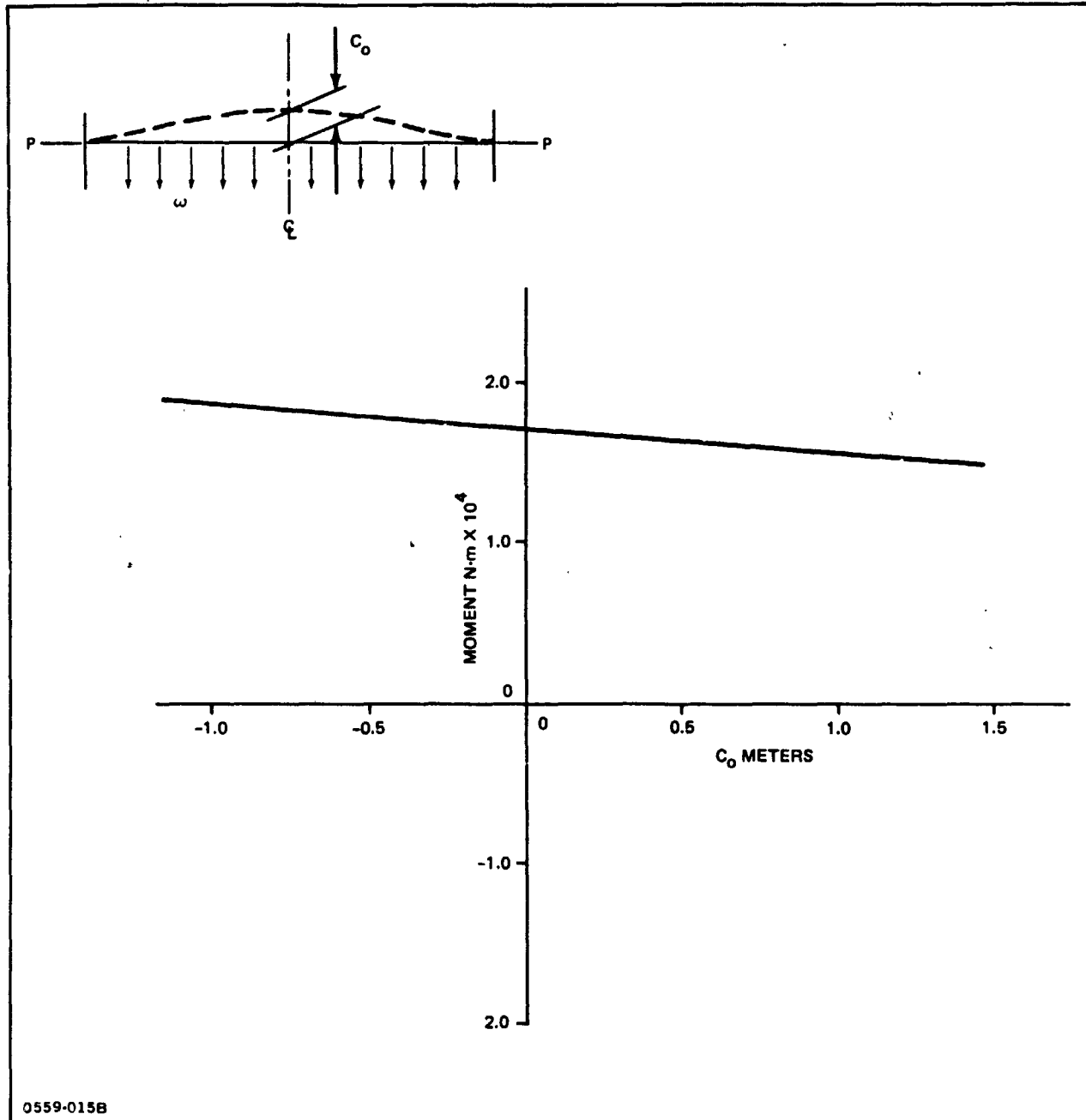


Fig. 2-12 Maximum Moment versus C_0 for 20 m x 493 m (Continuous Beam)

The incremental load on the 1-m x 40-m beam caused by bending on the 20-m x 493-m beam is

$$P = 912 \text{ N (205 lb) ultimate}$$

The axial load due to the primary solar array bending is 1647 N (370 lb) ultimate (i.e., $1111/3$). This force combined with $\Delta P = 205 \text{ lb}$ results in a total compression load at each end of 2558 N (575 lb) ultimate.

Estimate of the maximum moment at the centerline of the 1-m x 40-m pin ended beam (Fig. 2-13).

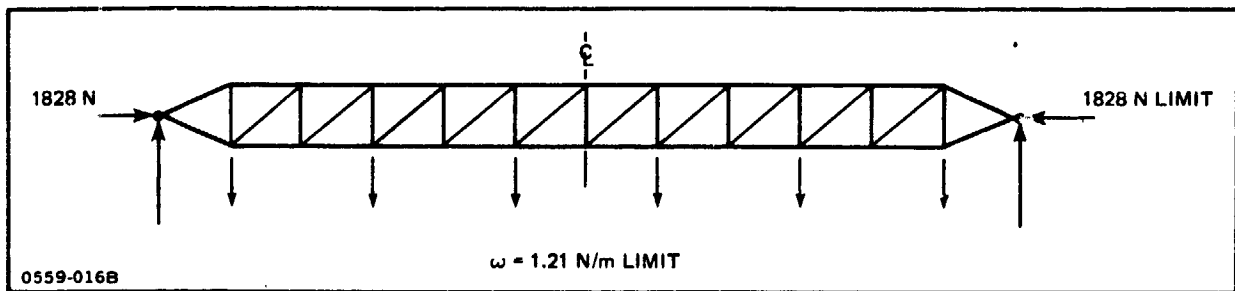


Fig. 2-13 Design Loading Condition for 1-m x 40-m Beam

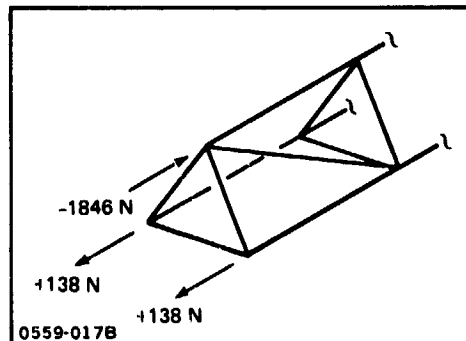
The maximum moment at the centerline is given by

$$M_{\max} = 2405 \pm 462 C_0$$

Where C_0 is the initial eccentricity at the beam centerline.

This equation is plotted in Fig. 2-14; an initial eccentricity of 0.5% (0.2 m) selected as a conservative initial imperfection for a 40-m long beam. The bending moment is 956 N·m (8460 in.-lb). The ultimate cap loads on the 1-m beam at the centerline are given by:

$$P = \frac{-575 \pm 223}{3} = \begin{matrix} -415 \text{ lb (-1846 N)} \\ +31 \text{ lb (+138 N)} \end{matrix}$$



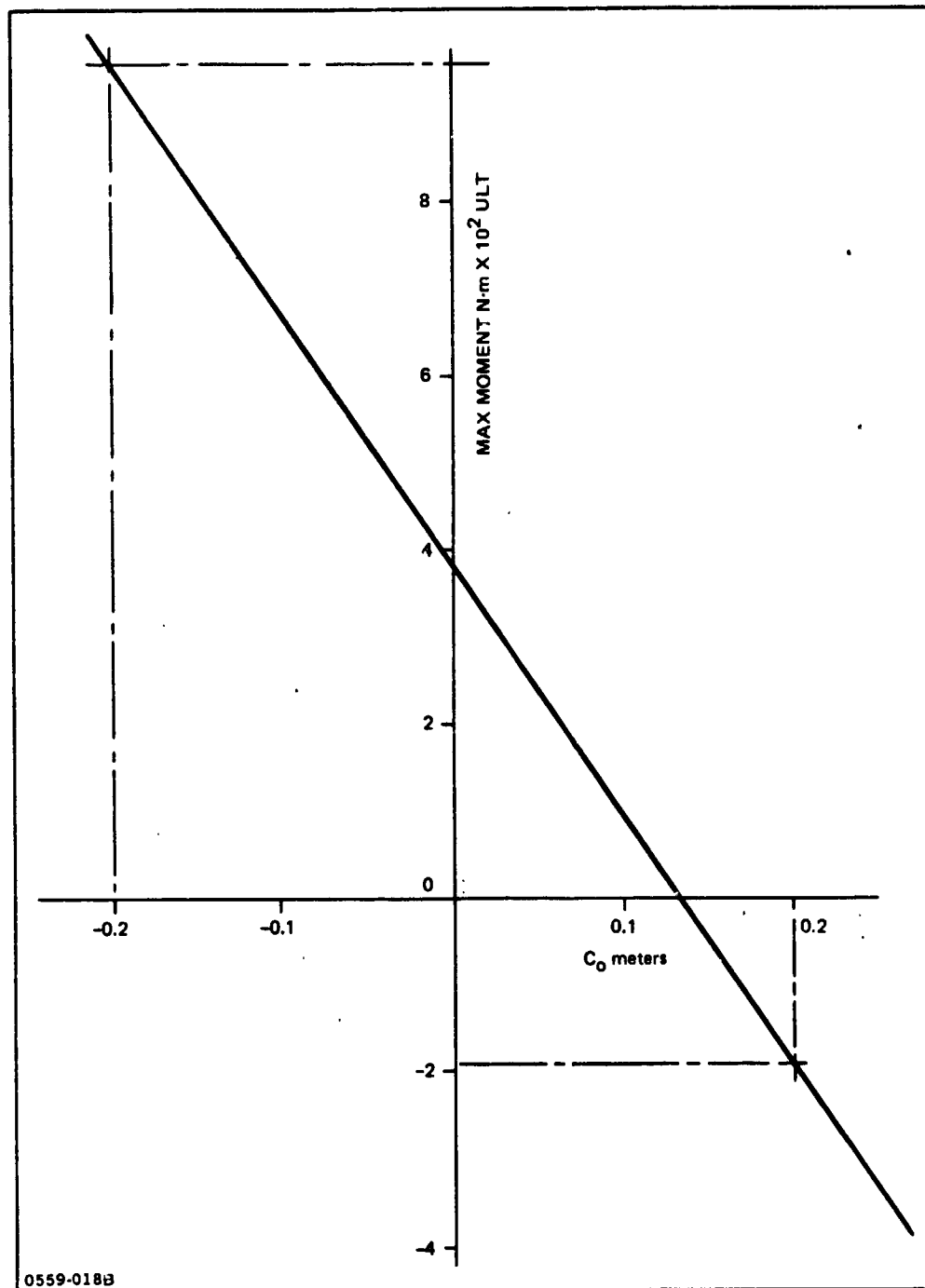


Fig. 2-14 Maximum Moment versus Initial Deflection (1-m x 40-m Beam Pin Ended)

The critical beam column load is 2558 N (575 lb) compression with a 1.69 N/m ($9.68 \times 10^{-3} \text{ lb/in.}$) lateral running load ultimate.

The critical cap load is 1846 N (416 lb) compression. In the derivation of these loads used to design the basic beam, a conservative approach was undertaken in order to achieve a design which had more than this extremely limited application.

2.3.2 Orbiter Payload Bay Operation

2.3.2.1 Modes & Frequencies 1-m Beam - A NASTRAN model (Ref. 6) was formulated to obtain modes and frequencies of a nominal 40-m long beam mounted in the Shuttle and also in the unconstrained state. Properties of the 1-m triangular beam and Shuttle mass properties are summarized in Table 2-2. The triangular beam was simulated as a series of axial load carrying members. The fundamental frequency is 0.57 Hz for the Shuttle mount and 3.6 Hz unconstrained (Table 2-3 and Fig. 2-15). Plots of the modes shapes are also given for typical cases. Figure 2-16 shows predicted variation in frequency with beam length using simple beam theory.

Table 2-2 Shuttle-Beam Mass Data

BEAM PROPERTIES		
LENGTH		39 m (1535 in.)
WGT		52.9 kg (116.7 lb)
C. G.	X	29.1 m (1146.7 in.)
	Y	0.0 m (0.0 in.)
	Z	30.13 m (1186.53 in.)
CAP AREA		0.65 cm ² (0.1014 in. ²)
BATTEN & DIAGONAL AREA		0.48 cm ² (0.0737 in. ²)
MATERIAL		ALUMINUM
SHUTTLE PROPERTIES		
WGT		96,717 kg (213,221 lb)
C.G.	X	28.7 m (1130.7 in.)
	Y	0.02 m (0.8 in.)
	Z	9.72 m (382.7 in.)
INERTIA	I _{xx}	1.22 X 10 ⁶ kg m ²
	I _{yy}	8.86 X 10 ⁶ kg m ²
	I _{zz}	9.24 X 10 ⁶ kg m ²
SUPPORT		
NODES 1, 2, 3		X, Y, Z
NODES 4, 5, 6		X, Y
0559-019B		

2.3.2.2 Forced Response - 40-m Beam to Orbiter RCS System Thrust - The modal data computed for the Orbiter supported 40-m beam (Fig. 2-17) was used to calculate the response of the beam (Ref. 2-7) to the RCS acceleration inputs given in NASA "Payload Accommodations Document," JSC 07700, Volume XIV. The primary RCS angular accelerations are 1.2 deg/sec² roll and +1.4 deg/sec², -1.5 deg/sec² in pitch. The vernier RCS

Table 2-3 Vibration Modes (1-m x 40-m Beam)

	FREQ (Hz)	GEN MASS (lb-sec ² /in.)	DESCRIPTION
MOUNTED IN SHUTTLE	0.570	0.124	1ST LATERAL BENDING (+X)
	0.575	0.116	1ST LATERAL BENDING (+Y)
	3.5	0.080	2ND LATERAL BENDING (+X)
	3.5	0.085	2ND LATERAL BENDING (+Y)
UNCONSTRAINED (FREE-FREE)	3.6	0.083	1ST LATERAL BENDING (+X)
	3.7	0.084	1ST LATERAL BENDING (+Y)
	7.6	0.153	1ST TORSION
	9.3	0.088	2ND LATERAL BENDING (+X)

0559-020B

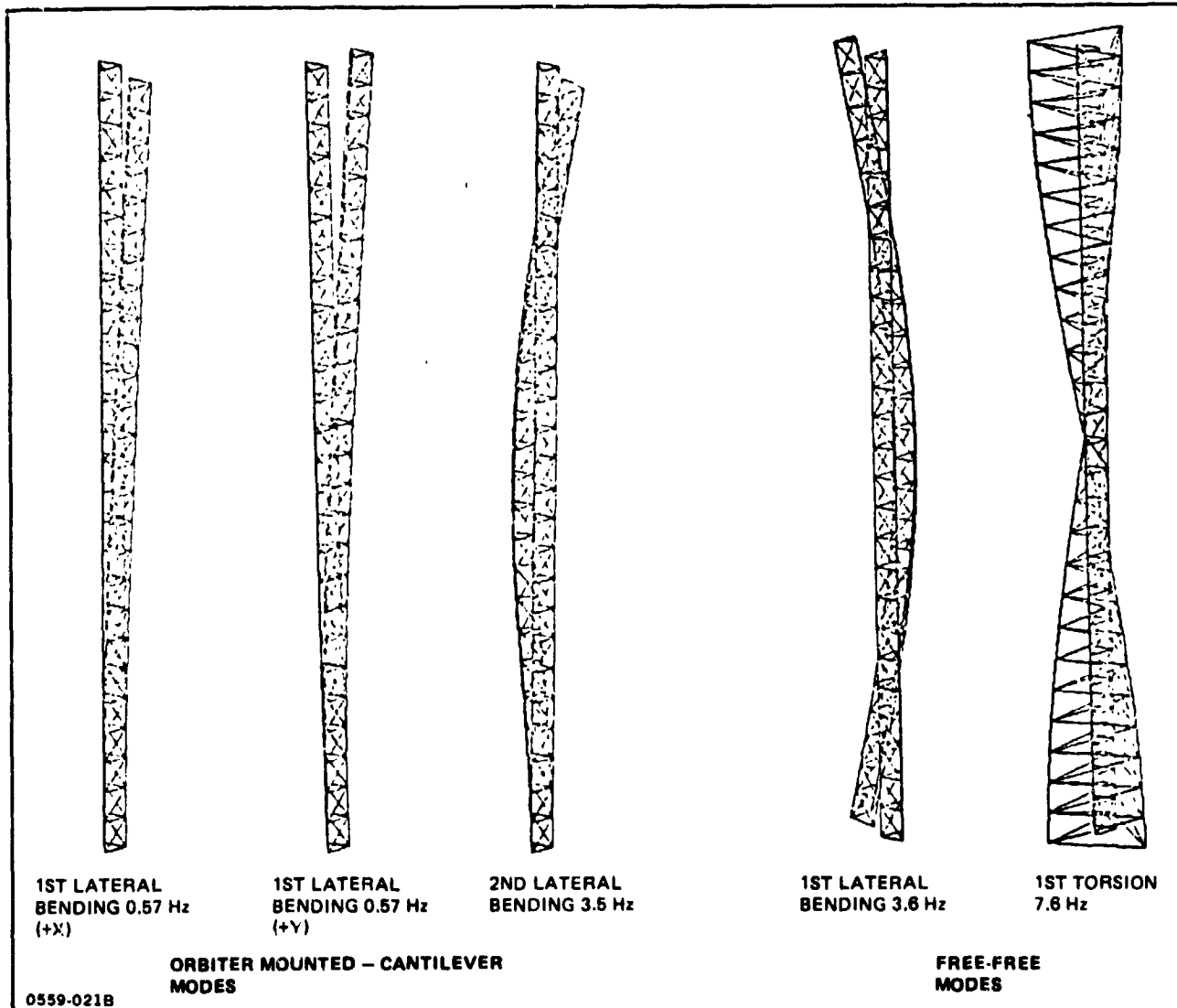


Fig. 2-15 Modes & Frequencies 1-m x 40-m Beam

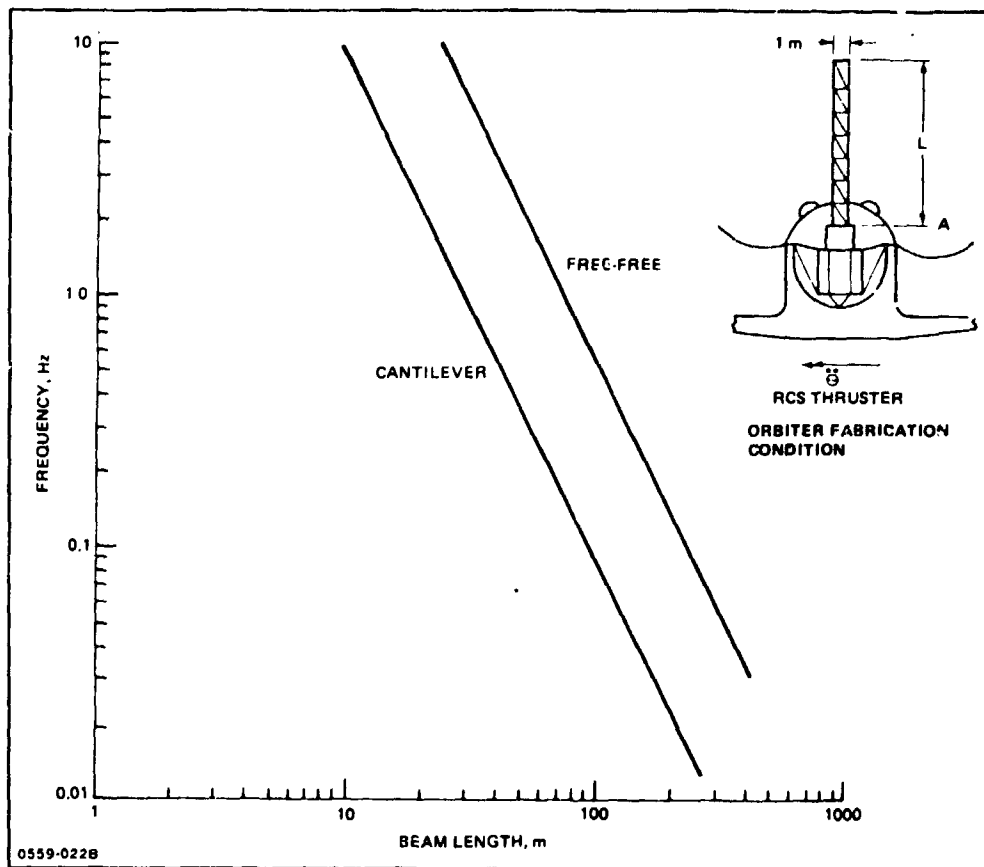


Fig. 2-16 Fundamental Frequency versus Beam Length

angular accelerations for the above cases are 0.04 and +0.03, -0.02, respectively. The acceleration inputs were applied in six selected modes varying from step inputs to double phased pulses up to 4 sec. The response data included:

- Tip displacement
- Tip acceleration
- Orbiter acceleration
- Load time histories of critical members.

Roll and pitch cases for the primary RCS were calculated for the selected input modes. Flexible modes were used for the roll condition; the peak limit cap loads was ± 672 N in members 105 and 107. The peak limit diagonal load was ± 307 N in members 104 and 106. These loads were for the step input from 0 to 2.5 sec.

Typical tip displacement, tip acceleration and orbiter acceleration curves are included (Fig. 2-18, 2-19, and 2-20). The rigid body positive pitch case was calculated for a step input acceleration resulting in a peak cap load of -1272 N and a tip deflection of

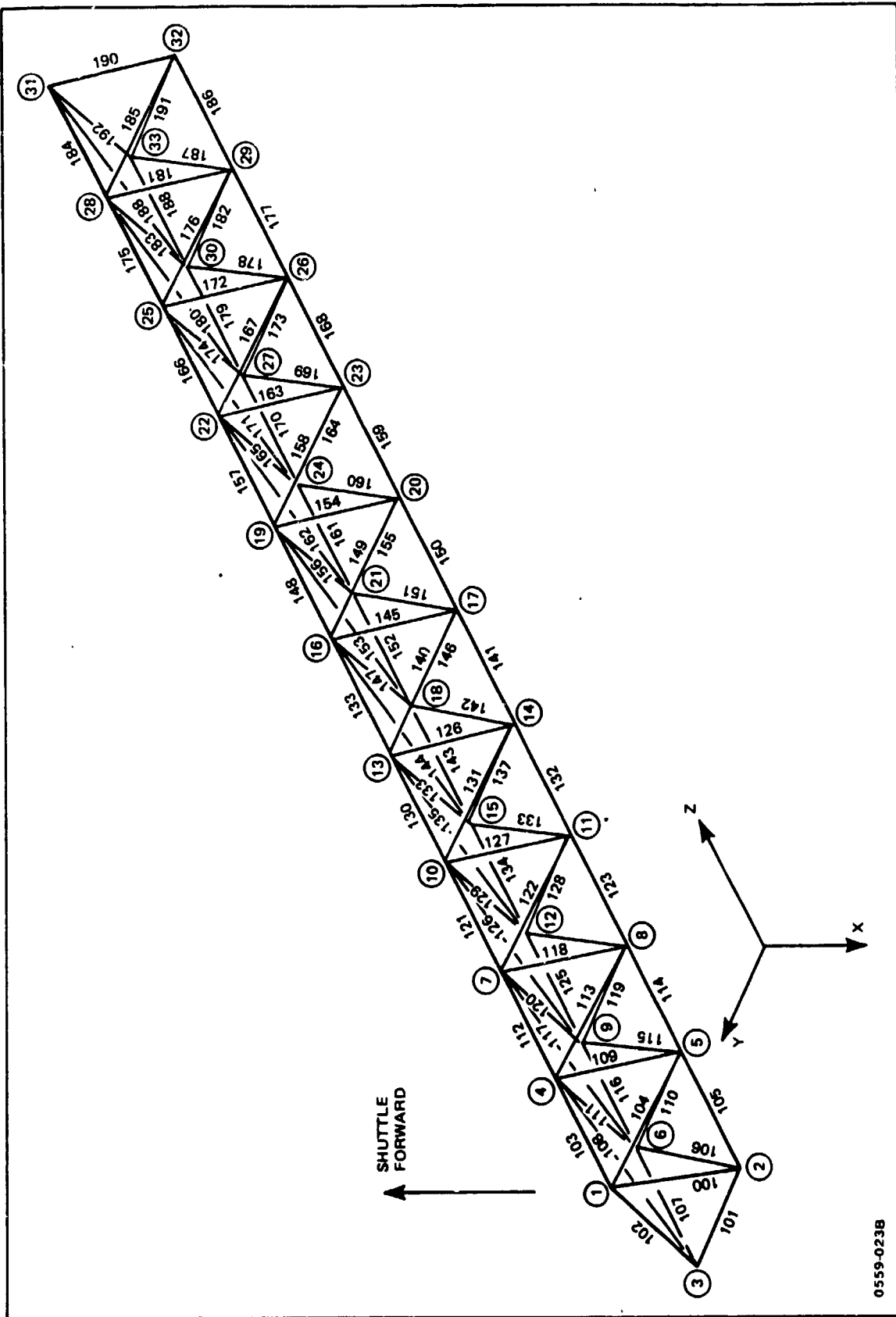


Fig. 2-17 Node & Member Designations

0.18 m. The maximum compression loads in the beam caps for the Orbiter primary RCS firing are lower than the loads obtained for the SSPS stationkeeping maneuver and, therefore, are not a design case. However, to avoid control system coupling it is recommended that only the vernier RCS thrusters be used if necessary during extended length beam fabrication operations. The primary system could be used as a backup for lengths up to 40 m.

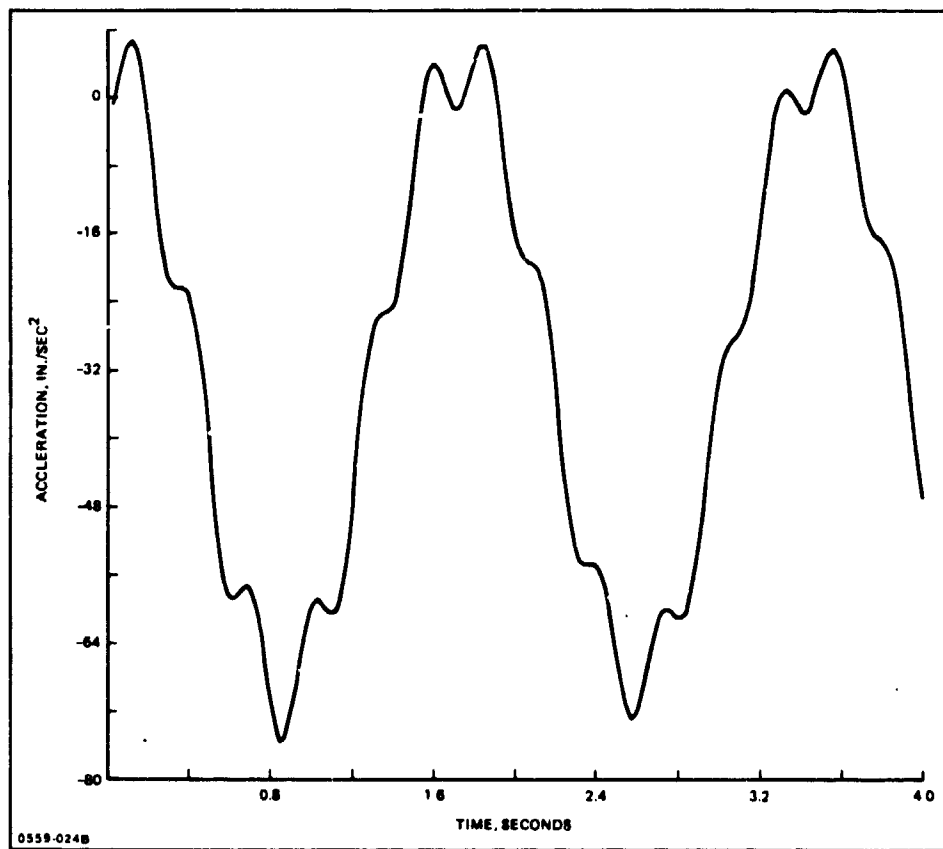


Fig. 2-18 Tip Acceleration versus Time

2.4 MATERIAL PROPERTIES

Aluminum alloys 2024-T3, 2219-T6, and 6061-T6 (Table 2-4) were selected as candidate materials for automatic beam builder fabrication of the 1-m beam. Of these alloys, 2024-T3 was selected for the beam material for its slightly higher compression yield strength and also because it is easier to roll form than the 2219-T6 alloy. These alloys all are resistance weldable and have relatively good mechanical property retention up to 450 °K (350 °F). Bend radii of 10T were used for all forming operations on the material.

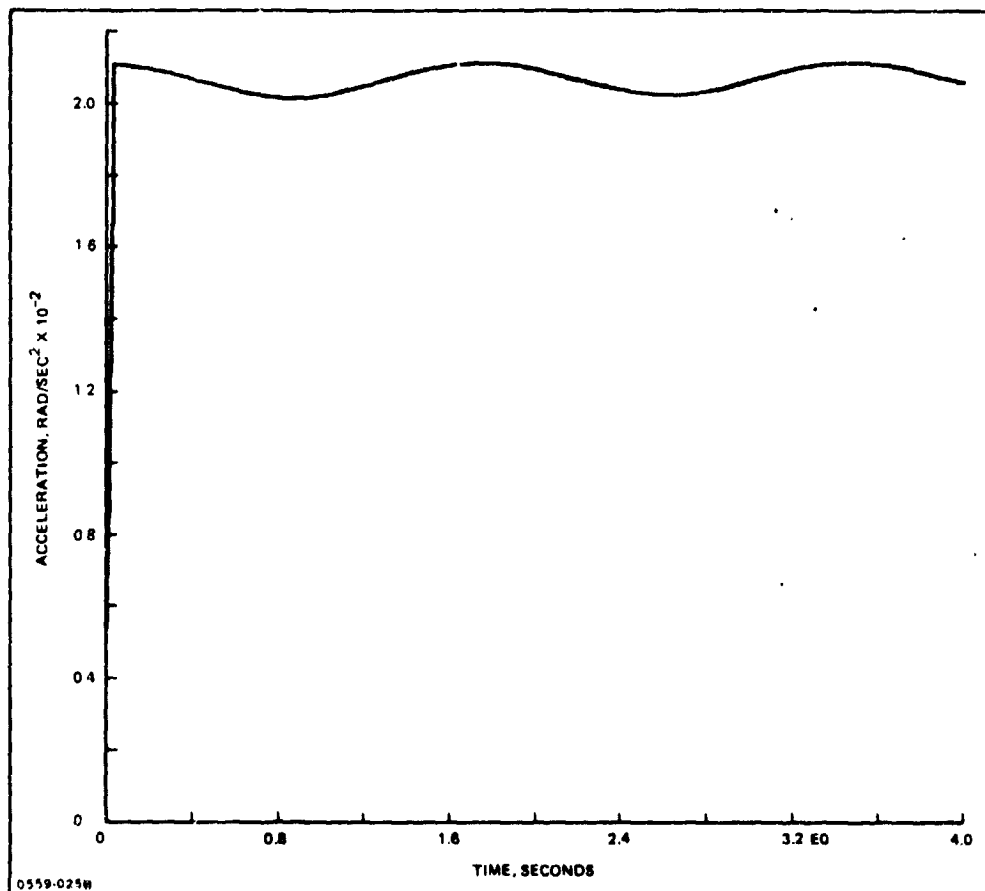


Fig. 2-19 Orbiter Acceleration versus Time

2.5 1-m x 40-m BEAM DESIGN DATA

2.5.1 Design Detail

Figure 2-21 shows the design configuration of the 1-m beam structure; end attachments were not included as part of this study, but a concept is described in a later section. The caps are roll formed in the beam builder out of 0.041 cm (0.016 in.) 2024-T3 aluminum alloy. Battens and diagonals, which have the same cross section, are ground roll formed from the same material as the caps; after positioning, these parts are attached to the caps by three spotwelds per leg in the automatic processing operations of the beam builder.

Diagonal members capable of supporting compression loads were selected instead of pretension cross cables in the early phases of beam builder studies. The rationale for selection of a compression capable diagonal was based on avoiding potential problem areas some of which included the following:

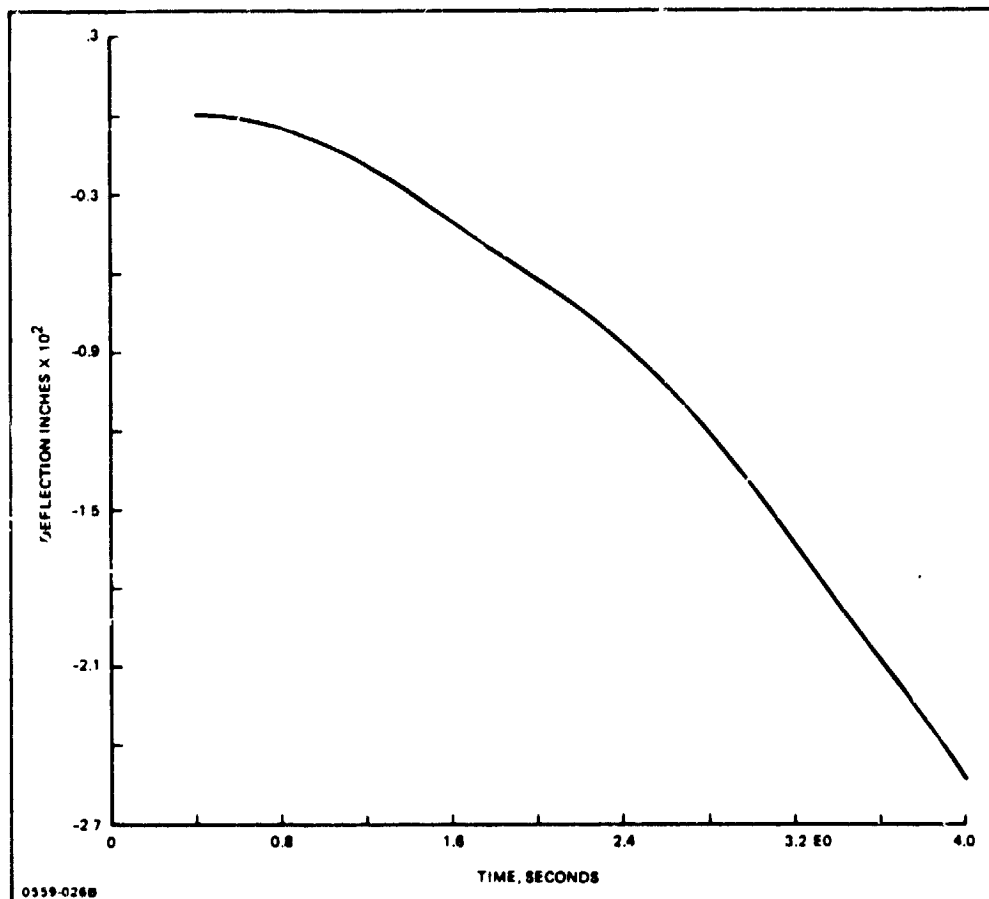


Fig. 2-20 Tip Deflection versus Time (Step 0 to 4 sec)

- Do the cross cable and low stiffness batten system have capability to provide sufficient end fixity for a cap which possesses low torsional stiffness characteristics ?
- What is the reliability of obtaining a structurally sound single point attachment of a small diameter preloaded wire during beam builder fabrication ?
- Does loss of several cable attachments to caps induce lattice column type failure due to inadequate residual stiffness ?
- Beam torsional stiffness is markedly greater with stiff diagonal than with crossed cables due to large area difference between the two diagonal design concepts.

Test data, which are discussed in later sections, show that the batten/diagonal design enforces a node at the batten spacing such that a joint fixity coefficient equal to 4.0 is attained.

Table 2-4 Candidate Material Property Data

	2024-T3		2219-T6		6061-T6	
• F_{TU} ksi (MN/m ²)	64	(440)	54	(370)	42	(290)
• F_{TY} ksi (MN/m ²)	47	(320)	36	(250)	36	(250)
• F_{CY} ksi (MN/m ²)	39	(270)	38	(260)	35	(240)
• E_C ksi (GN/m ²)	10.7 x 10 ³	(74)	10.8 x 10 ³	(74.5)	10.1 x 10 ³	(69.6)
• ρ lb/in. ³ (K kg/m ³)	0.100	(2.77)	0.102	(2.82)	0.098	(2.71)
• α in./in./°F x 10 ⁻⁶ @ 200°F (m/m/°C x 10 ⁻⁶ @ 93.4C)	12.9	(23.22)	12.4	(22.32)	13	(23.4)
• K BTU/(hr) (ft ²) (F)/ft	80		74		5	
• C BTU/(lb) (°F) @ 200°F	0.22		0.23		0.23	
0559-027B						

Figure 2-22 shows the detail dimensions of the cap and attachment between battens and cap.

The beam unit weight without end attachments is 0.85 lb/ft. (1.26 kg/m).

2.5.2 Beam Section Properties

Beam and detail parts properties are defined in Fig. 2-23 and 2-24.

2.5.3 Torsional Stiffness (Non-Buckled State)

A NASTRAN model of the 1-m beam with unbuckled members was used to calculate the torsional stiffness of the structure. The 1 in.-lb (0.113 N·m) torsion was applied at the center of the 40-m beam and reacted at each end (Fig. 2-25).

As previously noted the above data are for the unbuckled state for the 0.04-cm (0.016-in.) thick members. Some test experience for compression testing has shown that the onset of initial buckling in compression is at relatively low stress levels. The effect of the types of loading, stress state, and geometry on torsional stiffness can be evaluated by test.

2.5.4 Static Load Analysis

A 13-bay finite-element model, representing half of a 40-m column, has been generated using COMAP-ASTRAL. All elements are modeled as beams and have the section properties as presented in Fig. 2-26. These values represent the case for members in the non-buckled condition. All of the eccentricities, etc., of the specimen are incorporated.

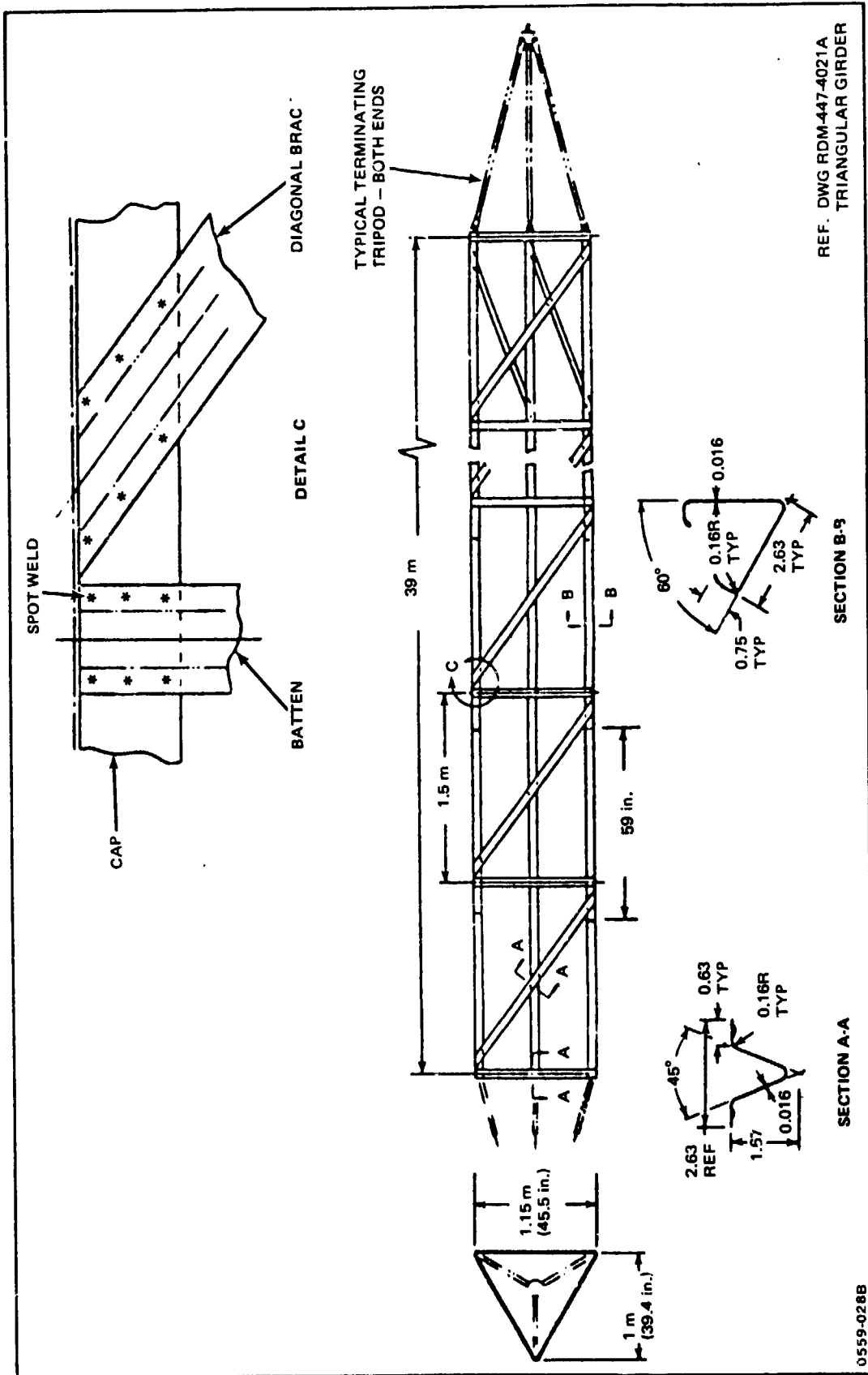


Fig. 2-21 1-m Beam Design

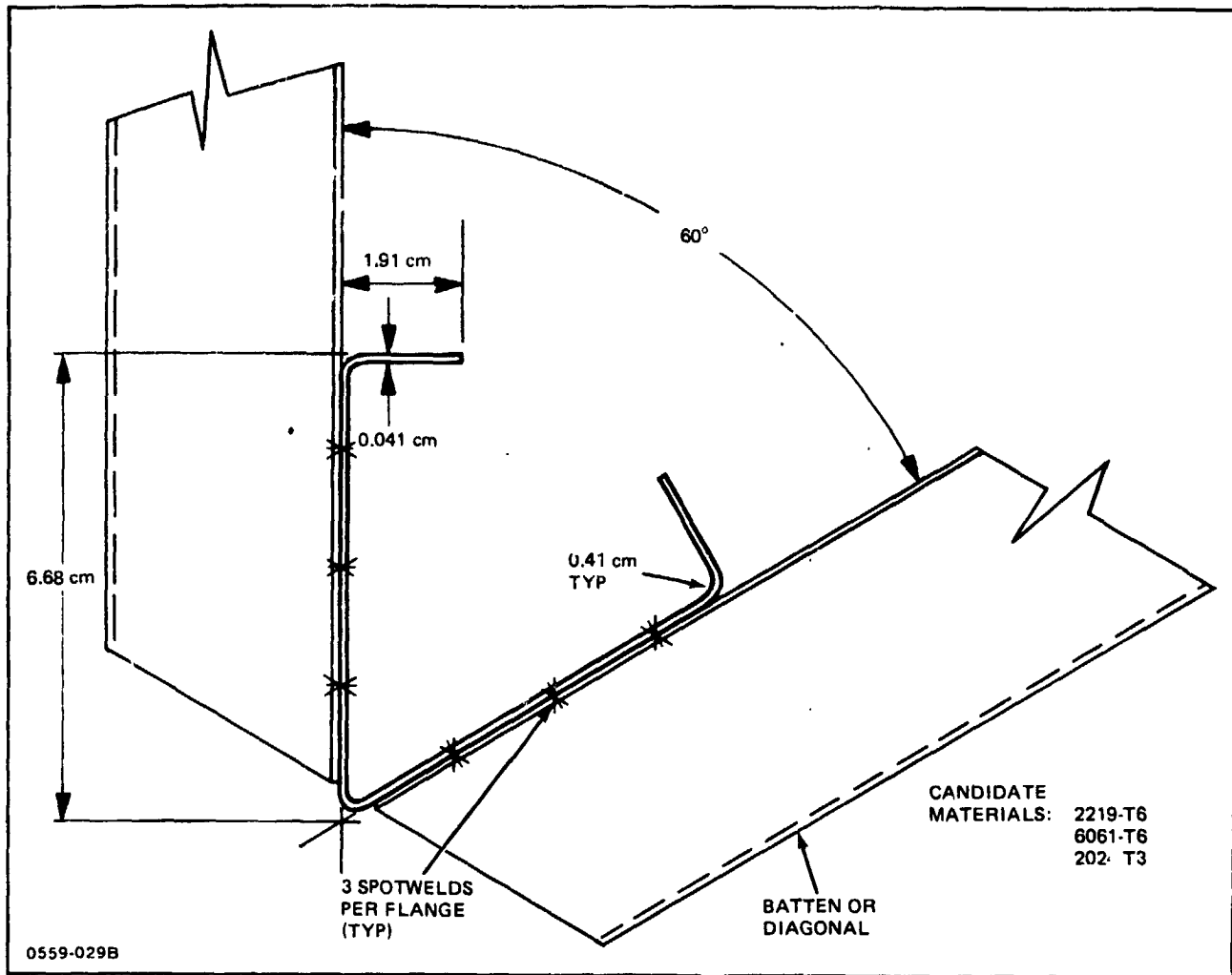


Fig. 2-22 1-m Beam Cap to Batten Attachment (2024-T3 Aluminum Alloy)

A total of two static and one thermal load conditions were run. It is anticipated that these, either separately or in combination, cover all the possible loading conditions.

Table 2-5 gives results of deflections and loads at the critical locations for each loading case.

2.5.5 Torsion at End Attachments

Torsion at end attachments caused by manufacturing misalignment of the 1-m x 40-m beam in the X-Y plane is shown in Fig. 2-27.

2.5.6 Summary Design Loads

- Solar Power operating Condition - Geosynchronous Orbit
 - 1-m x 40-m loading system (Fig. 2-28)

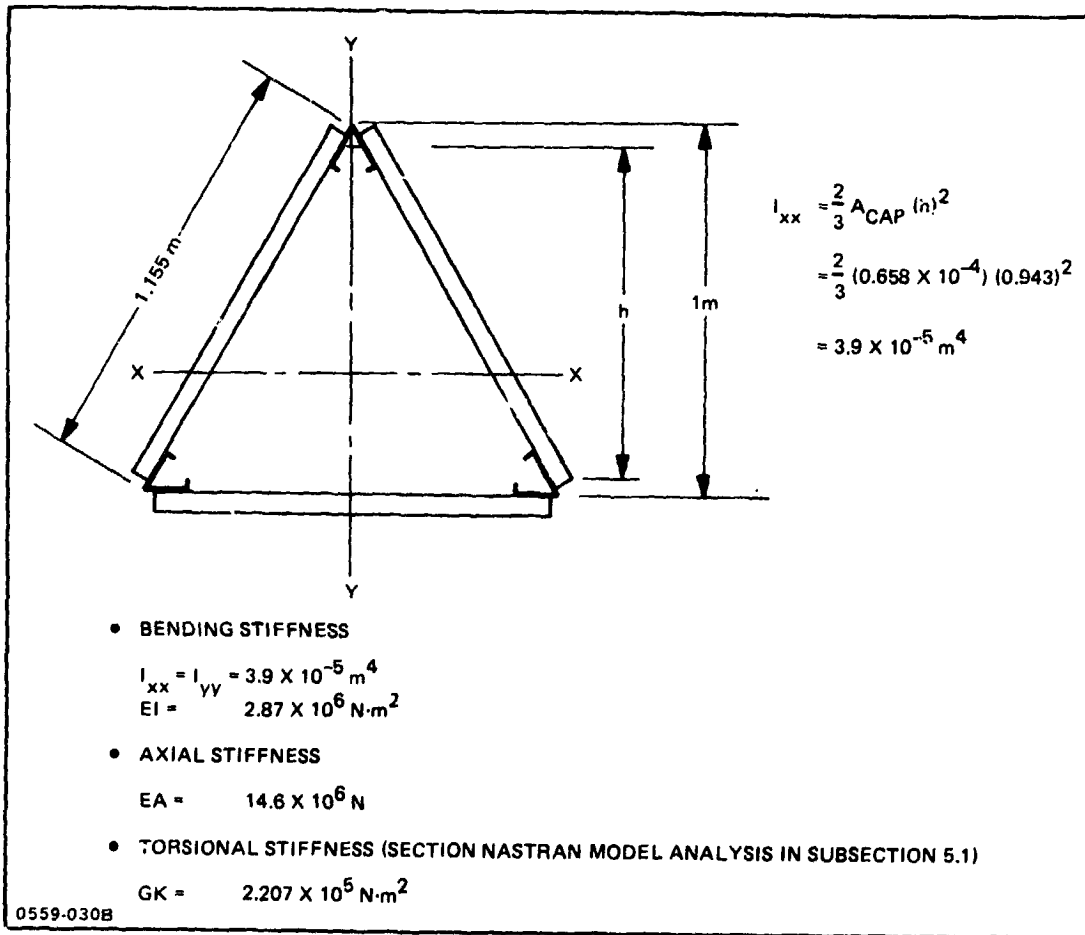


Fig. 2-23 Beam Cross Section

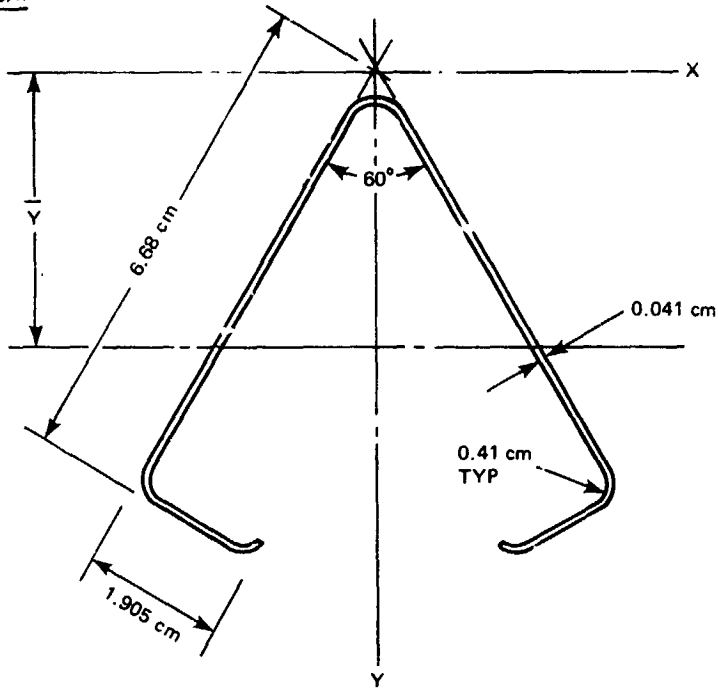
- Critical compression cap load at midspan of 40-m beam due to axial compression, lateral load, eccentricity, and non-linearity effect on bending (Fig. 2-29)
- RCS Firing During Fabrication - Orbiter Payload Bay - Low Earth Orbit (Fig. 2-30)
 - Maximum capload caused by primary RCS thruster firing in pitch -1272 N limit. For vernier RCS firing maximum load is -25 N; these loads are not critical.

2.5.7 Thermal Analysis

A thermal analyses was performed on the 1-m beam for a 400-km (215-n mi), 28.5° inclination earth oriented orbit at the vernal equinox. Figure 2-31 describes the orientation of the structure in the orbital plane. Early studies of various surface treatments showed that the black anodize coating 1 mil thick, MIL A-8625, with an absorptance to emittance ratio $\alpha/E = 0.86/0.83$, would provide the lowest temperature gradients for the conditions

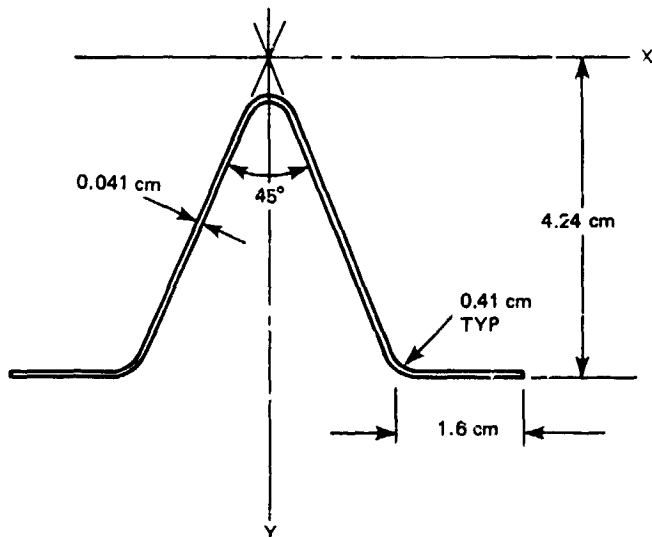
MEMBER SECTION PROPERTIES

CAP



AREA	= 0.658 cm ²
I _{xx}	= 2.422 cm ⁴
I _{yy}	= 3.25 cm ⁴
\bar{Y}	= 3.76 cm
\bar{X}	= 0

BATTEN & DIAGONAL



AREA	= 0.445 cm ²
I _{xx}	= 0.799 cm ⁴
I _{yy}	= 1.518 cm ⁴
\bar{Y}	= 2.72
\bar{X}	= 0

0559-031B

Fig. 2-24 Cap & Batten Cross Sections

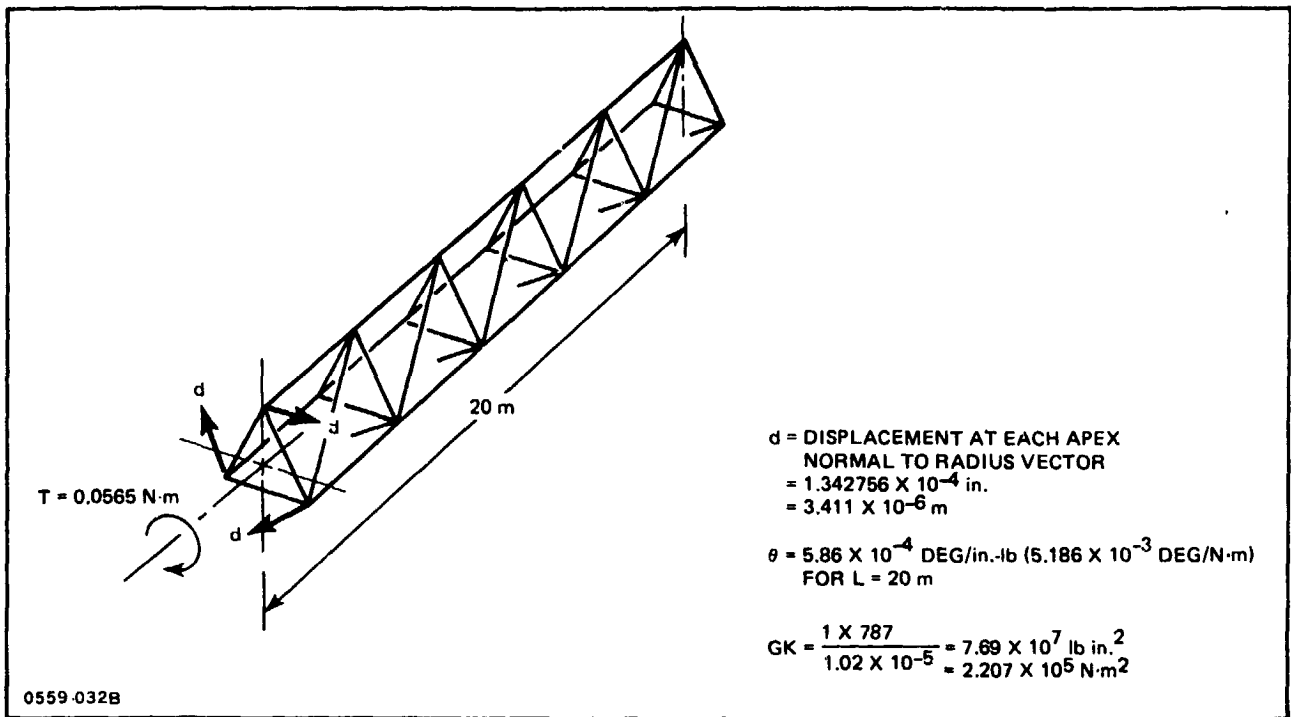


Fig. 2-25 Torsional Stiffness

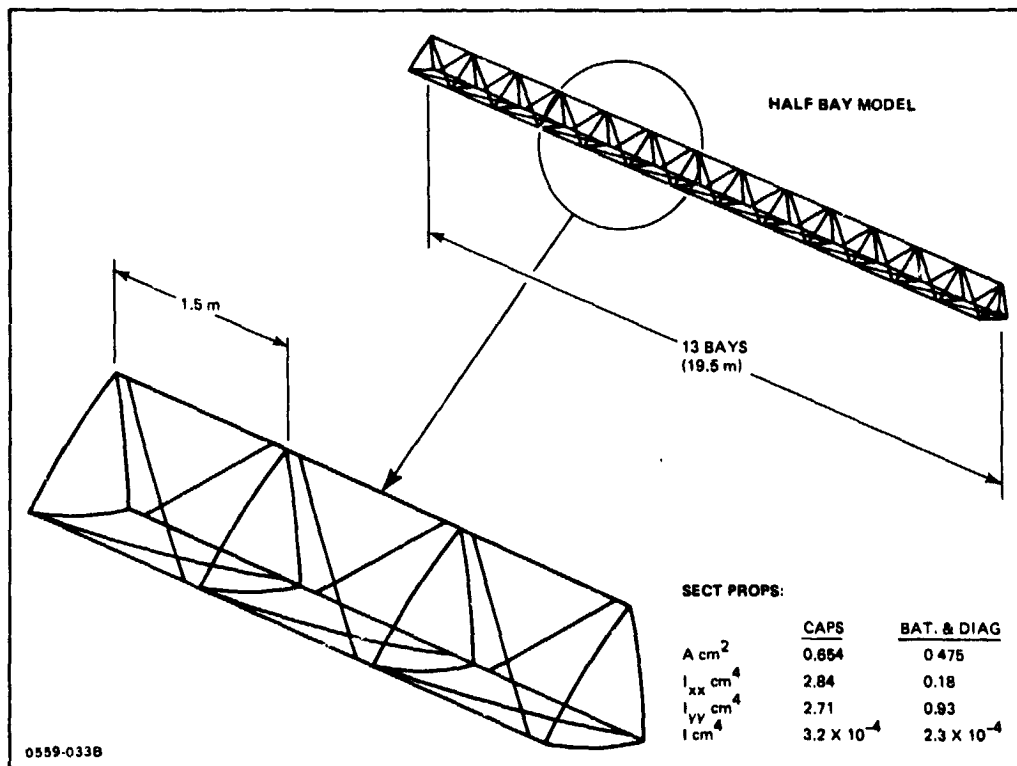
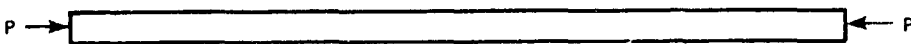


Fig. 2-26 1-m Beam Finite-Element Model

Table 2-5 Summary of Static Finite-Element Model Analysis Results

CONDITION 1 AXIAL LOAD	
	
L = 26 BAYS EACH 1.5 m, P = 2558 N ULTIMATE	
• COLUMN SHORTENING	6.99 X 10 ⁻³ m
• MAXIMUM LOAD IN BATTEN	1.87 N
• MAXIMUM LOAD IN DIAGONAL	5.83 N
• LOAD PER CAP	854 N
• INDUCED ROTATION AT EACH END OF BEAM	0.0127 RAD
CONDITION 2 REFLECTOR LATERAL LOAD	
	
P AT EACH BATTEN = 1.82 N	
• LATERAL DEFLECTION AT CENTER	1.52 X 10 ⁻² m
• SLOPE AT BEAM ENDS	3.66 X 10 ⁻³ RAD
• MAXIMUM LOAD IN BATTEN	14.23 N
• MAXIMUM LOAD IN DIAGONAL	22.51 N
• MAXIMUM LOAD IN CAP	264.2 N
CONDITION 3 TEMPERATURE DIFFERENTIAL T _u - T _L = 30° F; 16.7° K	
	
• LATERAL DEFLECTION AT CENTER	0.079 m
• SLOPE AT BEAM ENDS	2.15 X 10 ⁻² RAD
• MAXIMUM LOAD IN BATTEN	2.4 N
• MAXIMUM LOAD IN DIAGONAL	5.43 N
• MAXIMUM LOAD IN CAP	3.46 N

0559-034B

analyzed. This coating can be ground processed on the strip stock and will not be effected during roll forming in orbit. Other orbital orientations could have been chosen which might have resulted in more severe thermal gradients. However, for the known missions at the time of this study, this analysis represented a rational approach to the problem.

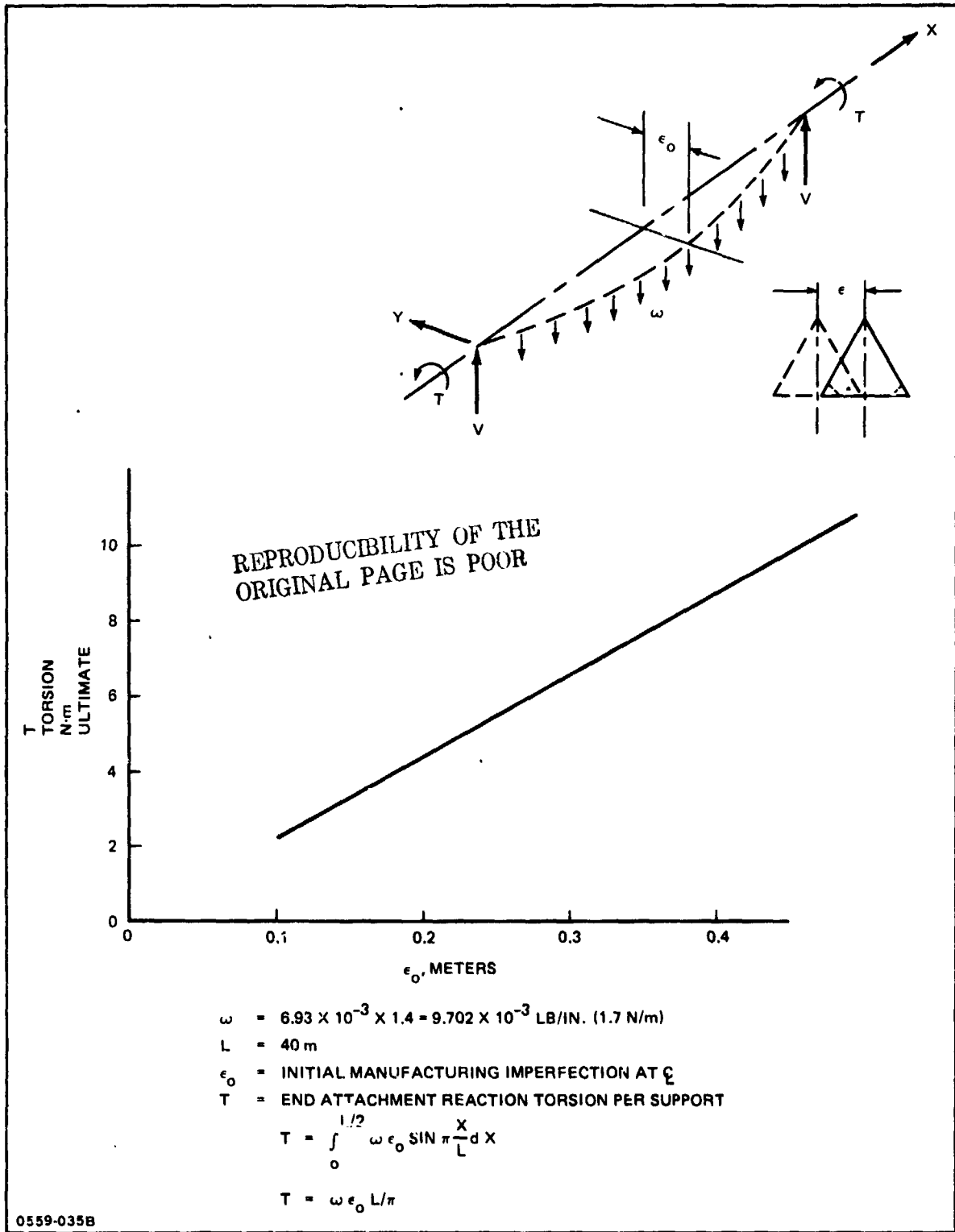


Fig. 2-27 End Torsion versus Manufacturing Eccentricity in X-Y Plane (1-m x 40-m Beam)

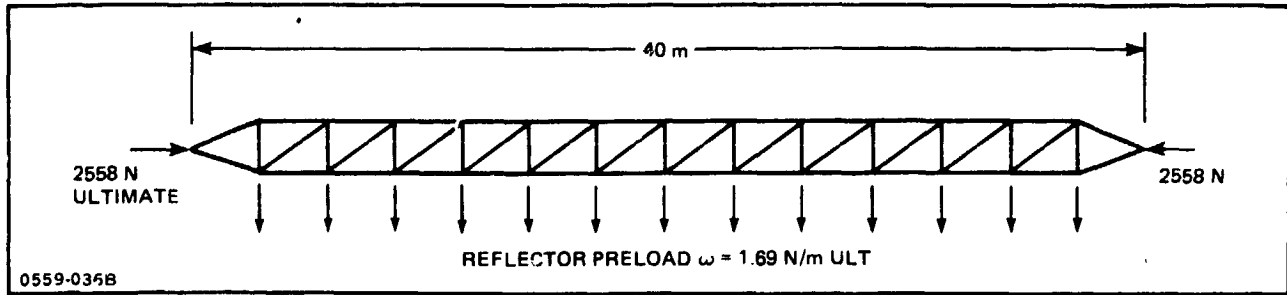


Fig. 2-28 1-m Beam Loading Conditions

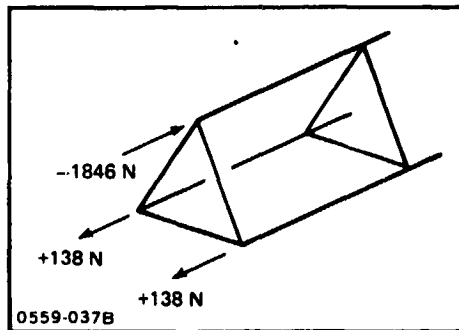


Fig. 2-29 Critical Cap Compression Load

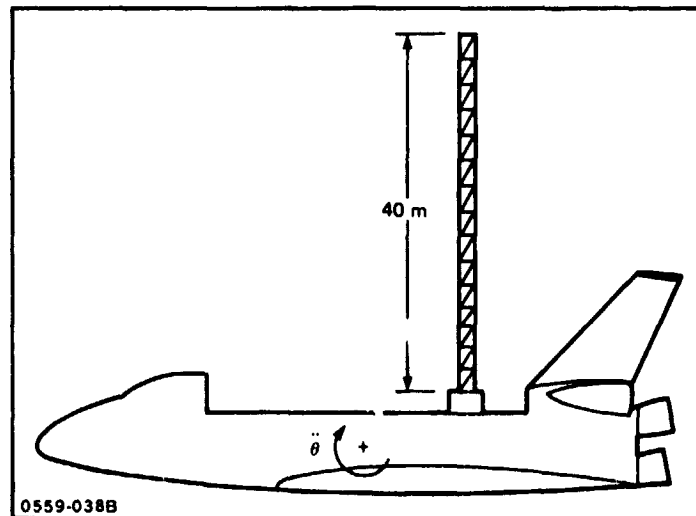


Fig. 2-30 Fabrication in Orbiter Bay

Figure 2-32 presents the temperature differences within a cap element and also the weighted average cap temperature for the sun vector oriented at 180° to the beam. The study was done for the sun angle rotated around the structure from 0° to 180° ; the 180° position resulted in the largest gradients. Thermal conduction and internal surface

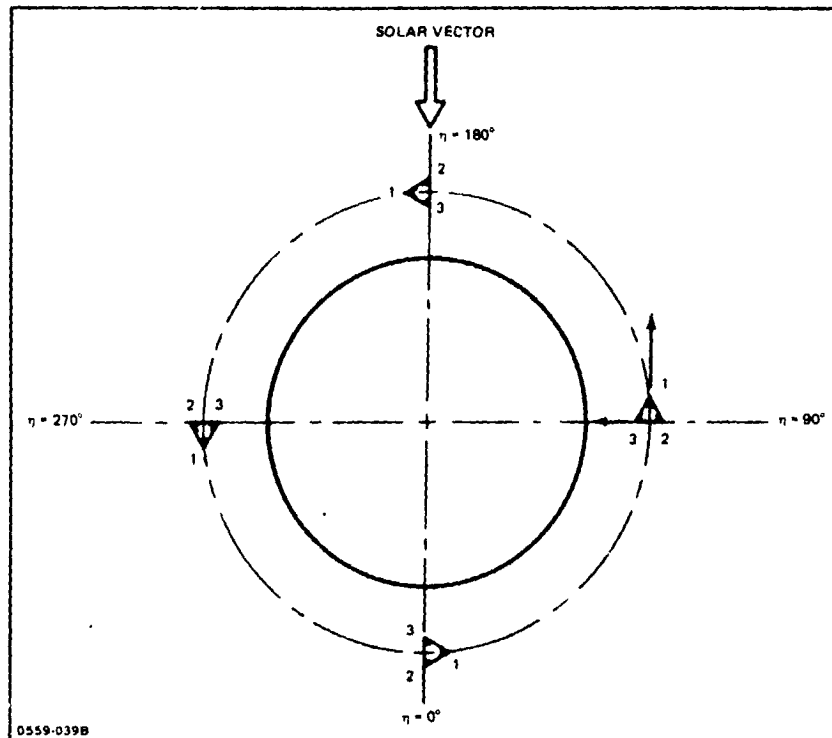


Fig. 2-31 Beam Orbital Orientation

radiation were also included in the analysis. Earlier calculations had been carried out for the 180° solar orientation condition and these data are summarized in Fig. 2-33 (Ref. 2-8). The reason for including these earlier data at this point is that the gradients are higher than those of Fig. 2-32; the data used in the thermal stress analysis shows the worst cap non-linear thermal gradient to be 50°F (27.8°K) compared to 49.1°F (27.3°K).

A transient thermal analysis (Ref. 2-9) was performed on the 1-m beam to evaluate the temperature differential which exists for the case where one cap occludes solar energy from impinging on another cap. Because of the low thermal mass of the structure, the shadowed member can experience a rapid cooldown thus increasing the thermal gradient between caps. The results of this analysis are illustrated in Fig. 2-34, wherein one cap can block another for as long as 6.1° rotation of the orbit or 95 sec of orbital time. The maximum differential is 20.6°K (37°F). The use of lightening holes to permit illumination of the occluded member could greatly relieve this type of condition if it had been shown to be critical.

A preliminary evaluation of temperature distributions (Ref. 2-10) was carried out on the SSPS at geosynchronous orbit; the temperature differential in the upper and lower chords of the 20-m beam was 31°F (17.2°K).

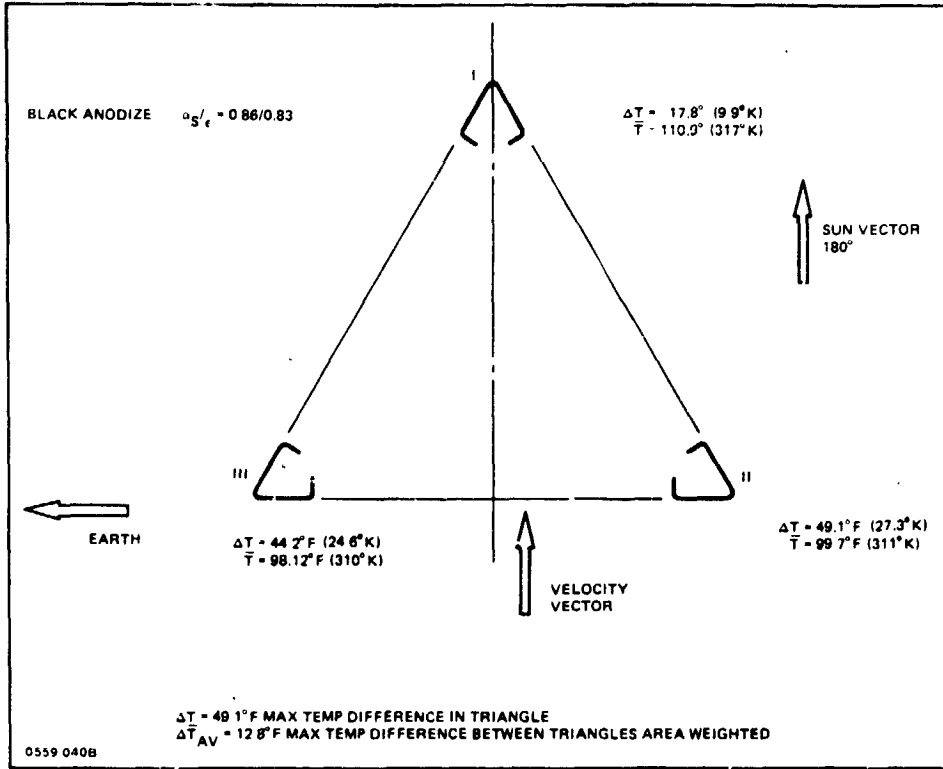


Fig. 2-32 Beam Temperature Response

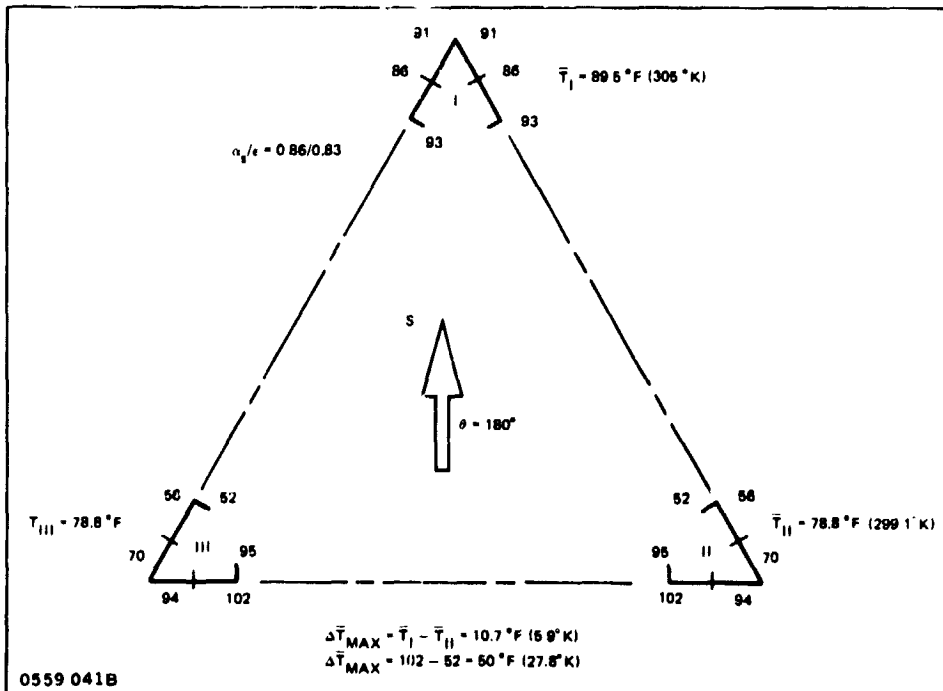


Fig. 2-33 Thermal Gradients at $\theta = 180^\circ$

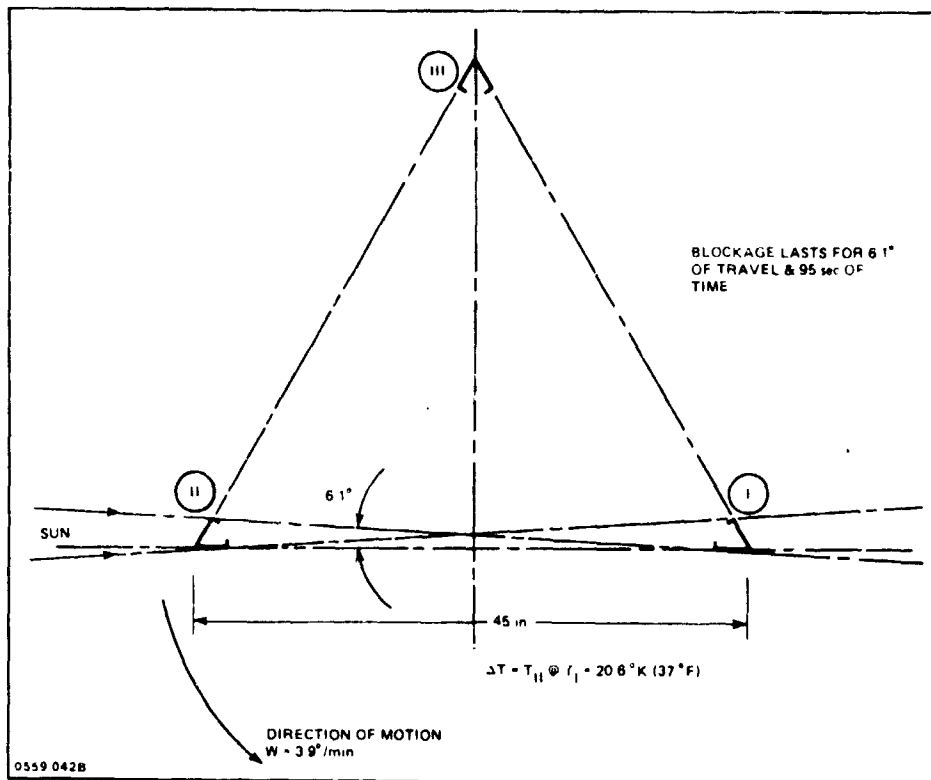


Fig. 2-34 Solar Blockage Geometry

2.5.8 Thermal Stresses

Thermally induced stresses in the beam caps were evaluated for the 180° sun orientation angle considering two temperature differential effects. The first of these was the non-linear temperature distribution across the cap cross section represented by the temperature curve in Fig. 2-33, the other is the temperature differential between the upper cap at 110.9 °F (317 °K) and the average of the two lower caps at 98.9 °F (310.2 °K). The non-linear temperature gradient in the cross section was analyzed assuming (1) a 1.5-m length cap with unrestrained ends and (2) fixed ends. The results of these analyses are shown in Fig. 2-35 and 2-36. The analyses are based on non-buckled elements of the cap cross section; the peak compression for the unrestrained case is $3.4 \times 10^6 \text{ N/m}^2$ compared to $20 \times 10^6 \text{ N/m}^2$ for the fully restrained boundary condition. The initial buckling for the flat sides occurs at an approximate average stress of $9.4 \times 10^5 \text{ N/m}^2$; the thermally induced stress for the fixed case requires re-estimation based on the redistribution caused by thermal buckling. It is assumed that the stress caused by the non-linear temperature is more closely approximated by the free boundary condition. The estimated stress caused by cap temperature differences is approximately $4.3 \times 10^6 \text{ N/m}^2$; this combined with the local stress gives a total of $7.7 \times 10^6 \text{ N/m}^2$ (1117 psi).

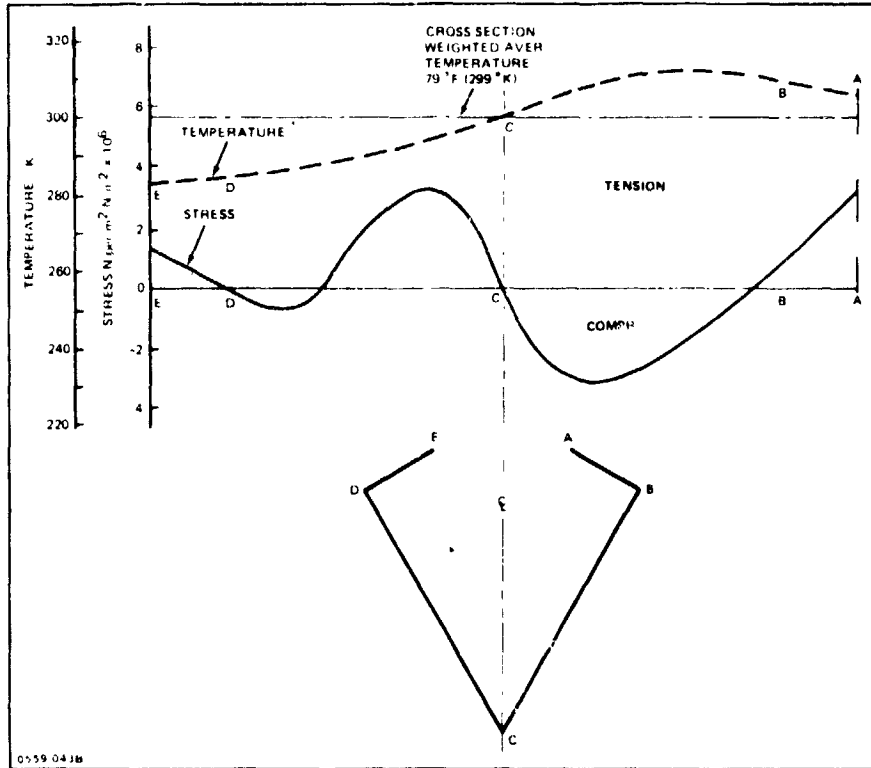


Fig. 2-35 Thermal Stress in 1-1/2-m Long Cap due to Gradient Unrestrained Boundaries

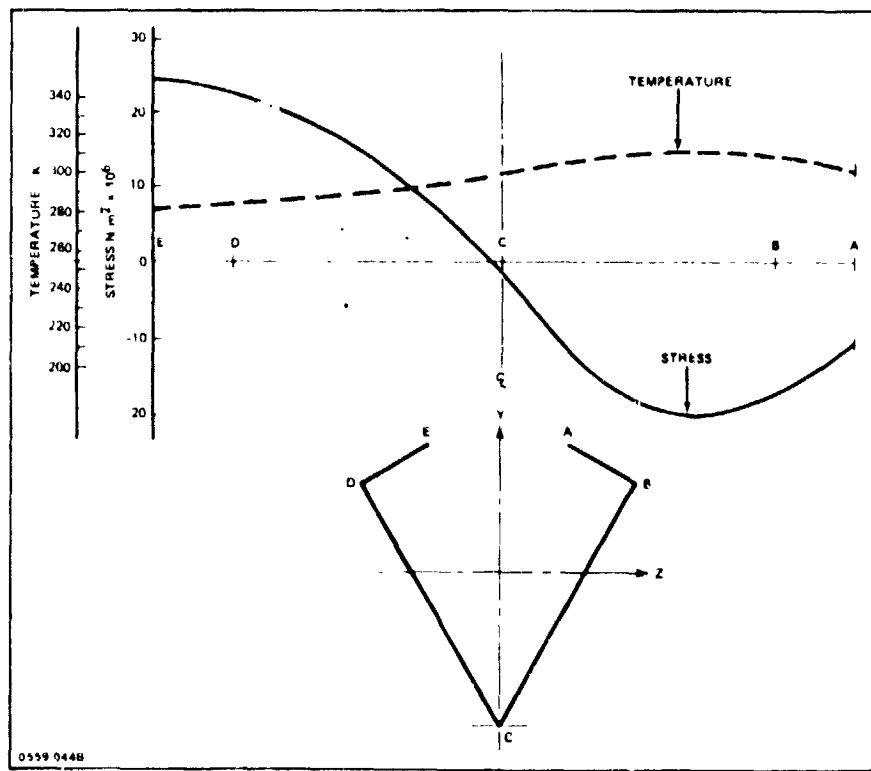
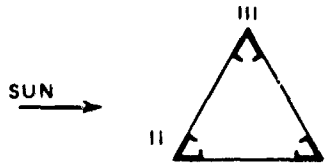


Fig. 2-36 Thermal Stress in 1-1/2-m Long Cap due to Gradient; Fully Restrained in Rotation about Y & Z Axis

A more accurate evaluation of thermal stresses induced in the very thin wall structural elements can be assessed by testing a two- or three-bay beam segment in a solar thermal vacuum test facility with proper instrumentation including thermocouples, strain gages, and deflection gages. The effect of local buckling caused by thermal loads can have significant effects on redistribution of member loads and on stiffnesses.

2.5.9 Deflection

Deflection of 1-m x 40-m beam due to thermal differential in caps is:



0559-0468

Differential: $\Delta T = T_{II} - T_I = 21 \text{ }^\circ\text{C} (37 \text{ }^\circ\text{F})$

Beam length: 40 m (1575 in.)

$$\alpha = 6.94 \times 10^{-6} / ^\circ\text{C} (12.5 \times 10^{-6} / ^\circ\text{F})$$

REPRODUCIBILITY OF THE ORIGINAL PAGE IS POOR

The temperature differentials and deflections (Fig. 2-37) are transitory inasmuch as they occur because of solar blockage of Cap I by Cap II during orbital motion; the total time of occlusion is approximately 1.6 min. In cases where temperature differentials due to solar blockage are a problem they may be alleviated by the use of lightening holes.

The other significant thermal deformation occurs during the satellite eclipse by the earth's shadow. The temperature excursion is in the order of 115 °F. This temperature change can result in a beam total maximum length change of approximately 0.055 m depending where in LEO the member is fabricated and integrated into the next assembly. The small length change can be corrected for by the design of a length adjustable attachment fitting at each end of the beam.

2.6 BEAM FAILURE MODES

The failure modes of a 1-m x 40-m beam analyzed in this section include the following:

- Cap section, 1.5 m long; critical segment is at center of 40-m beam where compression load is due to combined bending and axial force on 40-m beam
- Diagonal brace
- 40-m beam; load due to combined bending and axial load.

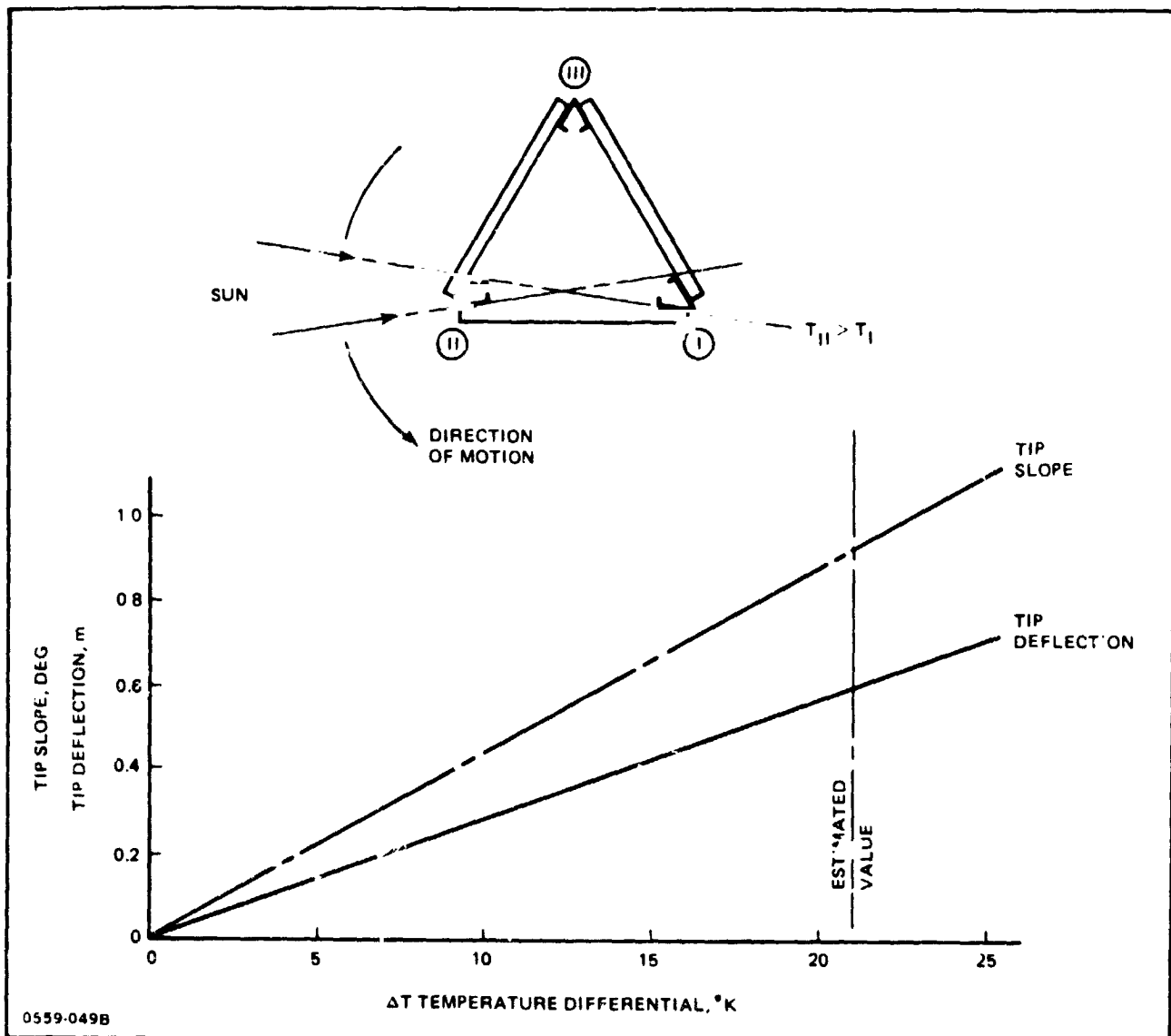


Fig. 2-37 Deflection & Slope versus Temperature Differential
(1-m x 40-m Beam)

2.6.1 Beam Cap

The open cap section shown in Fig. 2-21 evolved from early in-house studies on triangular cross section beams studied in various materials including metallics and composites. The design shown in the figure was finalized under study contract NAS8-31876 which was initiated in February 1976. The section is roll formed from 0.016-in. (0.041-cm) 2024-T3 bare aluminum alloy strip stock in the automatic beam builder. The ultimate design load is -115 lb (-1846 N) (Fig. 2-29). Torsion-flexure of the thin walled open cross section column supported at the battens is the primary failure mode based on analytic and test results and the degree of fixity in bending and torsion provided at the boundaries has a

significant effect on the load capability of the column. From data developed under this program and presented below, indications are that the support provided by the vee-hat section batten and diagonal induces a high level of end fixity in both torsion and bending; the effective column length appears to be one-half the batten spacing. Very early studies indicated that cross cable diagonal bracing and battens with very low torsional stiffness would not provide adequate support for the open cap section for the same batten spacing. The cable concept also presents quality assurance problems during automatic fabrication in preventing loss of cable attachment due to misalignment, etc.

Failure load prediction was approximated by modification of the techniques given by Timoshenko and Gere, "Theory of Elastic Stability" and Bieich, "Buckling Strength of Metal Structures." A method for an iterated solution was derived which accounted for local buckling and its impact in changing the section stiffnesses (Ref. 2-11).

The following critical loads were estimated:

- Torsion failure without buckling correction
- Torsion-flexure failure without buckling correction
- Torsion-flexure failure with buckling correction.

REPRODUCIBILITY OF THE
ORIGINAL PAGE IS POOR

The failure mode is predominantly torsion buckling of the column; there is a significant loss in strength caused by section stiffness reduction induced by buckling of the cap elements.

The purpose of these tests was to verify the capability of the cap to carry the design load as represented by beam bending and axial load; the critical section was at the center-line of the 40-m beam. The three compression tests of the beam specimens represent conservative simulations of the actual loading condition; for obvious reasons it was not feasible to conduct the full 40-m beam test in bending and compression. The tests, however, also provide data for a compression-only load condition on the beam in addition to verifying cap columnar stability with actual boundary conditions represented by the battens. Following is the list of the tests:

- Two 22-in. long cap specimens were tested in compression; the specimens failed at 770 lb (3425 N); failure mode was predominately local crippling because each specimen included a small segment of batten and diagonal. Test objective was to evaluate buckling across spotwelds, material 2024-T3 clad (Ref. 2-12)
- Two 48-in. long specimens were tested in compression machine. Specimens were made of clad 2024-T3 and had slight dimensional difference from final configuration. Test was part of in-house study. Failure load was 515 lb (2290 N) torsion-flexure mode (Ref. 2-13)

- Four 1.5-m caps tested in compression machine; sections were roll formed 2024-T3 and represented final configuration. Failure load was 507 lb (2255 N) for the two good quality specimens. Two roll formed specimens with initially rippled flanges due to forming were also tested. Their average failure load was 493 lb (2193 N) (Ref. 2-14)
- 4.5-m, 3-bay, beam tested in compression, sections were brake formed and beam hand assembled. Upper beam end was unrestrained in lateral directions and torsion. Failure load was 1260 lb (5604 N) or 420 lb (1868 N) per cap. Material clad 2024-T3 (Ref. 2-13)
- 6-m, 4-bay, beam tested in compression, sections were roll formed and beam was hand assembled. Beam ends were restrained in torsion. Failure load was 1507 lb (6703 N) or 502 lb (2234 N) per cap. Material 2024-T3 (Ref. 2-15)
- 6-m, 4-bay, beam tested as above. The beam was built entirely by the automatic beam builder; no manual operations were performed in fabrication. Several spotwelds between batten and cap separated just below limit load. In two such locations, small "C" clamps were attached and test proceeded to failure. Failing load was 1374 lb (6112 N) or 458 lb (2037 N) per cap. The failure was torsion buckling of cap apparently initiated by separation of several spotwelds due to local buckling of cap. Failure load was well above the cap ultimate design load of 1260 lb (5600 N) or 420 lb (1867 N) per caps (Ref. 2-15)

2.6.2 Diagonal Brace

Figure 2-38 presents the estimated critical compression load versus column length which was derived from the torsion buckling methods given in Timoshenko and Gere and Bleich. The curve is based on reduced stiffness properties caused by local cross sectional buckling and the axial load applied at the section centroid. The end fixity provided by the boundary conditions will require evaluation by test; it is assumed currently that the effective length is 1.5 m.

2.6.3 40-m Beam

The design condition for the 1-m x 40-m beam is a combined axial compression end load of 2558 N ultimate and a lateral distributed load of 1.69 N/m.

The beam was analyzed for overall compression stability using a finite-element model (Ref. 2-16); the influence of the simultaneously applied lateral loading was found to have a negligible effect on the buckling load. Figure 2-39 shows the unloaded model and the buckling modes for axial load only and axial load plus lateral load. The buckling load was

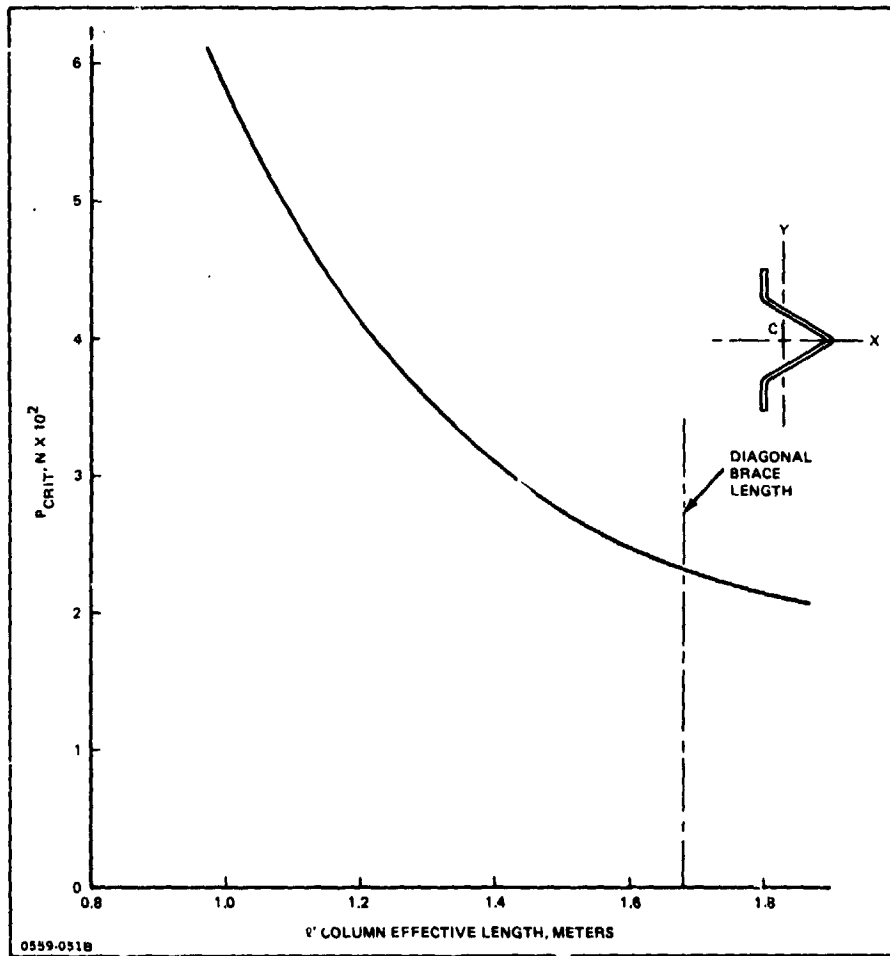


Fig. 2-38 Torsion-Flexure Buckling Load versus Effective Length of Diagonal Brace

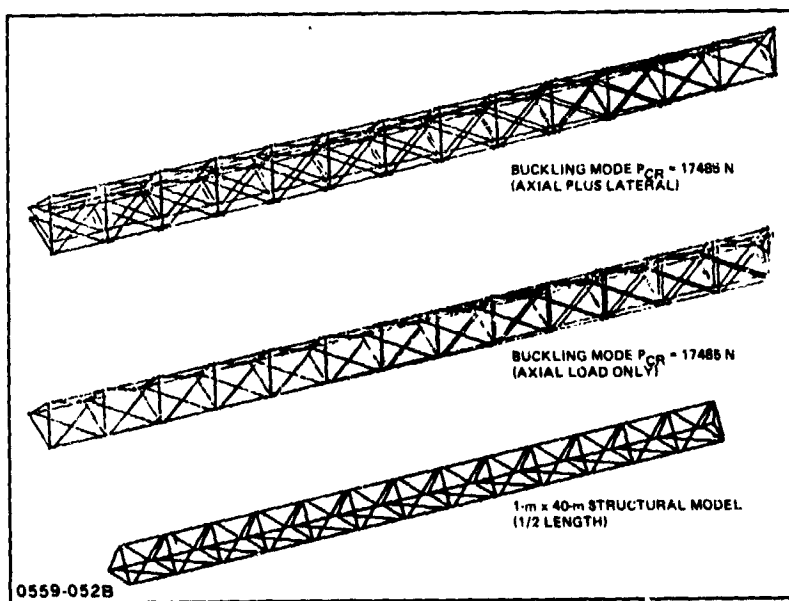


Fig. 2-39 Buckling Modes (1-m x 40-m Beam)

calculated to be 17485 N compared to an applied ultimate load of 2558 N.

Both this analysis and the results of the static finite-element analysis of the beam characteristics indicate an induced torsional deflection under axial load application caused by lateral force components in the diagonals. The static analysis of subsection 5.4 shows the induced rotation to be 0.009 radian for a limit axial compression load of 1829 N. The results of the static axial compression tests on the 6-m long beams show the measured reaction component forces in the plane of the beam cross section induced by loads in the diagonals to be 18 N (4 lb) for limit applied load. These three components produced an external end torque of 17.6 N·m (156 in.-lb). The effect of the end angular rotation did not appreciably reduce the failure load of the beam test Specimen (d) as shown in the figure summarizing critical load versus effective length. Specimen (d) had an upper end condition which was free to translate laterally and rotate about the beam major axis; no external support provision was provided. Based upon the data and tests carried out in developing the 1-m x 40-m beam within the conservative design envelop assumed for the SSPS missions, the basic requirements have been satisfied.

2.6.4 Combined Thermal & Mechanical Loading Conditions

- 1-m beam in orbiter - The mechanical load caused by the vernier RCS thruster firing is -25 N, the stress is -38 N/m^2 , Subsection 2.5.6 Thermal stress for the 180° sun angle is $-7.7 \times 10^6 \text{ N/m}^2$ (-1117 psi), Subsection 2.5.8. These stresses when combined are below allowable stresses based on test data
- 1-m beam SSPS mission -
 - Maximum mechanical loads
 - o Cap compression - 1846 N (415 lb), ultimate
 - o 1-m x 40-m Beam -2558 N axial, 1.69 N/m lateral, ultimate
 - Thermal

Thermal gradient within cap perimeter 13.6 °F (7.6 °K) for the 0° sun angle case.

2.6.5 References

- 2-1. "Space Fabrication Techniques," NASA Contract No. NAS8-31876, Report No. NSS-SF-RP004, Dec. 15, 1976.
- 2-2. "Payload Accommodations Document," NASA Report No. JSC 07700, Vol XIV.

- 2-3. "Solar Satellite Power Station (SSPS) Stationkeeping Thrust Duty Cycle and Thruster Analysis," Memo No. NSS-M0-76199, April 5, 1976.
- 2-4. "Space-Base Solar Power Conversion and Delivery Systems Study," Vol. II, Study for ECON Inc. under NASA Contract NAS8-31308, March 1977.
- 2-5. "Transient Temperature Response of SSPS Structure During Eclipse," 3 May 1976.
- 2-6. "Space Fabrication Demonstration System - 40M Beam Vibration Modes," Memo No. NSS-SF-M0019.
- 2-7. "Space Fabrication System - Forced Response of 40M Beam to RCS System Input," Memo No. NSS-SF-M0025.
- 2-8. "Preliminary Thermal Analysis of Large Space Structure," Memo No. HPM-77-026, May 11, 1977.
- 2-9. "Transient Thermal Analysis of Large Space Structure," Memo No. HPM-77-034, July 21, 1977.
- 2-10. "Preliminary Thermal Analysis of SSPS Structure," Memo No. HPM-77-040, July 28, 1977.
- 2-11. "Torsion Bending of Thin Wall Open Sections," Memo No. NSS-SF-M0017, Mar. 17, 1977.
- 2-12. "SFDS Reduced Quantity Attachment Spotwelds," Memo No. MP-AMPD-MO-78-15, Jan. 27, 1978.
- 2-13. "Space Fabrication Technique - Failing Tests of Truss and of Truss Cap Components," Memo No. SMETS-IOM 76/181.
- 2-14. "Compression Tests on ABB Cap Elements," Memo No. NSS-SFDS-M0043, June 26, 1978.
- 2-15. "Results of Compressive Failing Load Tests of Space Fabrication Technique Demonstration Basic Trusses (Hand Assembled and Beam Builder Assembled)," Report No. 380-48.11, Setp. 1, 1978.
- 2-16. "Overall Stability of Space Truss," Memo No. EG-STAN-77-059, July 21, 1977.

REPRODUCIBILITY OF THE
ORIGINAL PAGE IS NOT GUARANTEED

3 - SPACE FABRICATION DEMONSTRATION SYSTEM

The design, development and fabrication objectives throughout the program were to provide at minimum cost a fully operational ground Space Fabrication Demonstration System (SFDS) within the principal shuttle constraints, which would automatically produce the previously described 1-m beam (Fig. 3-1). The following general guidelines were used to achieve these objectives:

- Maximum use of off-the-shelf commercial hardware
- Application of high safety factors
- Modular equipment design.

Throughout the design and fabrication tasks, the primary approach has been to use existing state-of-the-art proven hardware and commercial expertise to minimize the costs and risks associated with constructing the beam builder.

The safety factors employed for special mechanisms and equipment were approached as in the design of ground operating equipment with little regard toward weight optimization. This was done to minimize analysis costs, expedite construction of the ground demonstration equipment, and place maximum emphasis on the functional aspects of the system. The modular design approach was employed for greater versatility in the system for future structural truss member configurations or modification to the machine.

3.1 OVERALL CONFIGURATION CHARACTERISTICS

3.1.1 General Arrangement

The demonstration machine (Fig. 1-2) has automatically manufactured the low-density aluminum beam structures of the configuration discussed in Section 2. The general arrangement layout for this equipment (Fig. 3-2) identifies the floor space, support equipment, and power services used in the program. The beam builder equipment can be broken into the following principal subsystems:

- Machine structure
- CAP member roll forming
- Brace member storage dispensing
- Beam cutoff

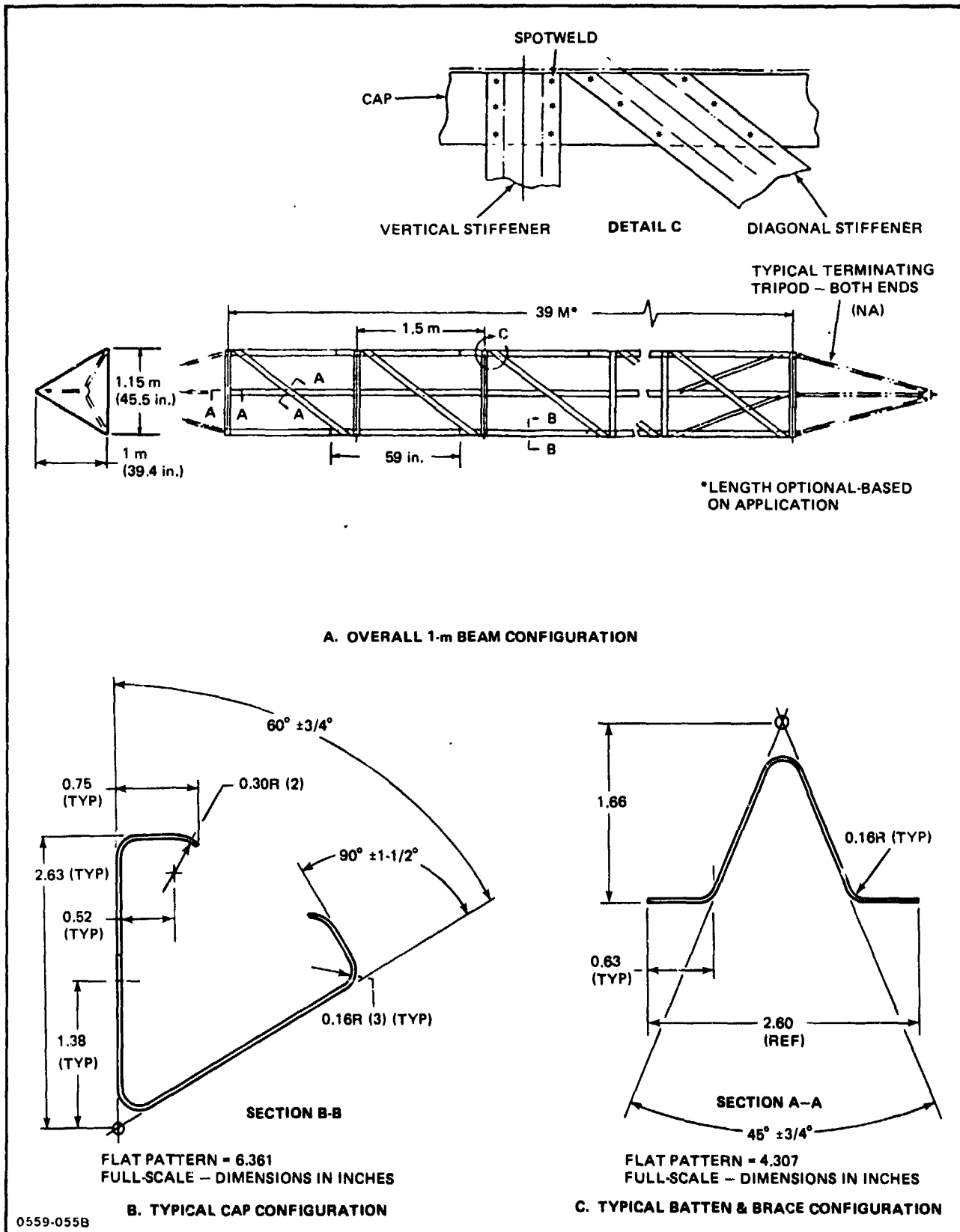


Fig. 3-1 1-m Beam Design Configuration

- Controls.

Each of these subsystems will be discussed in the subsequent subsections.

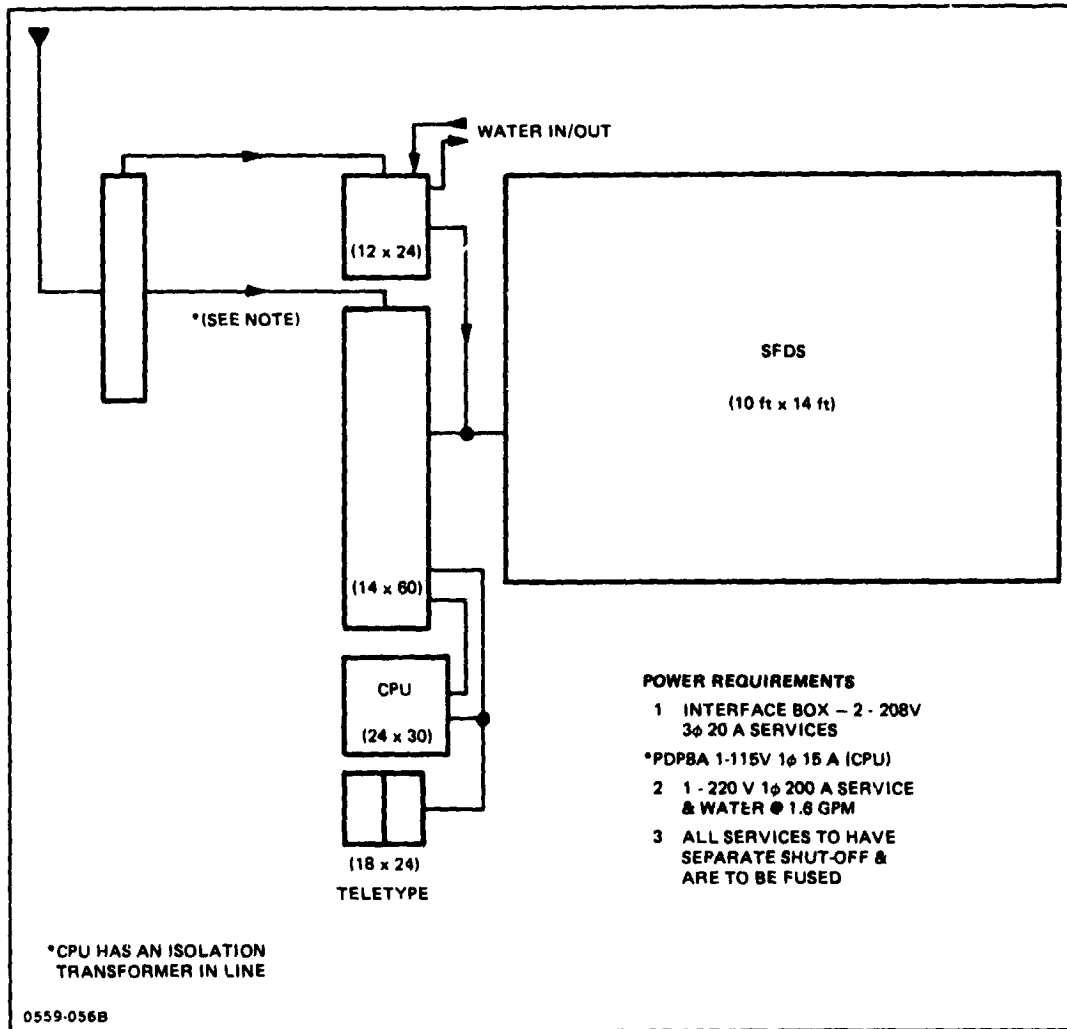


Fig. 3-2 Ground Demonstration Floor Plan & Facility Requirements

3.1.2 Operation

The machine produces a beam structure by performing the following basic sequence of operations:

- Coiled aluminum strip stock is fed to the roll forming mill to be formed into three continuous cap members for the beam
- The control system coordinates the speed and position of these members as they are projected from the rolling equipment to ensure overall beam straightness

- Transverse and diagonal brace members are prefabricated on earth, stored in magazines, and dispensed to the beam caps as required
- Resistance spotweld equipment is used to attach the brace members to the caps
- When the preprogrammed length of beam is achieved, a guillotine shear mechanism is activated to cutoff the three cap members.

3.1.3 Mass Distribution

The approximate weight distribution of these principal subsystems in the ground demonstration machine is illustrated in Fig. 3-3 with a detailed breakdown provided in Table 3-1.

3.1.4 Power Requirements

The estimated average power distribution for these principal subsystems in the ground demonstration machine is illustrated in Fig. 3-4.

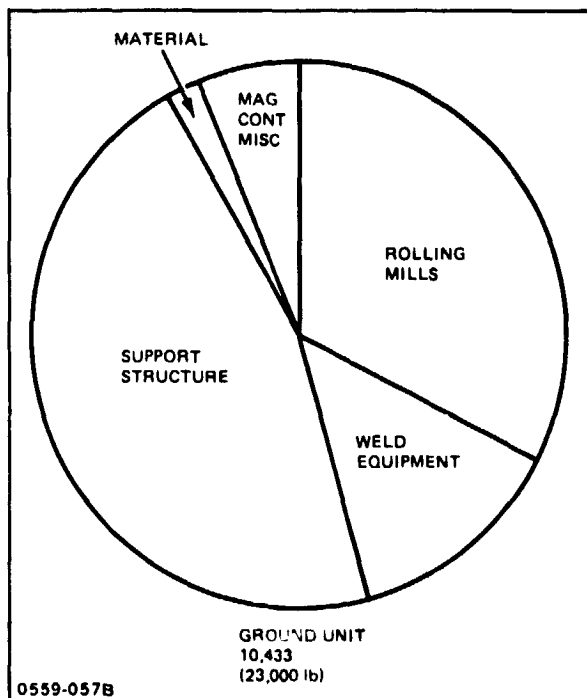


Fig. 3-3 Ground Demonstration System Weight Distribution

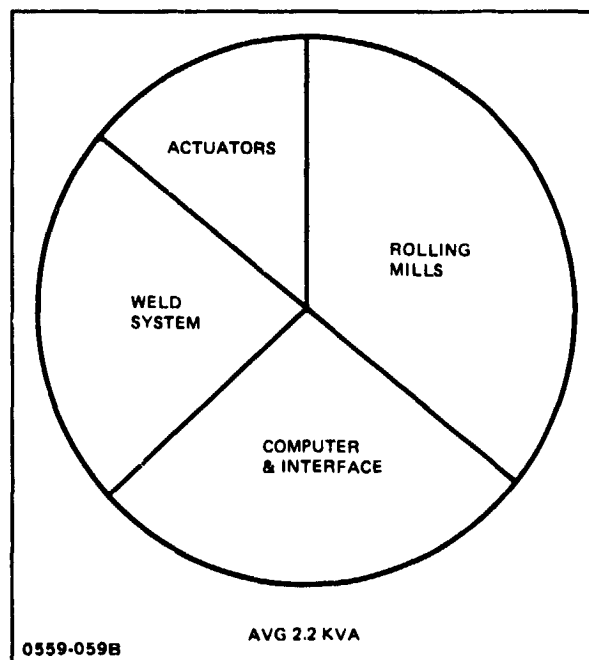


Fig. 3-4 Ground Demonstration System Estimated Average Power Requirements

Table 3-1 SFDS Estimated Weight Breakdown by Subsystem

Sub-System	Component	Drawing Number	Ground Test Article		
			Unit Wt (lb)	Qty	Total Wt (lb)
Roll Forming	Yoder Mill	AD-6911-1	1800	3	5400
	Mill Base Plate (Incl With Yoder)	2060	(512)	3	
	Drive Motor (Control Sys)	709	60	3	
	Gear Box (Sumitomo Co.)	HJ51A		3	
	Yoder Mill Drive Brackets	2112	51	3	
	Bushings	2138	1	3	
	Raw Material Spools	2085	211	3	
	Feed Spool Mechanisms	2136-1	129	3	
		-3	70	3	
	Encoder (Dynamics Research) Thru-Transmission Detector	29-21-804-200 1874-1		3 2	
				(6996)	
Magazine Dispenser	Vertical Cannister	2100-1	254	3	762
	Diagonal Cannister	2100-3	255	3	
	Supt Struct-Diag Magazine	2131	103	3	
				(1836)	
Weld Processor	Vertical Clamp Assy	2051	140	3	420
	Clamp-Aft Diag Brace	2103	83	3	
	Clamp-Fwd Diag Brace	2104	75	3	
	Carriage-Bracehandling	2102-1	39	6	
		-91	5	3	
	Transformer Mtg Brkts	2137	3	12	
	Transformers (Conrac)	T1671	240	6	
	Trans/Weld Head Cables		85	9	
				(2696)	
Truss Cutoff/Support Structure	Cutoff Upper Moveable Die	2107	77	3	231
	Cutoff Stationary Die	2108	9	3	
	Cutoff Lower Moveable Die	2109	53	3	
	Cutoff Assy	2181			
	Diagonals - Req'd Struct				
	Box Beam Weldment	2062	858	3	
	Box Beam Details	2071	8	3	
	Bulkhead 1	2063	1281	1	
	Bulkhead 2	2065	1568	1	
	Bulkhead 3	2067	1438	1	
	Brackets	2068	3	6	
	Brackets	2072	47	6	
	Internal Support Struct	2076	744	1	
	Installation Hardware	2070			
	Weldblock Int Supts	2069	31	3	
	Base Frame	2077	1962	1	
	Base Frame Brackets	2078	66	3	
				(10764)	
Orbiter Interface	Fittings				
	Truss + End Fittings				
Power & Controls	Computer Console				340
	Rack(s)				
	Weld Control Unit (Sciaky)				
	Inverters (Weld)				
	Inverters (Controls)				
	Batteries				
	Cabling				
				200	
				150	
				300	
				(990)	
Thermal	Thermal Control System				
Fit Instrument	Instrumentation Hardware				
Totals					23272
0559-0588					

3.2 MACHINE STRUCTURE

The ground demonstration machine structure is composed of three major assemblies:

- Base mounting stand
- External support structure
- Internal support structure.

3.2.1 Base Mounting Stand

The base mounting stand (Fig. 3-5) is a hot rolled steel weldment which is not actually a functional part of the machine. The stand provides a practical mounting platform for the external structure so the equipment can be operated in the horizontal position.

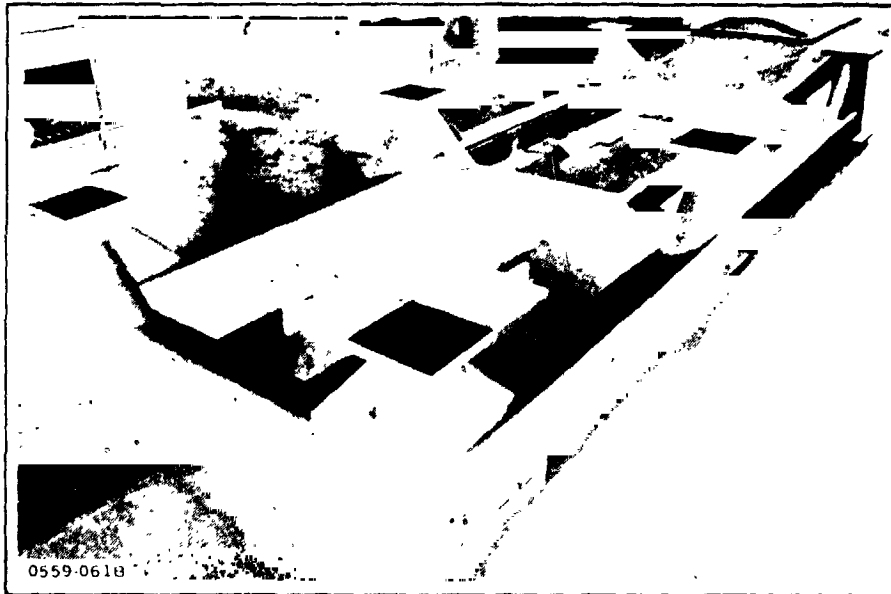


Fig. 3-5 Base Mounting Stand

3.2.2 External Support Structure

The external support structure (Fig. 3-6) is the principal equipment support frame and consists of three major 1-in. thick steel bulkheads. The bulkheads are attached by three pairs of 10-in. deep channels, 20 in. apart, located at 120° intervals. The channels are on a radius of approximately 40 in. and extend continuously from the aft bulkhead to the forward bulkhead through slots in the mid bulkhead. In the lower bay, the rolling mills are bolted to a 7/8-in. steel base plate which is bolted to the inner flanges of the channels. A closure plate welded to the outer flanges of the channels in the bay supports the lower transformers and the raw materials spools. Each roller base plate penetrates through the aft bulkhead and supports its feed spool system.

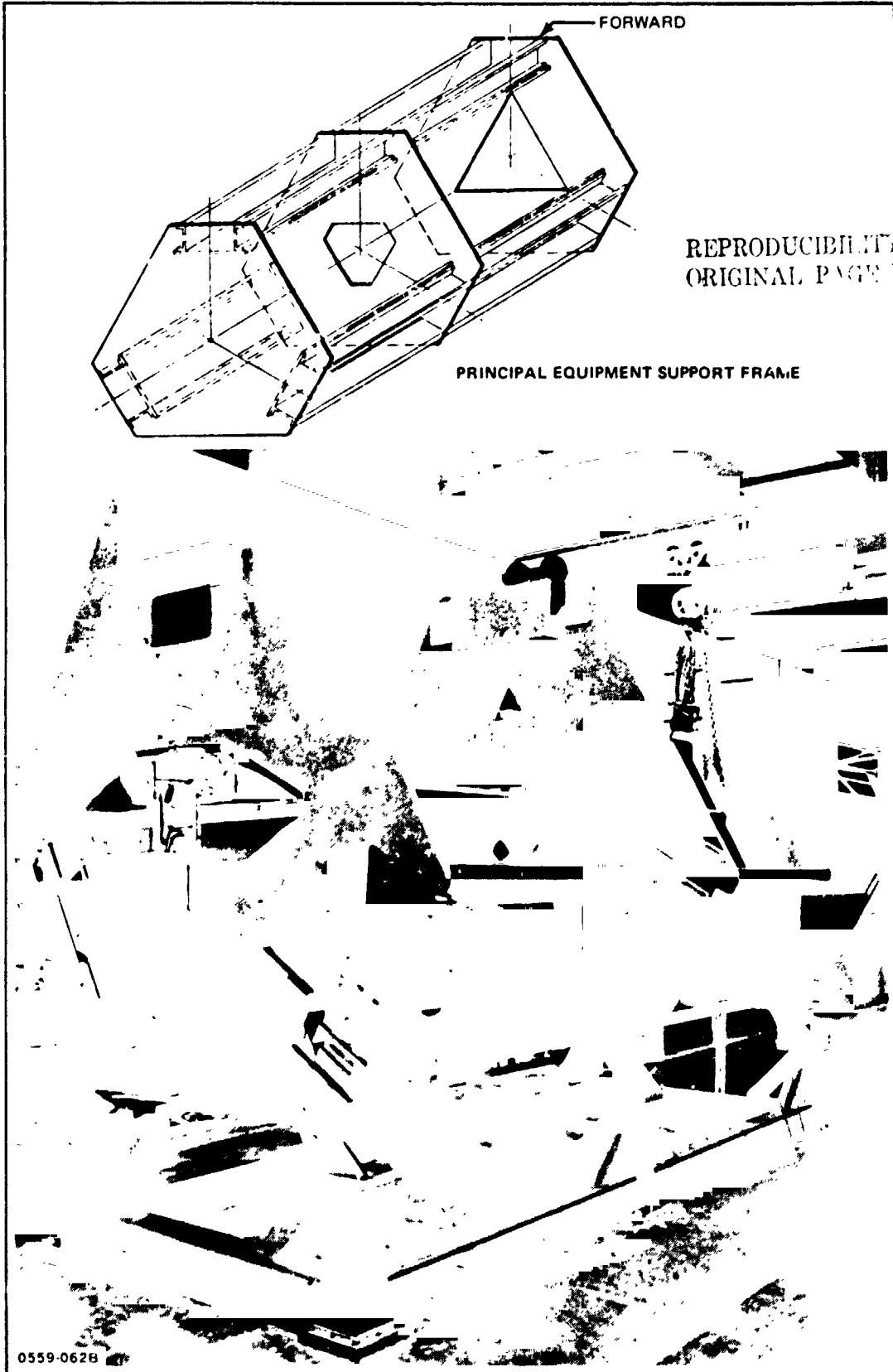


Fig. 3-6 Ground Demonstration Machine External Support Structure

Mounted to the mid-bulkhead are the vertical (batten) weld mechanism and the batten transfer mechanism (carriage). Also mounted to this bulkhead are the vertical (batten) magazine support fittings. Mounted on the forward bulkhead are the mobile portions of the guillotine and the aft diagonal weld mechanism, in addition to the upper ends of the diagonal magazine and carriage support beams.

The channels in the upper bay (between the mid and forward bulkheads) support the forward diagonal weld mechanisms, the upper transformers, and the lower ends of the diagonal magazine the carriage support beams.

3.2.3 Internal Support Structure

The internal support structure (Fig. 3-7) extends from the aft to the forward bulkheads along the SFDS centerline. This core structure weldment is mounted to the aft bulkhead and extends through a cutout in and is cantilevered from the mid-bulkhead. In the upper bay, it provides internal support for the weld subsystem anvils which also provide a guide for the formed caps. At the forward bulkhead, the internal support structure supports the plate to which are mounted the stationary portions of the guillotines.

3.3 CAP MEMBER ROLL FORMING SUBSYSTEM

The aluminum cap member roll forming subsystem (Fig. 3-8) consists of the following principal components:

- Feed roller and guides
- Roll form equipment.

3.3.1 Feed Roller & Guides

The spool storage assembly provides a capability to store up to 1000 ft of 0.016-in. (0.41-mm) thick aluminum flat stock. A spring loaded cam driven spool assembly permits easy loading of the slit coils of aluminum strip stock onto the storage spool. Several guide rollers are used to feed the material to the rolling mill strip guide table.

The guide table manufactured by the Yoder Company provides precise adjustment of the strip stock materials entrance position into the rolling mill. Proper alignment of this guide is critical to obtaining a properly formed cap configuration. Once the adjustment was properly made, the configuration remained stable and only required readjustment if the aluminum strip material width were changed.

3.3.2 Roll Form Tooling

The roll form tooling approach for the program was initially evaluated at Grumman on

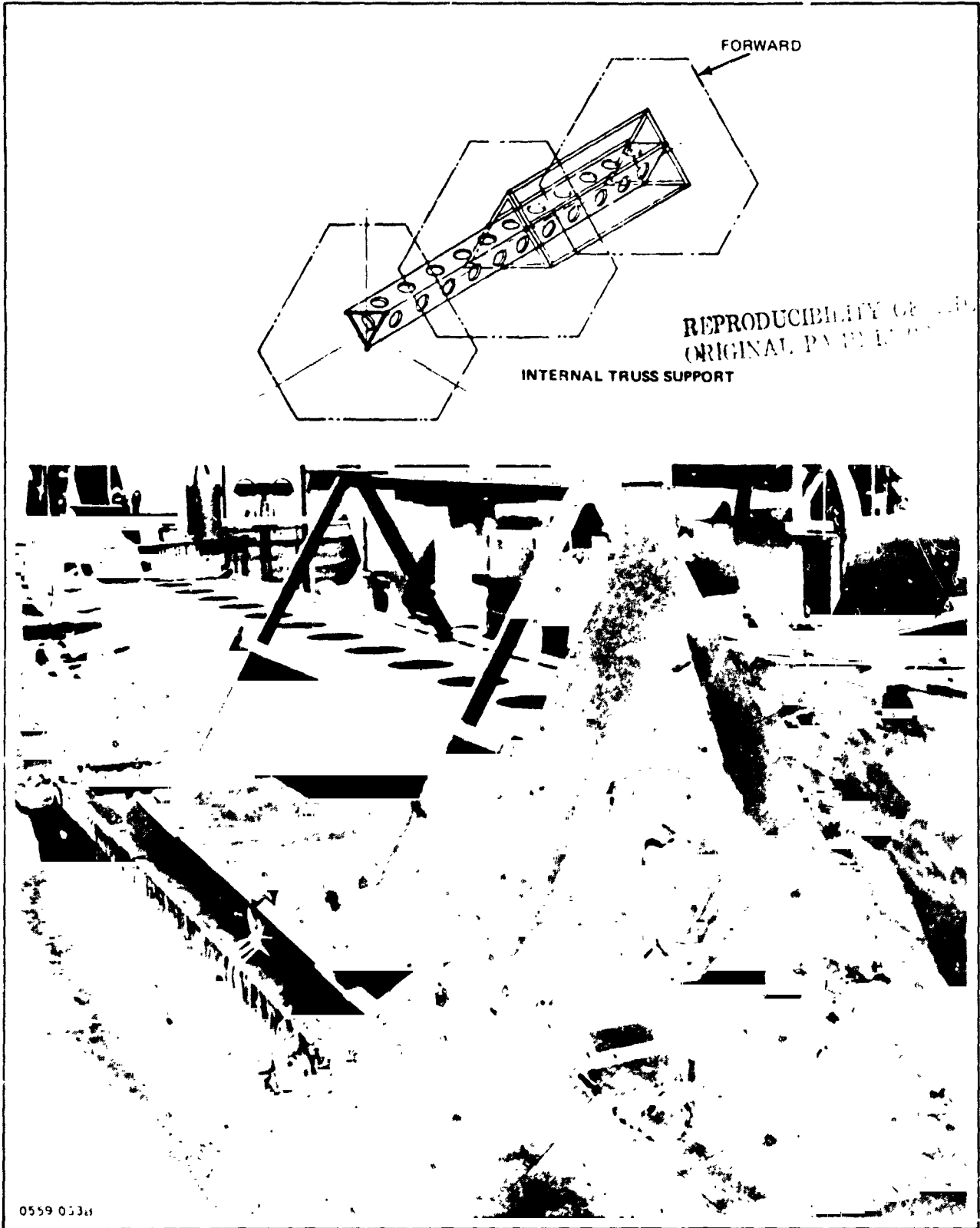


Fig. 3-7 Ground Demonstration Machine Internal Support Structure

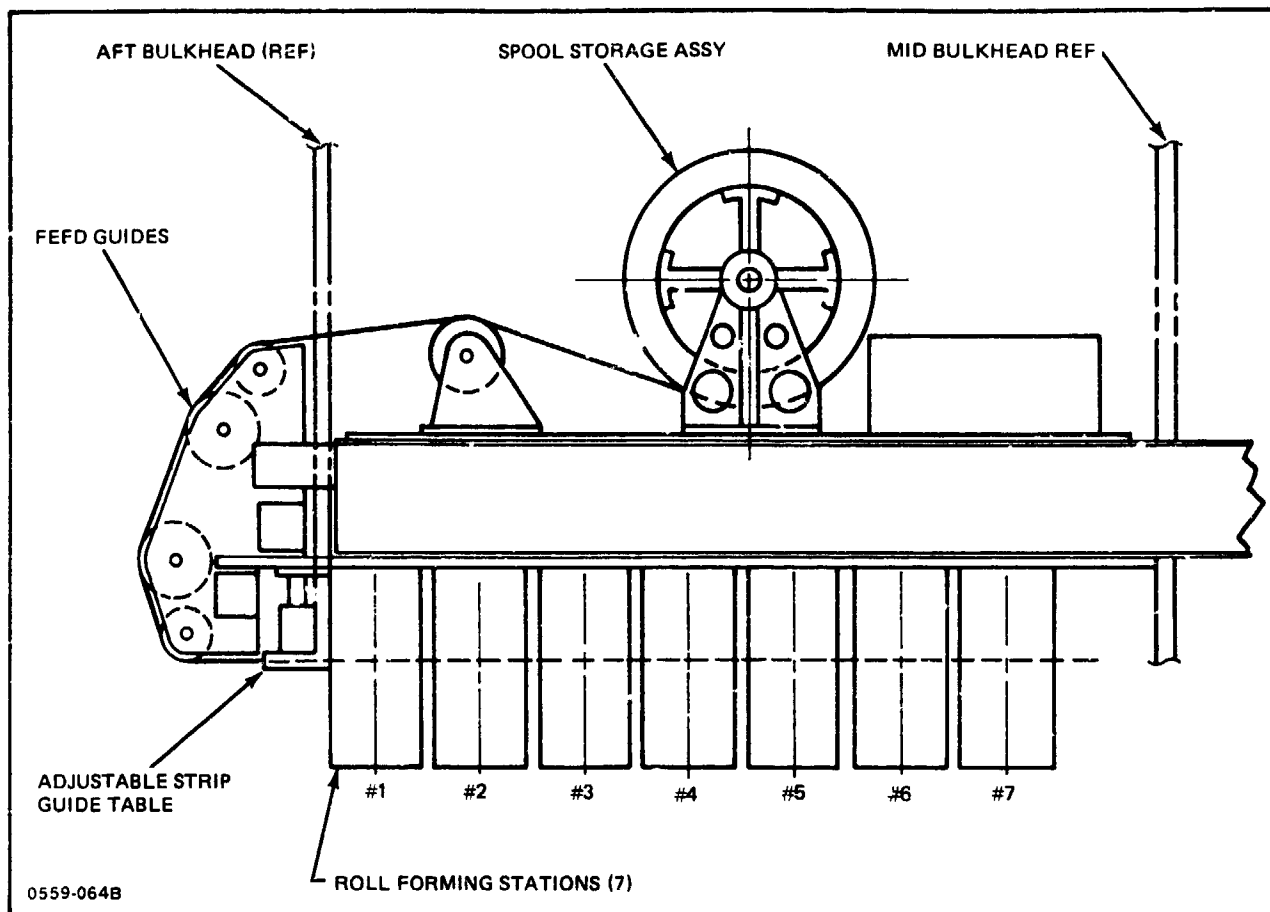


Fig. 3-8 Cap Roll Forming System

a production machine (Fig. 3-9) to establish the feasibility of producing a satisfactory cap configuration and establish preliminary equipment requirements.

3.3.2.1 Roller Configuration - As a result of the initial roll forming tests of the cap member, and a material change from 2219-T6 aluminum alloy to 2024-T3, the following roller modifications were made:

- Springback allowance changed from the 10° to 2° to accommodate material change
- Corner radii changed from 4t to 10t due to material change
- Roll stations changed from eight stations to seven stations at 9-1-1/4 in. centers to comply with machine/shuttle cargo bay configuration constraints.

The configuration of the rolls and the number of stations required was established after reviewing the initial roll form tests at Grumman with a die design specialist from the Yoder Company. Follow-up roll forming tests with the seven-station configuration

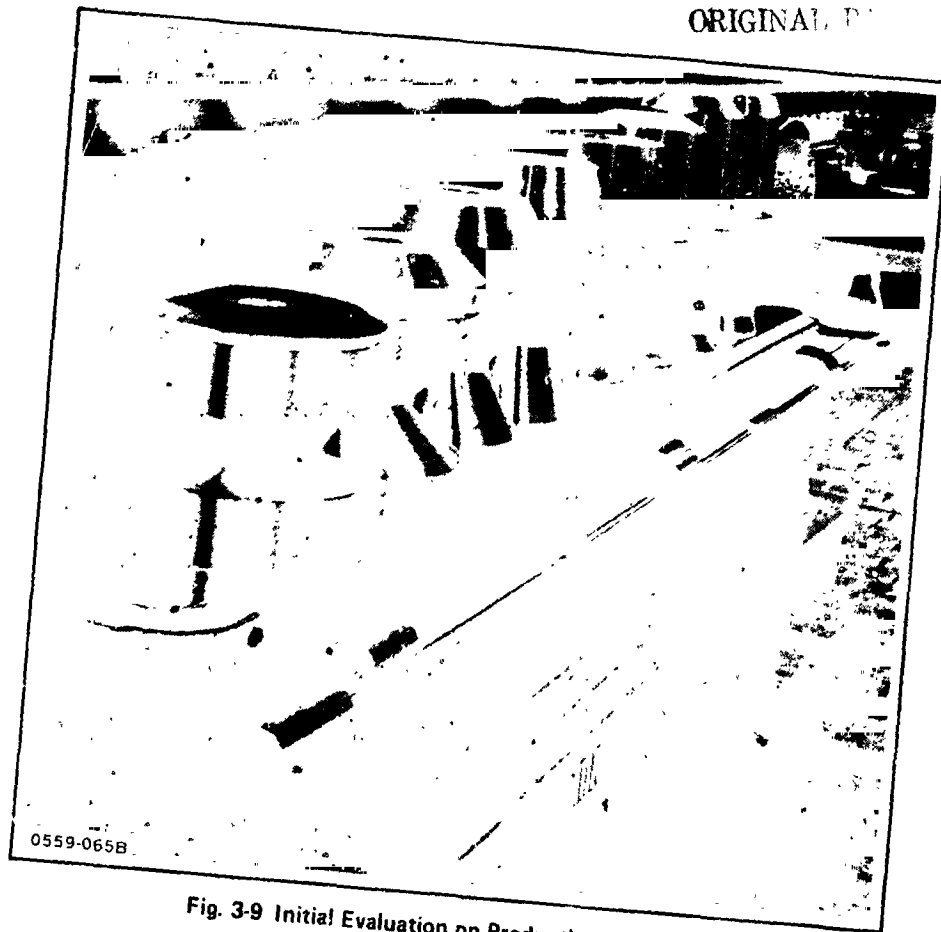


Fig. 3-9 Initial Evaluation on Production Equipment

(Fig. 3-10) were performed. This setup is compatible to the length constraints as defined in the configuration layout. Positive results were: seven-station configuration is acceptable, i.e., no bow, twist, nor flatness anomalies were apparent; and a good geometric configuration was obtained. The seven-step roll forming process is shown in Fig. 3-11. These tests also illustrated that bending of the flange angle must be distributed over five stations. A minor wave condition noted in the return flange was addressed by modifying two rolling stations to redistribute the workload of station five.

3.3.2.2 Cap Configuration Produced - The final cap configuration was modified to permit a modification the return flange of the cap (Fig. 3-12). The change was made as an aid in minimizing a ripple being formed in the flange.

The cap material is prepared for the roll forming operation by being slit on production slitting equipment to a 6.360-in. (16.154-cm) flat pattern width and recoiled. A rectangular index hole is then die punched into the strip at precisely one bay intervals 59.055-in. (1.5 m) (Fig. 3-13). This hole is used as a control point on the beam to assure proper synchronization of the three cap members. The actual control system is discussed in Subsection 3.7.

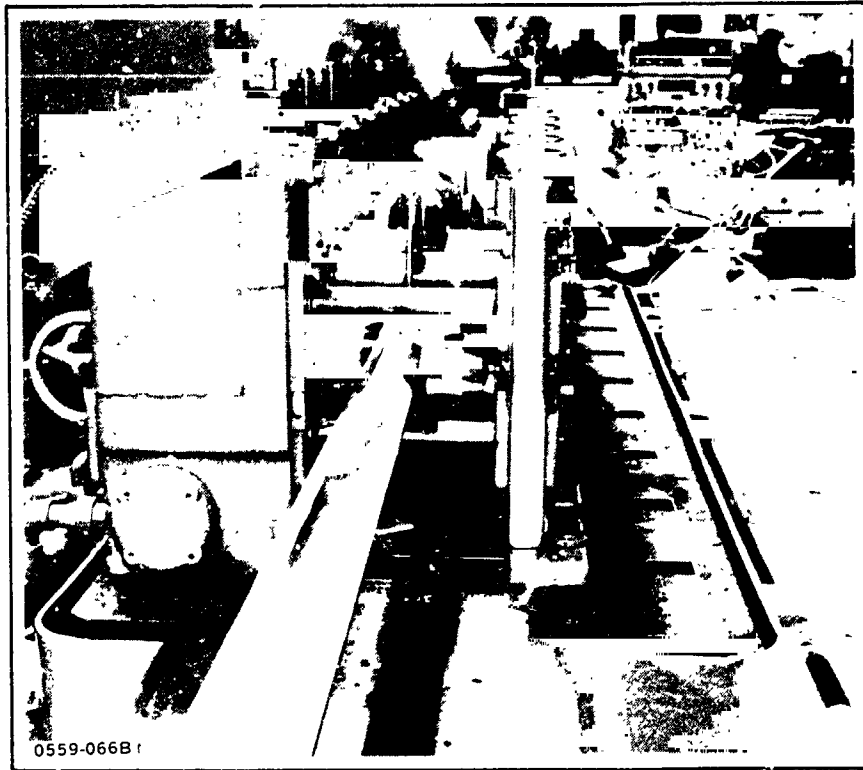


Fig. 3-10 Seven-Station Roll Form Tests

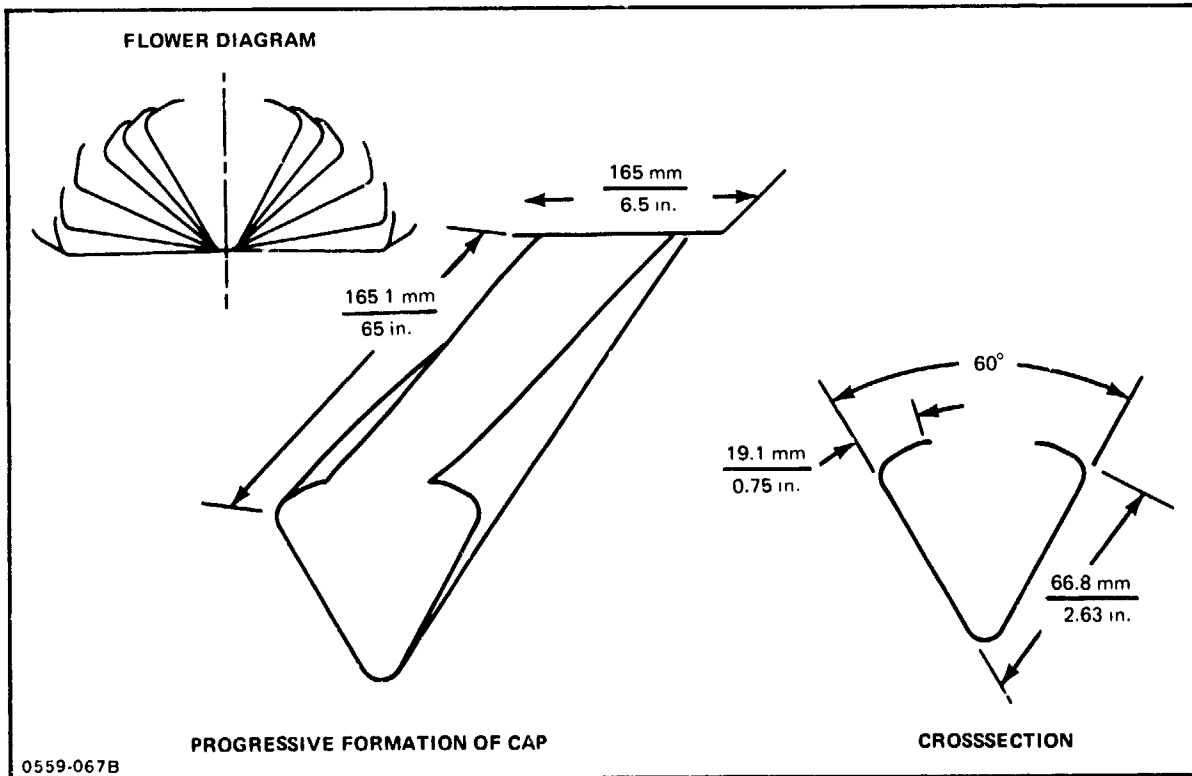


Fig. 3-11 Seven-Station Progressive Roll Form Steps

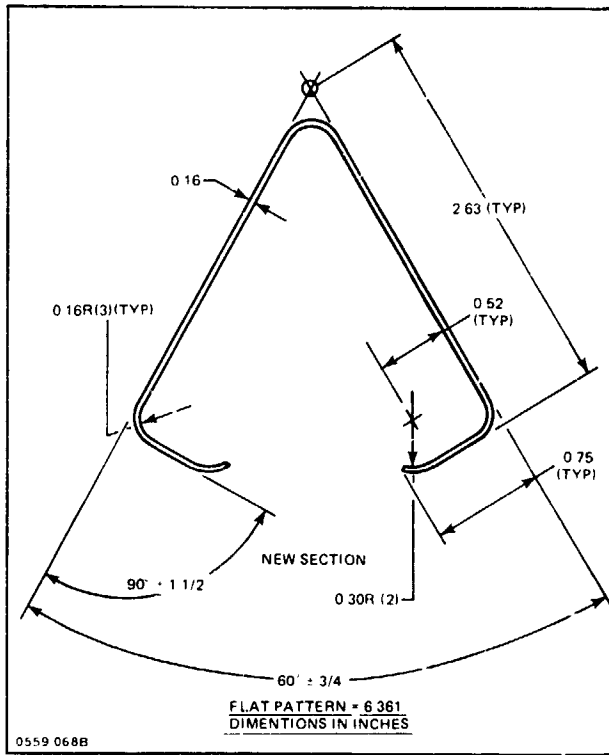


Fig. 3-12 Cap Configuration

REPRODUCIBILITY OF THE ORIGINAL PAGE IS POOR

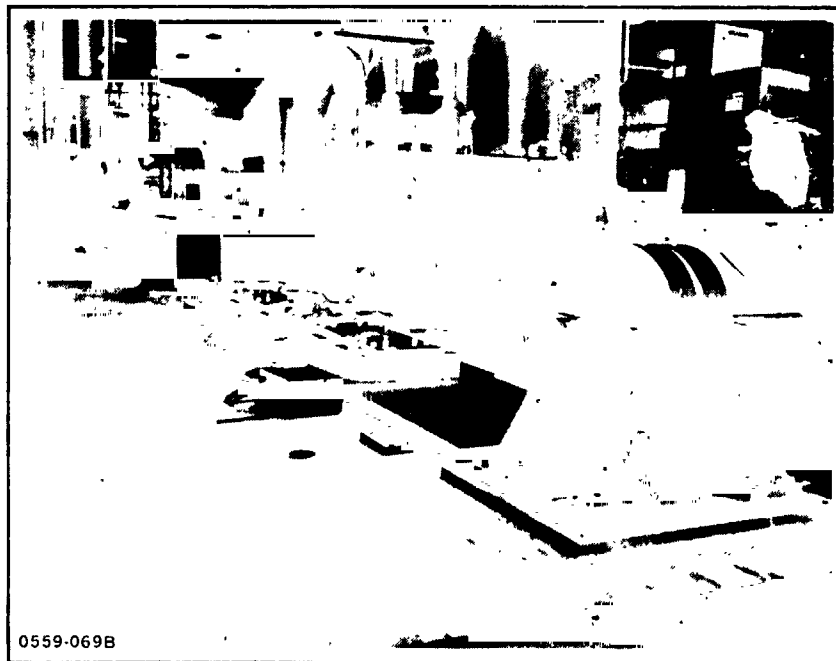


Fig. 3-13 Index Hole Blanking Setup

3.3.3 Roll Form Equipment

3.3.3.1 Equipment - The three rolling mills used in the beam builder were built by the Yoder Company. The "M" series equipment was selected for its roll drive gearing built into the inboard housing to reduce machine size and provide good drive control conditions (Fig. 3-14).

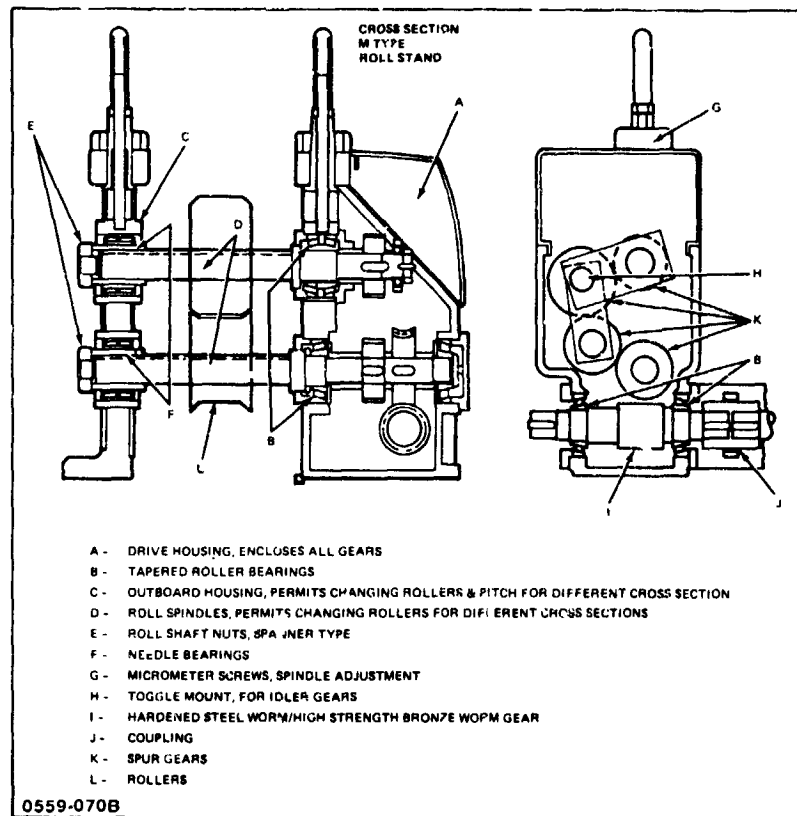


Fig. 3-14 Typical Rolling Mill Cross Section

The actual torque requirements to drive the rollings are as shown in Table 3-2. The servo motor drive system and position control is discussed in Paragraph 3.7.2.

Table 3-2 Rolling Drive Torque Values

MILL NO.	BREAKAWAY TORQUE* (in.-lb)	RUNNING TORQUE* (in.-lb)
1 (TOP)	140	120
2 (LEFT)	84	60
3 (RIGHT)	140	85
*WITH MATERIAL		
0559-071B		

3.3.3.2 Equipment Adjustments - As a result of the roll forming performed on the ground demonstration machine, the following roll adjustment settings were established to produce the desired cap configuration (Table 3-3).

Table 3-3 Rolling Mill Roll Adjustment Settings

ADJUSTMENT LOCATION	STATION NO. MICROMETER SCREW SETTING*						
	1	2	3	4	5	6	7
MILL NO. 401 INBOARD	5.390	6.013	5.990	6.024	5.990	6.002	6.100
OUTBOARD	5.990	6.013	5.990	6.026	5.990	6.038	6.097
MILL NO. 401A INBOARD	5.973	5.975	6.000	6.032	5.982	6.017	6.096
OUTBOARD	5.972	5.970	6.000	6.032	5.982	6.015	6.098
MILL NO. 401B INBOARD	6.014	5.975	6.003	5.995	5.981	5.994	6.073
OUTBOARD	6.015	5.982	6.003	5.991	5.980	5.997	6.075

*SEE "G", FIG. 3-14
0559-072B

The final drive configuration was modified as shown in Fig. 3-15 to eliminate localized section compression between stations no. 3 and 4.

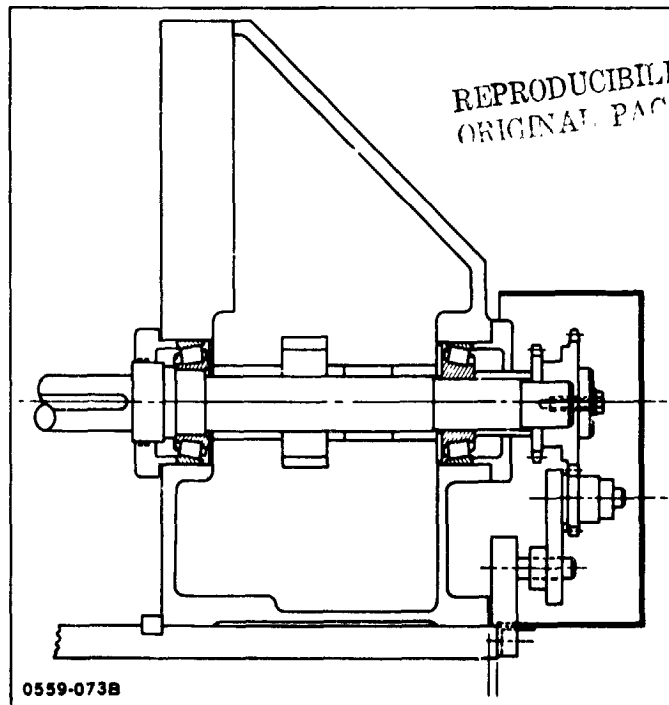


Fig. 3-15 Typical Section of Modified Mill Drive

The drive train for the Yoder machine normally consists of in-line worm gears for station. However, because of peculiarities related to the part shape and tool design, the material attempted to drive faster through the first three mill stations than the last four. Initially, the first three stations were disconnected (idled) so that the material would be kept in tension. This approach was successful for improving part quality. So that the machine would regain its self threading feature, a new drive ratio was experimentally determined. In the interest of schedule and economy, a chain and sprocket drive was selected using this developed drive ratio for station no. 1 through 3. These first three stations are now driven by station no. 4.

3.4 BRACE MEMBER STORAGE DISPENSING SUBSYSTEM

3.4.1 Brace Storage & Dispenser - Design Approach

The function of this subsystem is two-fold:

- Store the ground fabricated brace members
- Select a brace from the stored members and transport it into position on the caps.

In contrast to the continuous cap manufacturing approach discussed in the previous subsection, the relatively shorter brace members were prefabricated in a conventional production facility and stored in a magazine to be dispensed at the proper time. The prefabrication and magazine storage approach was selected for the following reasons:

- Part geometry lends itself to a high stacking density
- Part length is short enough to be stored and handled in a practical manner
- Part configuration and quality can be readily checked prior to use in space
- Members can be stored in their proper orientation relative to the truss structure minimizing the number of motions required for proper positioning
- Forming and cutoff machinery does not have to be included in the space fabrication facility.

The specific design approach selected for use in the beam builder incorporates the following principal features:

- Modular design
- Helix selector
- Separate brace transporter.

3.4.2 Equipment Design

The magazine design was determined after evaluating two approaches. The initial approach incorporated both the brace transport mechanism and magazine into one unit. A functional mockup of the unit was built (Fig. 3-16) and tested. The subsystem

operated in the following manner:

- The brace feed spring presses the stack of braces against a main stop shelf (MSS)
- To separate the first brace from the main stack of braces, a temporary stop shelf (TSS) is moved inward so a thin selector finger on the front can separate the first brace from the remainder while the main stop shelf is being retracted
- As the first brace is pushed away from the stack by the TSS, the MSS is brought into position and continues pushing the brace away from the stack to the brace transporter stop
- The transporter device rotates 90° to capture the edge of the brace at four points and moves the brace to the cap.

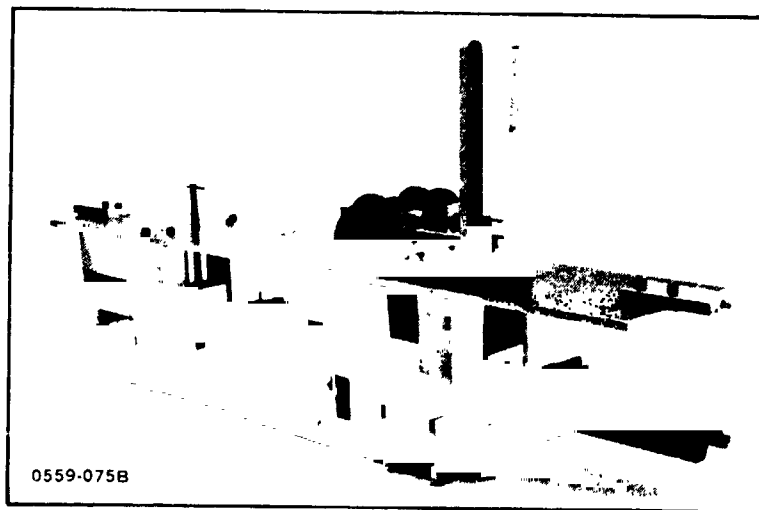


Fig. 3-16 Magazine/Dispensing Mechanism Fixture

REPRODUCTION OF THE
PAGE IS POOR

This approach was modified as a result of evaluation tests with the mockup and a need for a more compact modular unit which could be removed from the basic machine. The final design is shown in Fig. 3-17, and 3-18. It utilizes a helix selection for dispensing braces. The system operates in the following manner:

- The brace feed spring presses the stack of braces against the upper portion of four single-turn helixes
- The brace transporter gripper is rotated 90° to act as a stop for the next brace to be dispensed
- The helixes are rotated 360° with the leading edge of each helix acting as a selector which separates the first brace from the remainder of the stack by about 3/8-in. to the surface of the brace transport gripper mechanism

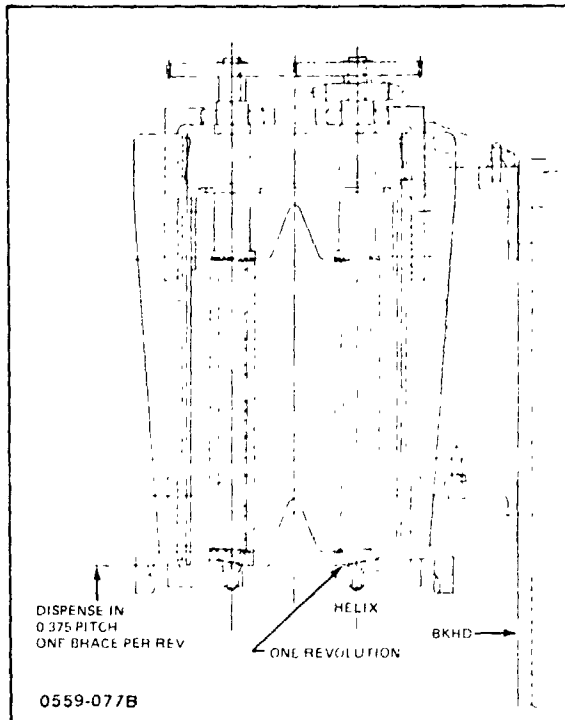


Fig. 3-17 Magazine & Helix Dispenser

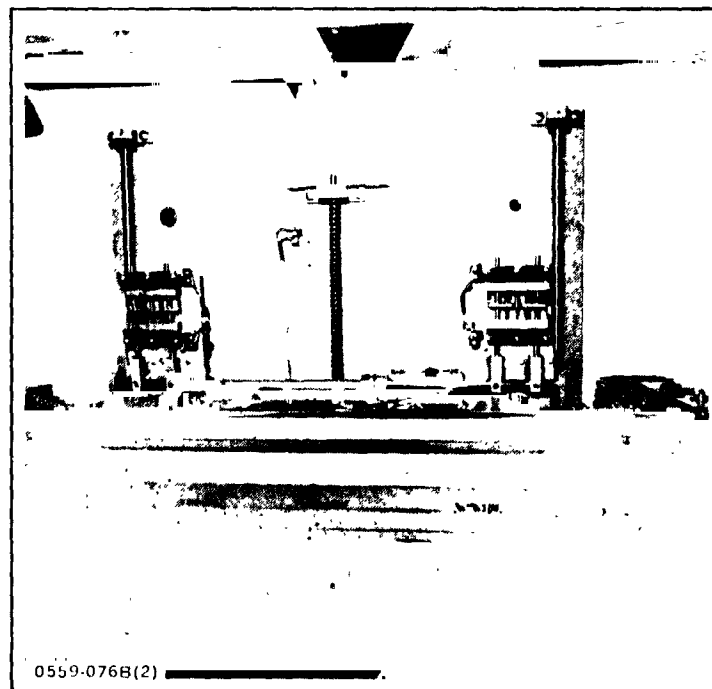


Fig. 3-18 Brace Transporter Carriage

- The gripper fingers are closed on the brace capturing the brace flange at four joints
- The transporter with the brace is driven by a ball screw so the brace is in contact with the cap members
- The brace is then clamped to the cap with a weld clamp mechanism described in Subsection 3.5
- The gripper fingers are retracted releasing the brace flange
- The gripper is rotated 90° so the mechanism will clear the brace and can be retracted to its park position.

The first two approaches provided restricted reliability in brace selection because of variations in the straightness and configuration of the thin 0.016-in. thick aluminum alloy parts. The latter approach with 0.063-in. thick crescent shaped spacers provided a reliable gap at the selection points with minimal dependence on part configuration.

3.4.3 Fabrication Method

The actual brace members were fabricated using a production rolling mill with the roll forming sequence shown in Fig. 3-19. Actual part cutoff was accomplished with the diagonal and vertical brace member shear cutoff dies.

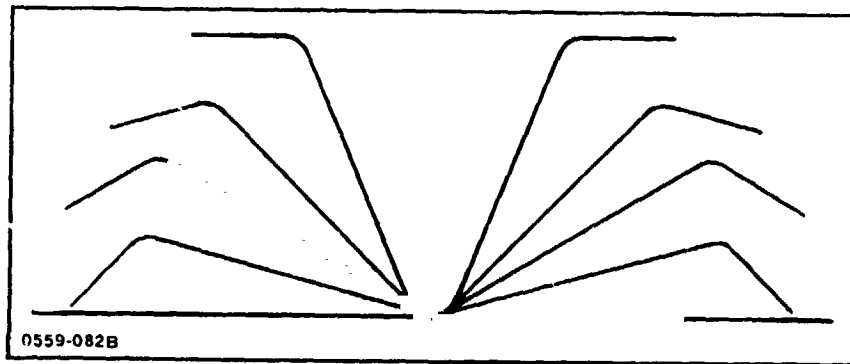


Fig. 3-19 Brace Roll Forming Sequence

3.5 BRACE CLAMPUP & ATTACHMENT SUBSYSTEM

3.5.1 Design Approach

This subsystem (Fig. 3-20) was designed and built to perform two primary functions:

- Clamp the brace members to the cap members with sufficient force to offset weld electrode clamp forces
- Resistance spotweld the brace members to the caps.

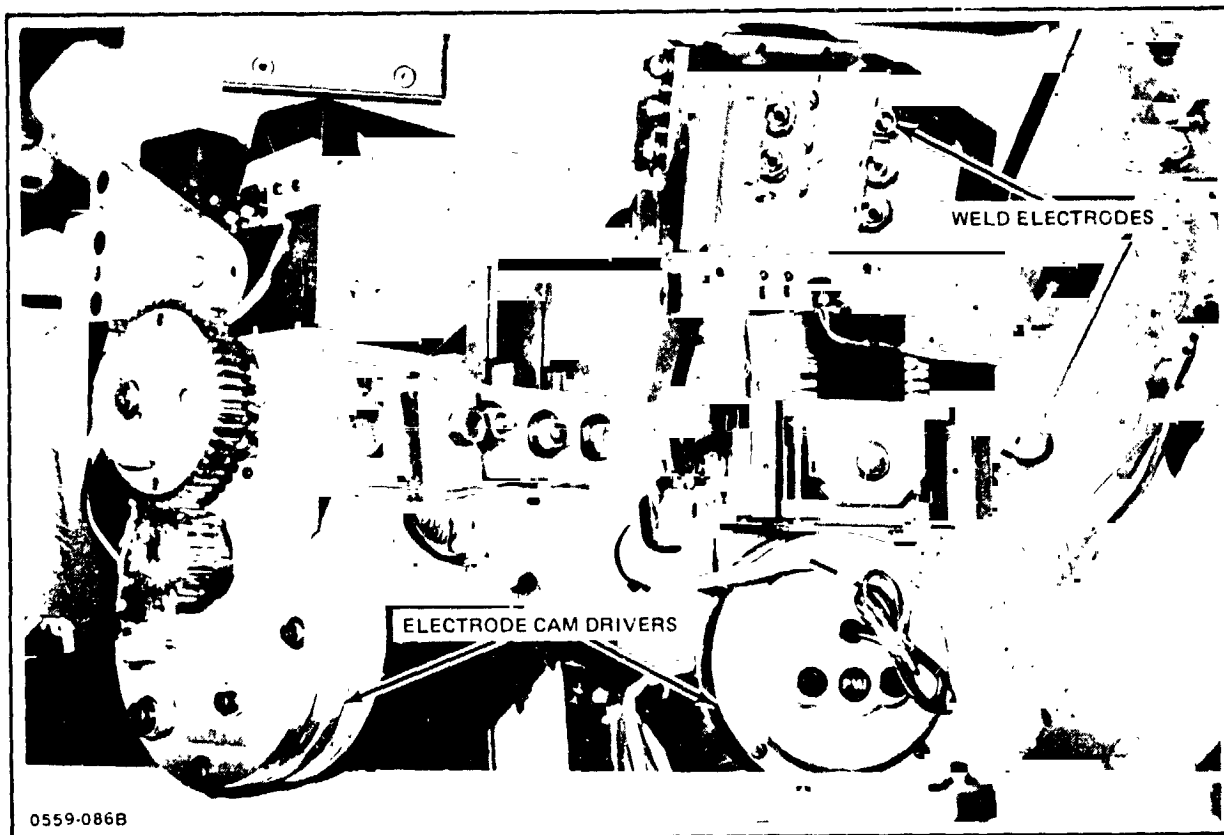


Fig. 3-20 Brace Clampup Attachment Subsystem

These functions are accomplished through the integration of the following principal devices: a mechanical scissor clamp mechanism, cam actuated weld electrodes, and a resistance spotwelding system. After evaluating several alternatives, discussed later in this subsection, the following approach was used:

- Once the brace members have been transported from the magazine, brace dispenser to the cap, a clamp mechanism is advanced to a fixed position
- A scissor mechanism driven by a ball screw is used to apply the clamping force through a pair of polyurethane plastic blocks to the brace and cap. An internal copper guide block prevents collapse of the cap member during clampup
- After the three vertical or diagonal brace members are clamped, a cam mechanism (Fig. 3-21) is actuated to permit individual pairs of spring loaded weld electrodes to be driven into the brace member
- A limit switch is used to confirm the proper cam position and resulting pair of electrodes permitted to be in contact with the brace. The confirmation signal is sent to the computer which directs the firing of the spotweld system.

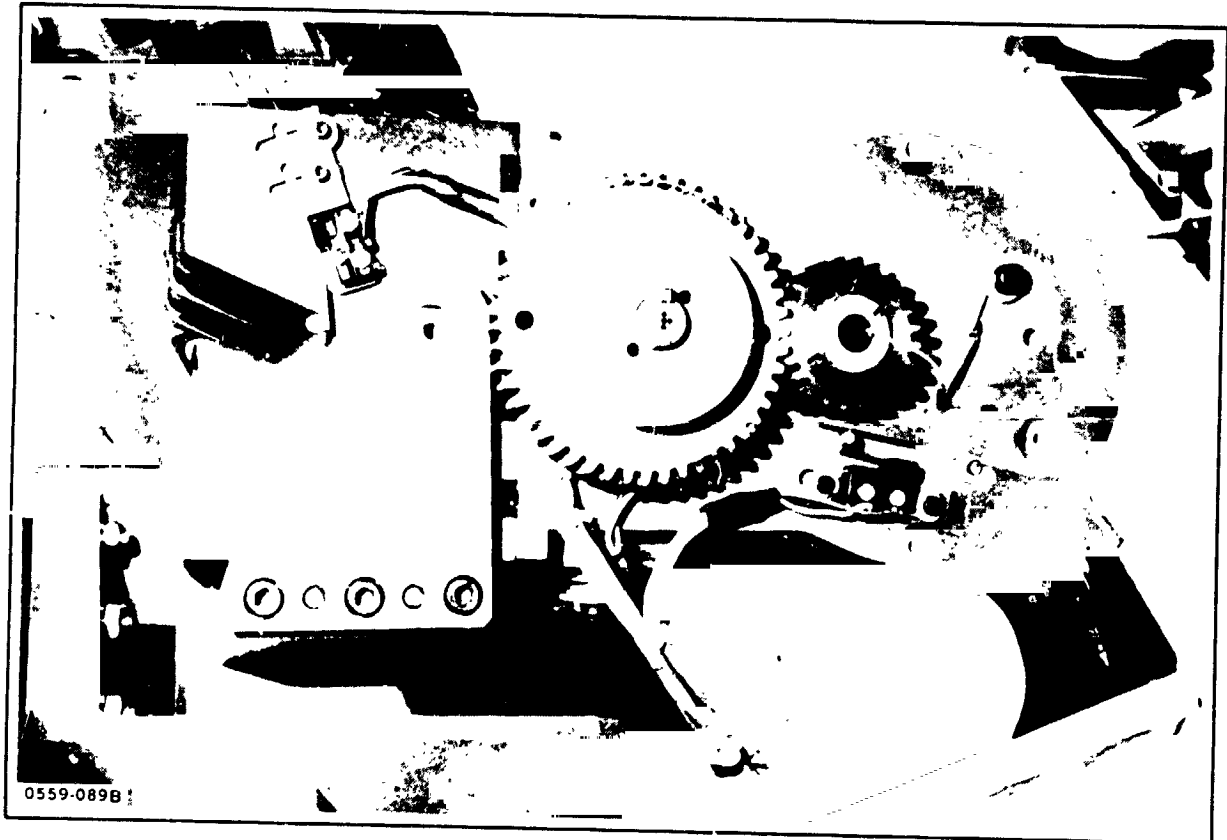


Fig. 3-21 Wild Electrode Cam Mechanism

The one pair of electrodes in contact provide the only complete circuit (Fig. 3-22) through the brace and cap, with the copper guide bar acting as a shunt from one spot to the other

- As each pair of welds are produced, the cam is cycled introducing the next pair of electrodes into the circuit until all electrodes have been fired
- The clamp mechanism scissor is opened and the entire mechanism retracted clear of the cap so the next brace can be advanced into position.

Resistance spotwelding was selected as the attachment technique on the ground demonstration system for the following reasons:

- Process is a common commercially available approach to attaching thin gage metal components
- Considerable experience has been accumulated in aerospace industry using this process
- Process has a fast cycle time

REPRODUCIBILITY OF THE
ORIGINAL PAGE IS POOR

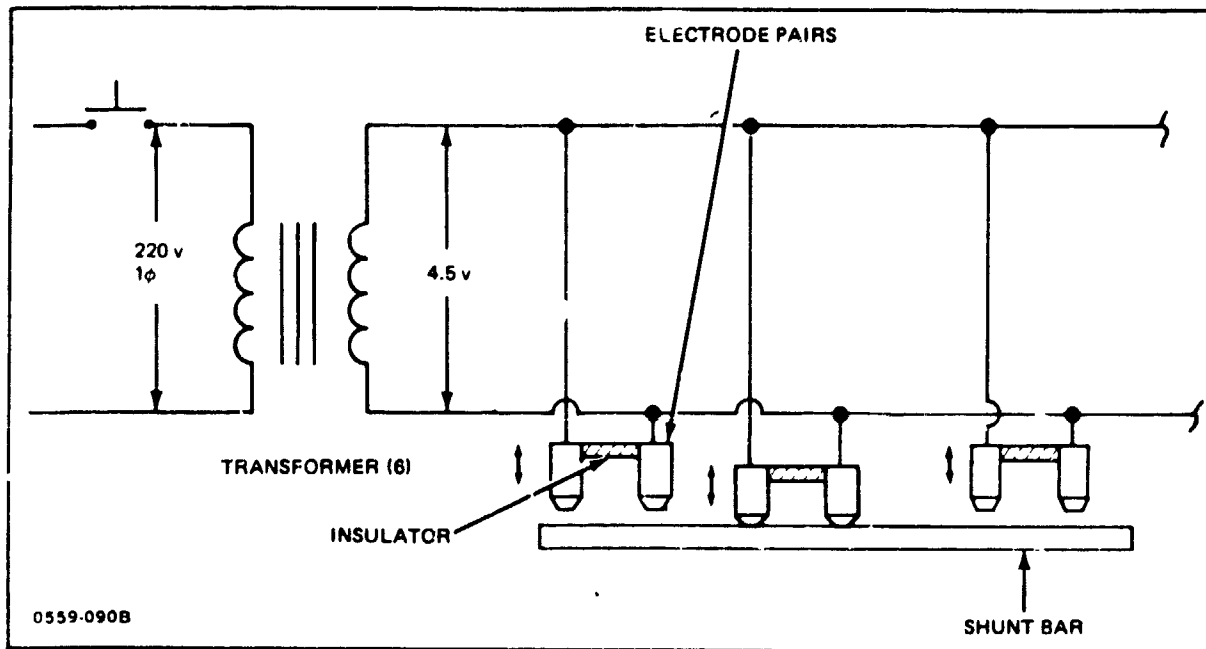


Fig. 3-22 Welding Process Schematic

- Process does not have any obvious space environment deterrents, such as material vaporization
- Electrodes are small and compatible with automated mechanisms.

3.5.2 Welding Equipment

The equipment used was a Selaky single direct energy system with SCR contactors with six 220-v input 63 KVA transformers with an output rating of 4.5 v, 14,000 A. Six 63 KVA transformers were used instead of one 75 KVA unit to reduce the electrical losses in the power cables to the weld electrodes.

The six transformers were positioned on the machine as close as practicable to the brace attachment points on the beam being produced. An alternate energy source was considered in the initial system evaluation. Various capacitor discharge systems were considered. In order to weld two spots in a series weld configuration, a capacitor discharge system would cost 4 to 10 times the cost of the planned unit and the recycle time would be 15 to 30 sec. This was considered too costly and too slow for the ground demonstration system.

Three types of resistance welding were considered: normal, indirect, and series. All three require application of pressure for less than 1 sec prior to the discharge of welding current. Normal resistance welding uses electrodes on both sides of the two

sheets of aluminum. The electrodes press against each other through the weld. Indirect resistance welding permits one of the electrodes to be at a distance from the spot weld. Both normal and indirect resistance welding produce a single spotweld from one current discharge between two electrodes. The selected approach is to use series resistance welding, which produces two spotwelds using two electrodes and a single discharge of welding current. The two electrodes are the hot lead and ground of the same open circuit. When they are properly separated and compress both thicknesses of aluminum (from the outside against a rigid conducting block within a cap member), most welding current flows from one electrode through a brace and into a cap member (forming a spot between cap member and brace). This current then flows through the conducting block and exits into the cap member and brace under the other electrode (forming a second spot), and completes the closed circuit path by leaving the brace and entering the second electrode. The spots are formed at the aluminum/aluminum interfaces rather than the copper/aluminum interfaces because contact resistance is much higher at the former.

As part of the initial weld tests, both static and fatigue tests were run on sample coupons for the 300-lb weld clamp conditions used in the ground demonstrator. These results are discussed in Section 4.

Ultrasonic welding was considered as an alternate approach (see Paragraph 4.1.1). This system had the advantage of requiring less power, but, due to accessibility problems, multiple heads with modified anvils would be required. Such a change would increase the equipment cost significantly over that for resistance welding.

Tests were conducted to determine the anticipated time between cleaning or replacement of electrodes. All tests were conducted using series welding at a spring loaded electrode force of 300-lb (1334 N). Weld time was 0.017 sec at a level of approximately 10,000 A. Electrodes were RWMA Class I with a 3/16-in. diameter x 4-in. spherical radius face. The backup shunt was RWMA Class 2. Over 200 firings were made before the electrodes stuck to the work pieces. The test was terminated at this point and the results considered acceptable. Weld strength averaged 126 lb (560 N) with no welds below the minimum required 75 lb. The electrodes could easily have been abrasively cleaned and rinsed because pitting and aluminum pickup were less than 0.005-in. in depth. The backup bar showed no signs of pitting or excessive pickup.

3.5.2.1 Weld Pattern - During the preliminary design of the ground demonstration equipment, a choice between a six-weld or eight-weld pattern was required to determine final mechanism design. The four-weld pattern would require an extra movement because four electrodes with their springs would not fit in the attachment space required,

and the pattern would have been attained with two firings of the same set of electrodes per joint. A pattern of six electrodes could be spaced so that a single firing position would provide the necessary attachment pattern. In order to check the structural integrity of the six-spotweld configuration, six and eight spotwelded components were fabricated from 0.016-in. thick, 2024-T3 clad material and tested. These tests are described in Section 4. Based upon the test results, the six-spot, 1.375-in. spacing weld configuration was selected.

3.6 BEAM CUTOFF

The output beam is cut to length using the truss cutoff mechanism shown in Fig. 3-23. This device is comprised of a screw-driven guillotine and a lower die which has both an internal support mandrel and a retractable die section. The truss cutoff utilizes a double shear approach to severing the beam cap member. A slit of 0.170-in. wide cap material is removed during the shearing operation; therefore, neither the fabricated beam nor the formed cap have to be displaced. The excess material is captured in a cavity in the lower die. In addition to imparting no relative motion to the cap and beam, the principal advantages of this approach are absence of extraneous particles and a clean cut.

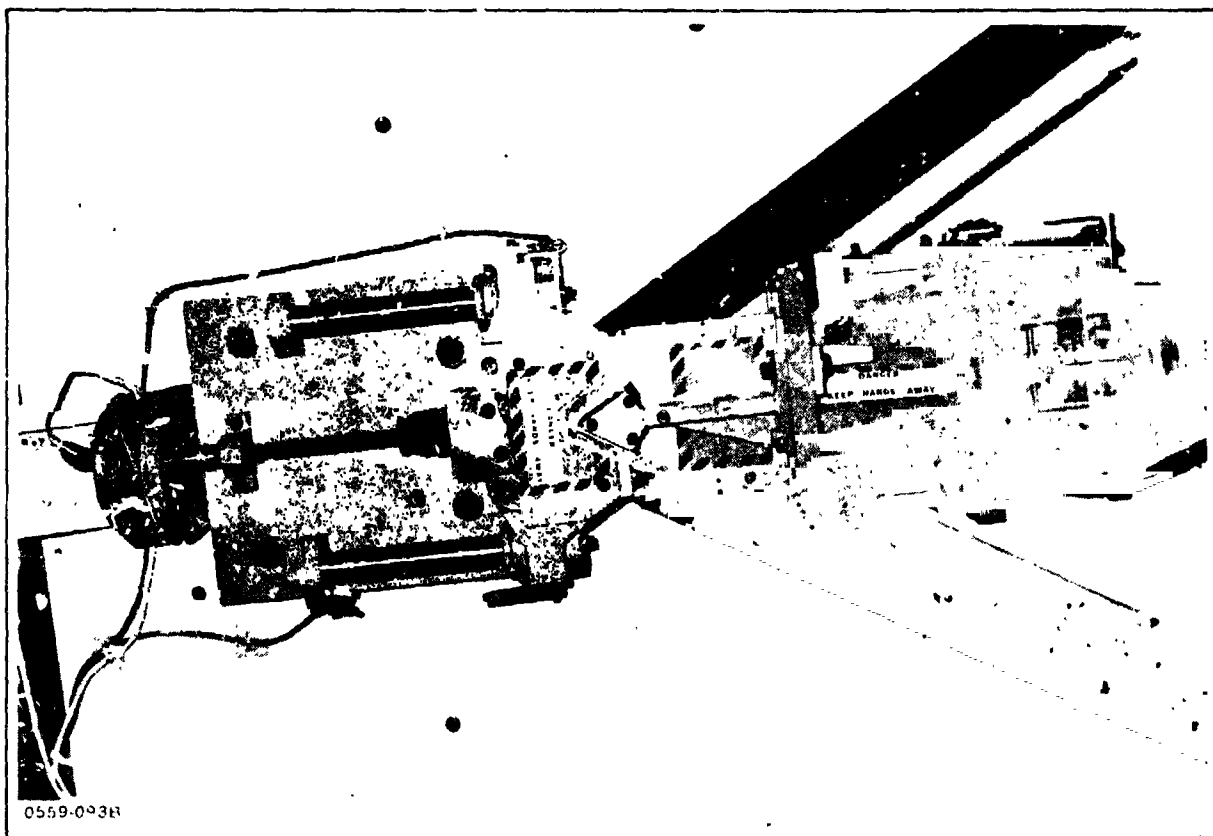


Fig. 3-23 Shear Assembly

3.7 CONTROLS

The control system for the Space Fabrication Demonstration System is responsible for overall automatic control of beam fabrication (Fig. 3-24). As such, it drives each of the three rolling mills in closely synchronized fashion to ensure that the three associated cap sections are formed at the same rate and have the same length. In addition, the control system directs the sequence for the assembly/fastening cycle which consists of

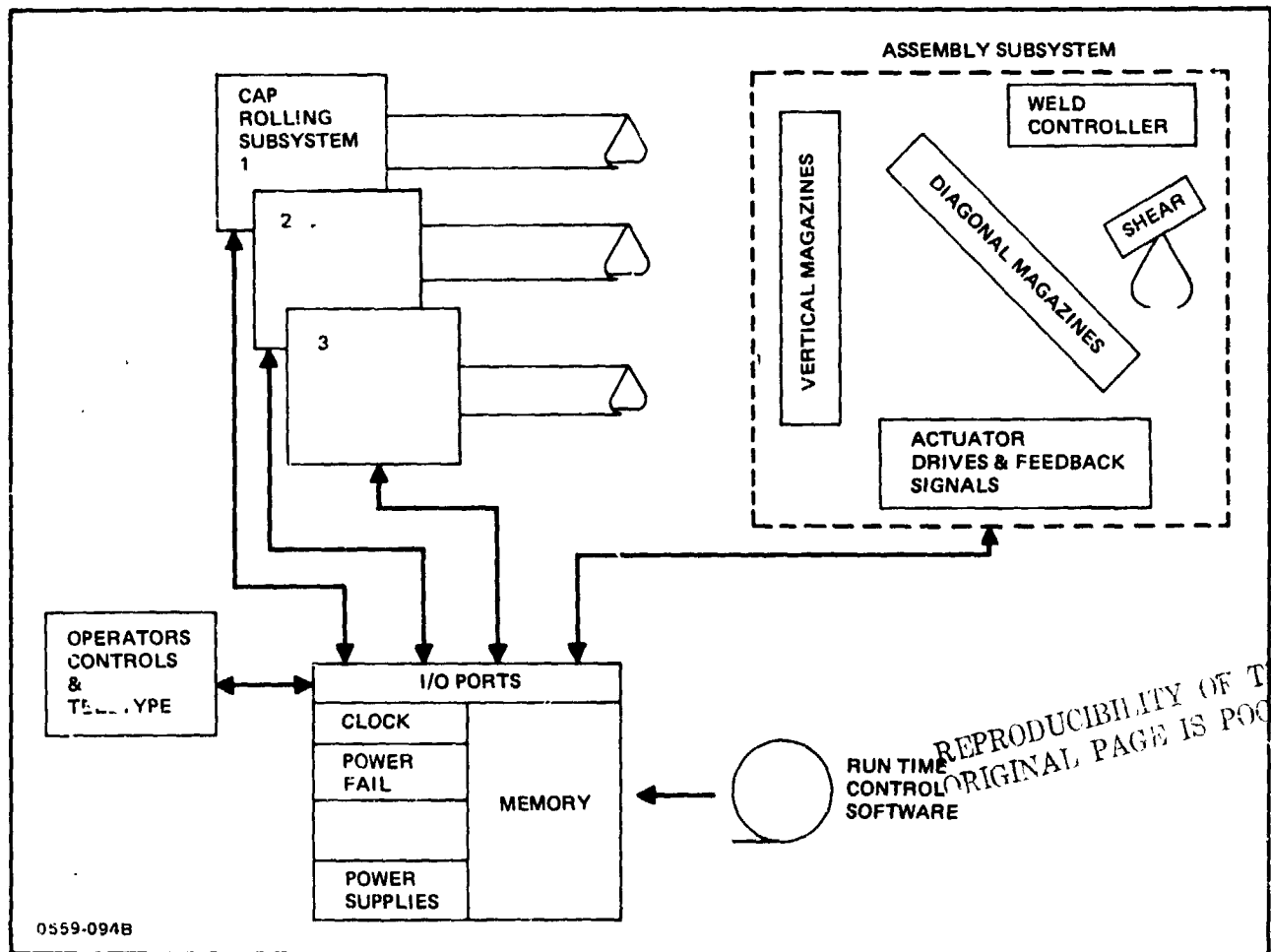


Fig. 3-24 Control System Block Diagram

alternating stops of cap positioning, fastening, and ultimately cutoff. The heart of the system is a Digital Equipment Corporation PDP-8A computer. The PDP-8A is a general purpose single address, fixed word length, parallel transfer computer. The PDP-8A was chosen for its proven off-the-shelf reliability and large library of previously developed and debugged software. The computer subsystem includes a non-volatile core memory, power fail-auto restart capability, and a real-time clock.

3.7.1 Rolling Mill Control

The cap positioning controls drive each rolling mill so that the caps are formed at precisely the same rate and so the that rolled lengths are equal prior to fastening the vertical and diagonal supports. It accomplishes this by sending out a synchronized serial pulse train to each of three servo translators. It is known that there is a slippage between rollers and cap members and that this slippage is not consistent. Therefore, a mechanism is employed to determine this slippage on the fly; that is, while the caps are being formed. The technique uses an encoder feedback device driven by the cap material being fed through the roller.

All calculations are done while the motors are in motion. There is no stop/start motion involved. After the motion start of the beginning of cap formation, they do not stop until they have formed the one bay length of section.

In addition to ensuring that the final position is reached by all three caps at the same time, the controller makes forced corrections to bring the caps into synchronization as soon as possible by withholding pulses to one or two of the rolling mills. Thus, for a case when the slippage factor of one or more rolling mills changed suddenly, the controller would try to re-synchronize the caps quickly without simply re-scaling to ensure that the final position were correct.

3.7.2 Controlling Bay Length

A check on the accuracy of the encoder measurement is also made on the fly. This may be necessary due to slippage of the friction drive wheel used to couple the encoder to the material. It also compensates for changes in the dimension of the encoder drive wheel. The method used (as shown in Fig. 3-25) consists of putting slots in each of the caps spaced one bay length apart. A light source and photo detector arrangement is used to determine when these slots pass the viewing station. Each time a slot passes a viewing station, the computer reads the encoder associated with that rolling mill and compares the reading to the one taken the last time a slot passed the viewing station for that mill.

The readings should differ by exactly 1.5 m (the distance between bays). If this is not the case, the weight given to the encoder counts will be modified by the computer. Of course, limits are placed on the amounts that these and other factors are permitted to change. An excessive change in a factor is a sign of a system malfunction which must be corrected. With this control technique, the length of a 10-bay beam (Fig. 3-26) was found to be within ± 0.03 in. (± 0.8 mm).



Fig. 3-25 Cap Member Feed Strip Length Encoder Setup

REPRODUCIBLE FROM THE
ORIGINAL DRAWING

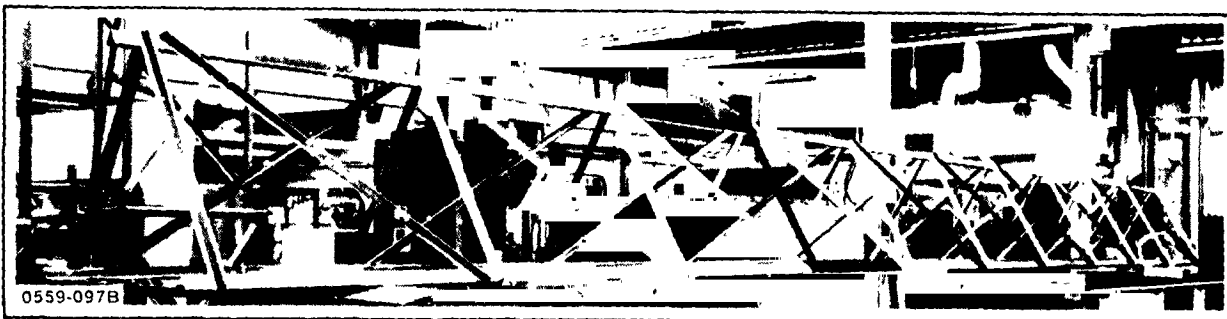


Fig. 3-26 Ten-Bay Beam

3.7.3 Fastening Cycle

Once the caps have been formed to the proper length, the computer directs the sequential operations necessary to insert and fasten the vertical and diagonal stiffeners. The computer (CPU) will direct a device to turn on or off and wait for a confidence signal that this action has occurred. When it has, it will direct the next sequence to be performed. To save time, some operations can be performed in parallel. An example is in the motion of the spotwelding electrodes, two can be moving up to position while the two that had been in position are moving to the retracted position. Approximately 80 actuators and 90 confidence signals are included in the control system.

4 - TESTING

Various tests were conducted to support design development trades and to verify the operation of the ABB and the structural integrity of the product (1-m deep beam) produced by the ABB. In addition, inspections were conducted during the fabrication and assembly of the ABB as part of our quality assurance program.

The following paragraphs discuss the components tests, the quality assurance inspections, and the structural tests conducted during this program.

4.1 COMPONENT TESTS

4.1.1 Ultrasonic Spotwelding

A brief summary of results obtained from initial tests of ultrasonic spotwelding bare 2024-T3 aluminum (0.016-in. thick) is presented. The following objectives were addressed:

- Mechanical strength of joints (lap shear and peel)
- Process reliability, maintainability, and accessibility
- Fabrication of sample truss joints.

Two welding machines were used for these tests:

- Branson 3000 W, Model 3301
- Sonobond, M-1200 Bench Welder.

Photographs of the ultrasonic welds produced by these machines are shown in Fig. 4-1.

Although these initial results were generally considered acceptable, the following major problem areas would have to be fully addressed before final acceptance of the process is possible:

- Tip and mandrel sticking occurred frequently (mostly tip)
- Excessive surface indentation (particularly on Sonobond welds)
- Limited accessibility in truss welding
- High cost of equipment.

Other less serious problems that must also be considered include frictional heating and effects of vibration on successive spots, and the optimization of weld time dwell (the Sonobond weld time of 1 sec is too long).

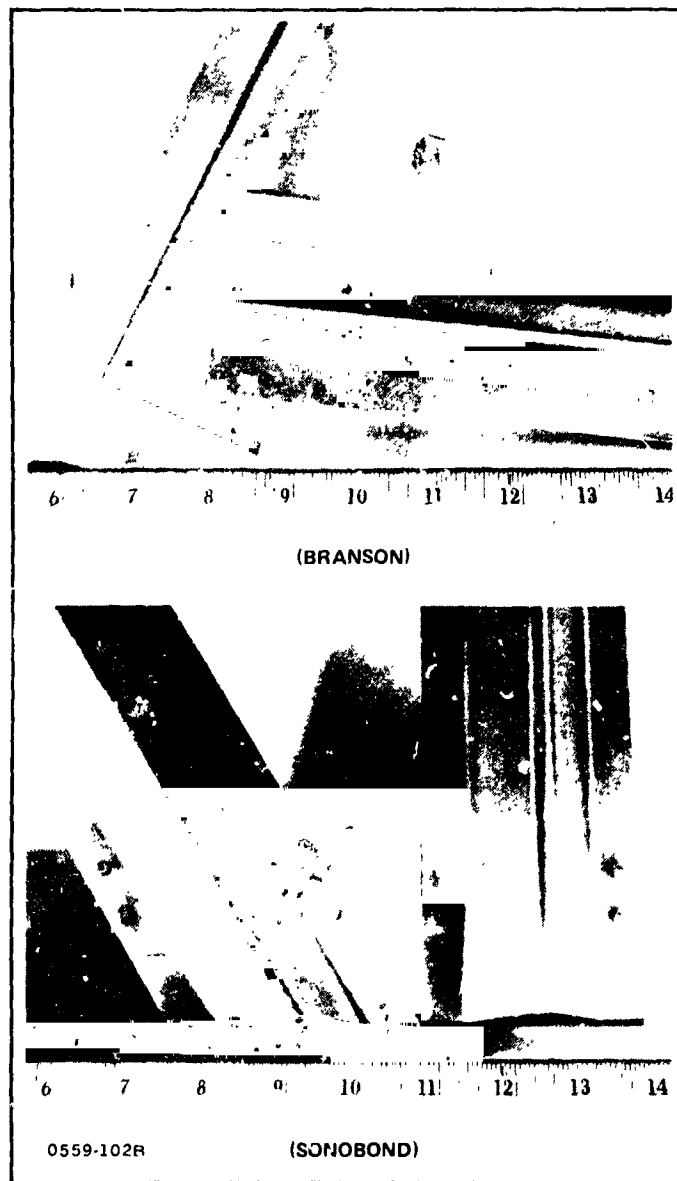


Fig. 4-1 Ultrasonic Spotwelding

In the case of the Branson machine, rectangular-shaped welds were produced with a knurled welding tip and backup mandrel. For the Sonobond weld, the welding tip was not knurled, but the mandrel was and the welds produced were essentially circular. The Branson welds were made in 0.075 sec at a power input of about 200 W-secs; the Sonobond welds were produced in about 1 sec at a power input of 550 W-sec. These schedules were not considered to be optimized, nor were tip selections, but they were considered reasonable for this evaluation.

The following analysis of the obtained lap shear data resulted:

	<u>Branson</u>	<u>Sonobond</u>
No. of tests	10	10
Load, lb (range)	170-350	250-330
Load, lb (average)	299	290.5
3 σ Load, lb (range)	129-469	211-370

The peel tests results showed that Sonobond welds averaged 26.8 lb and the Branson welds around 10 lb. In the case of lap shears, about 50% of the welds pulled nuggets for specimens produced by both machines. In the case of the peels, only one out of five was a shear failure, the remainder pulled partial nuggets.

When welding truss corner joints, problems were experienced with accessibility for each machine. It became apparent that multiple heads would be required using gun-type welding heads with modified anvils. This would increase the equipment cost significantly over that for resistance welding.

4.1.2 Static & Fatigue Characteristics of Spotwelded 2024-T3 Aluminum Joints

As part of an effort to evaluate techniques for joining structural elements fabricated in space to form a truss, resistance spotwelded 2024-T3 aluminum alloy (0.016-in. thick) was tested for static and fatigue properties. Test specimens, consisting of single lap shear joints, were resistance spotwelded to each of four configuration shown in Fig. 4-2. Welding was performed on a 100 kva welder using 300 lb per spot electrode pressure. Single spot direct welding using one cycle of heat was employed to simulate the series resistance welding concept proposed for space fabrication. Three samples of each configuration (Fig. 4-2) were statically tested. Results are shown in Table 4-1.

Configuration "D" (four spots in-line) resulted in the highest total (700 lb) or a 175 lb per spot shear load carrying capacity and was therefore selected for fatigue testing. Twenty-six additional samples were welded. Twelve specimens were tested in constant amplitude tension-fatigue (R=0.05) in an unrestrained (free) manner and 12 restrained between oiled Micarta to prevent end curling or lifting in the lap joint area. The three remaining specimens were statically tested to determine the shear ultimate strength of the lot. Test results are tabulated in Table 4-2 and plotted as an S-N curve in Fig. 4-3.

Fatigue testing in the unrestrained condition resulted in a predominant failure mode consisting of spot pull-out, attributed to a tension component induced by sample curling or lifting in the lap joint area. Fatigue endurance limit occurred for loads below 10% of the ultimate shear load. Restraining the fatigue specimen in the lap joint area prevented

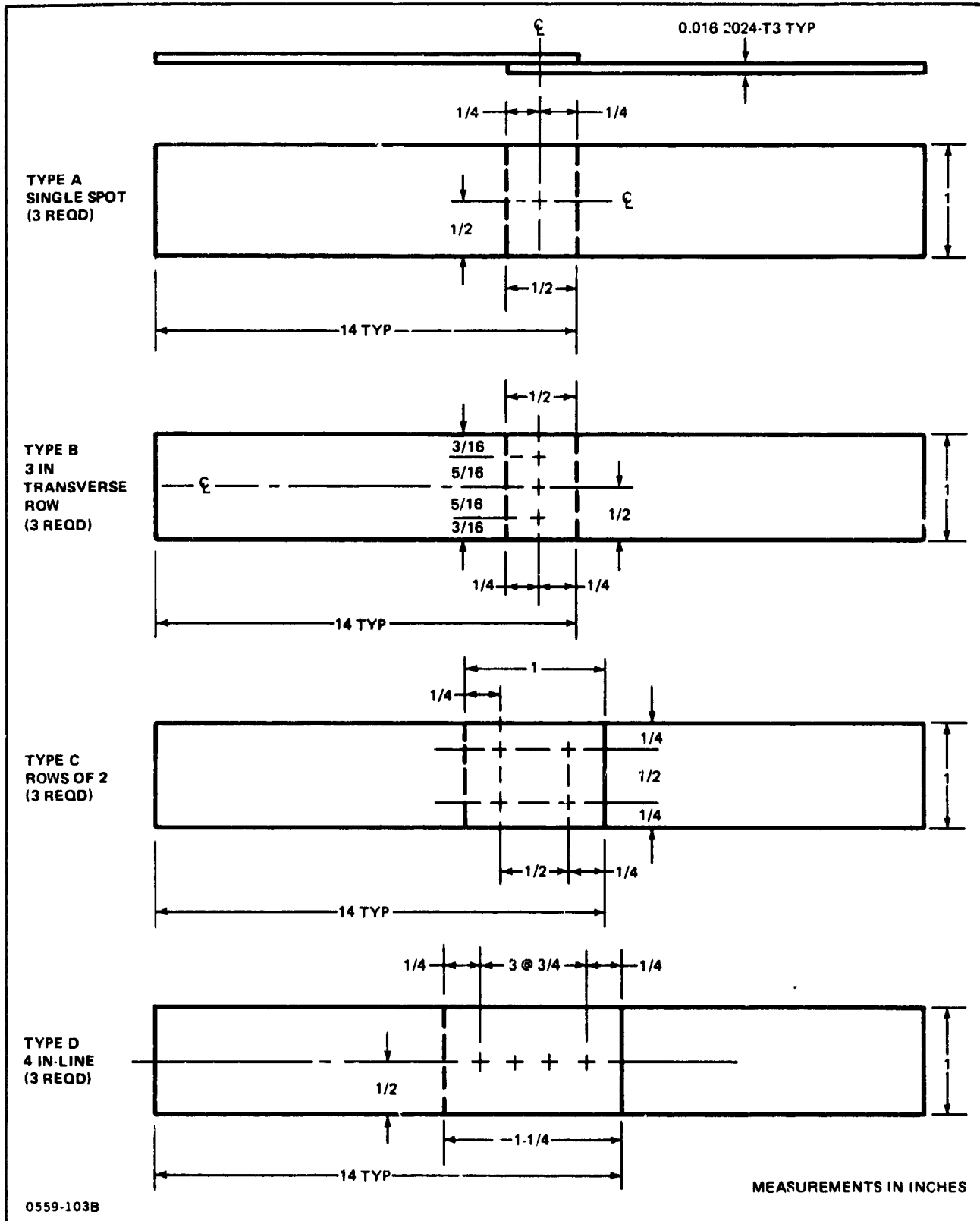


Fig. 4-2 Spotweld Evaluation Static & Fatigue Test Specimen Configuration

Table 4-1 Spotweld Evaluation: Static

SPEC NO.	NO. OF SPOTS	ULTIMATE FAILING LOAD (lb)	FAILING LOAD PER SPOT (lb)	COMMENT
A-1	1	170	170	
A-2	1	150	150	
A-3	1	191	191	
		170 AVG	170 AVG	
B-1	3	467	156	CONSIDERABLE BENDING EXTRACTED SPOTS AS "PLUGS"
B-2	3	479	159	
B-3	3	473	158	
		473 AVG	158 AVG	
C-1	4 (2)	676	169	SLIGHT BENDING
C-2	4 (ROWS)	652	163	
C-3	4 (of 2)	685	171	
		671 AVG	168 AVG	
D-1	4 (4)	715	179	SLIGHT BENDING SELECTED FOR PHASE II
D-2	4 (SPOTS)	675	169	
D-3	4 (IN LINE)	709	177	
0559-104B		700 AVG	175 AVG	

Table 4-2 Spotweld Evaluation: Fatigue Test Results

SPEC NO.	MAX. LOAD (lb)	% STATIC TEST ULTIMATE	CYCLES TO FAILURE	MODE OF FAILURE
UNRESTRAINED JOINT				
1	350	55	6,000	SPOT
2	210	33	106,000	AL
3	140	22	238,000	AL
4	175	27.3	177,000	AL
5	280	44	31,000	SPOT
6	280	44	19,000	SPOT
7	245	38.3	65,000	SPOT
8	245	38.3	68,000	AL
9	227-1/2	35.8	100,000	SPOT
10	227-1/2	35.8	100,000	SPOT
11	140	22	255,000	AL
12	70	11	10,000,000	NO FAILURE
12R	350	55	8,000	SPOT
RESTRAINED JOINT				
13	210	33	109,000	AL
14	140	22	483,000	AL
15	140	22	235,000	AL
16	315	49.3	38,000	AL
17	315	49.3	2,000	SPOT
18	210	33	106,000	AL
19	140	22	510,000	AL
20	105	16.4	2,580,000	AL
21	70	11	10,000,000	NO FAILURE
21R	245	38.2	63,000	AL
22	175	27.3	280,000	AL
23	105	16.4	8,345,000	AL
STATIC				
	ULT LOAD (lb)		LOAD PER SPOT (lb)-4 SPOTS IN LINE	
24	660		165	
25	631		158	
26	627		157	
AVG	639		160	
0559 105B				

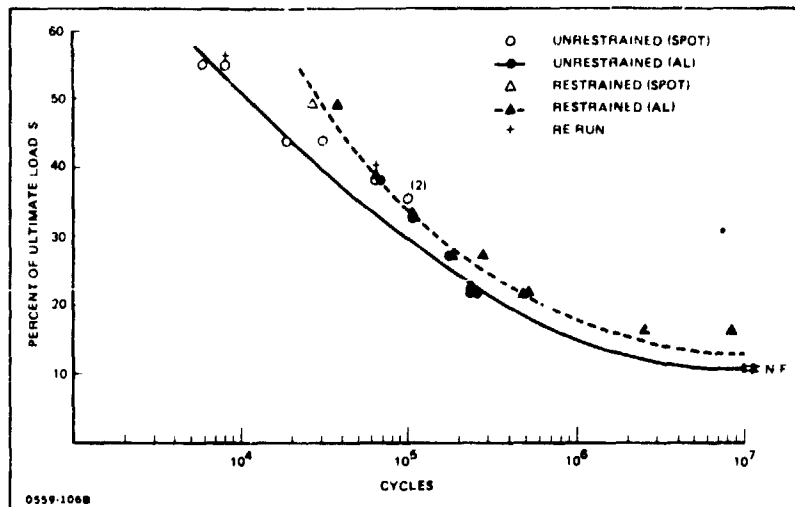


Fig. 4-3 Spotweld Evaluation Fatigue Test Results

curling or lifting and resulted in a predominant failure mode consisting of fatigue failure through the aluminum, initiating at one of the end spotwelds. Fatigue run-out occurred between 10 and 15% of the shear ultimate load.

In conclusion, spotwelds which are representative of those that would be made in space (i.e., single spot direct welded) produced ultimate shear tension strengths of 700 lb using four spots in-line. Fatigue run-out averages 10 to 15% of shear ultimate load, which is within the range of values obtained by other programs (e.g., Goodyear spotwelding studies).

4.1.3 Six Spotweld Attachment Component Tests

The initial SFDS truss design utilized eight spotwelds per brace attachment as shown in Fig. 4-4. A reduction from eight to six spotwelds yields the following advantages: 25% reduction in power requirements, 100% increase in electrode life, and reduced time weld cycle. To verify the integrity of the reduced quantity weld configuration, two alternate attachments were selected (Fig. 4-5 and 4-6) and tested against the eight-weld baseline.

4.1.3.1 Procedure & Results - Three components (Fig. 4-4 through 4-6) were fabricated from 0.016-in. thick, 2024-T3 clad material and tested per the general arrangement shown in Fig. 4-7. Each component was compression loaded 15 times up to 300-lb (limit load) then to ultimate failure (Fig. 4-8). Ultimate failure results were as follows:

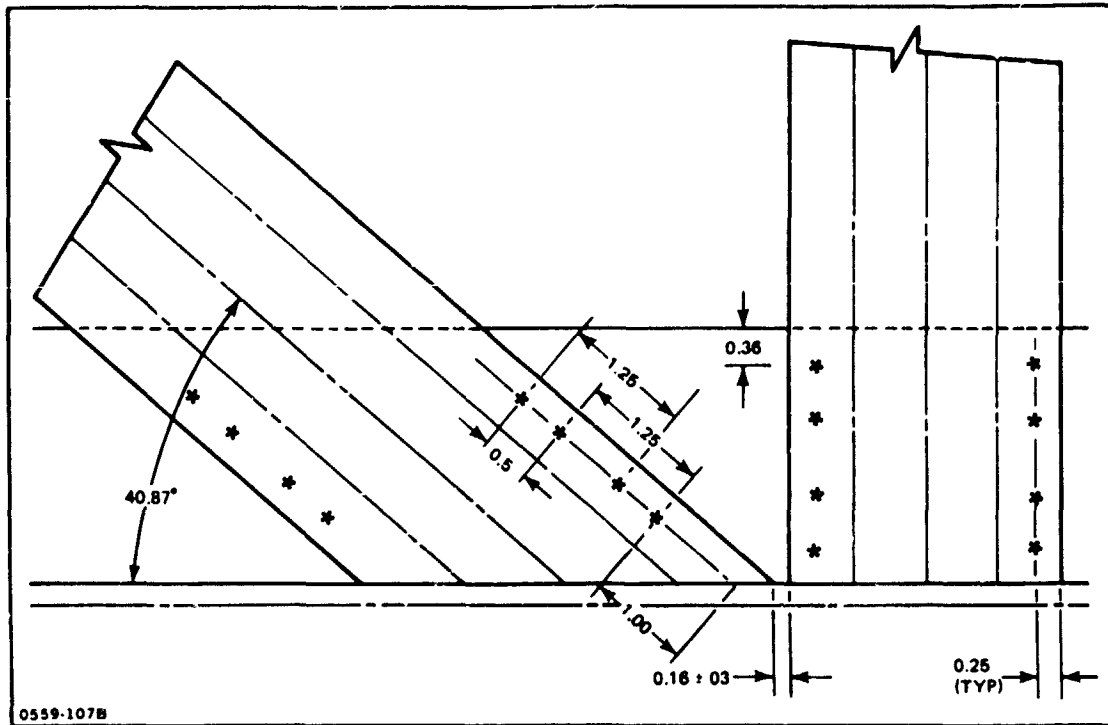


Fig. 4-4 Spotweld Configuration No. 1: S Weld/Junct

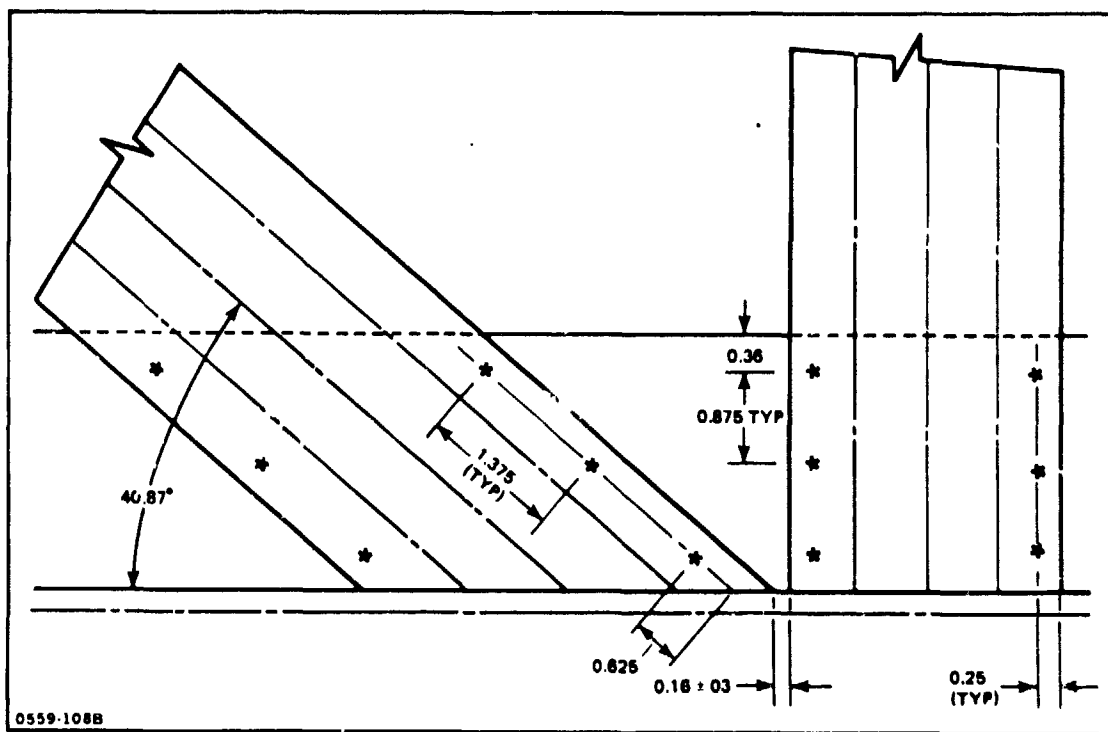


Fig. 4-5 Spotweld Configuration No. 2: S Weld/Junct, Maximum Spacing

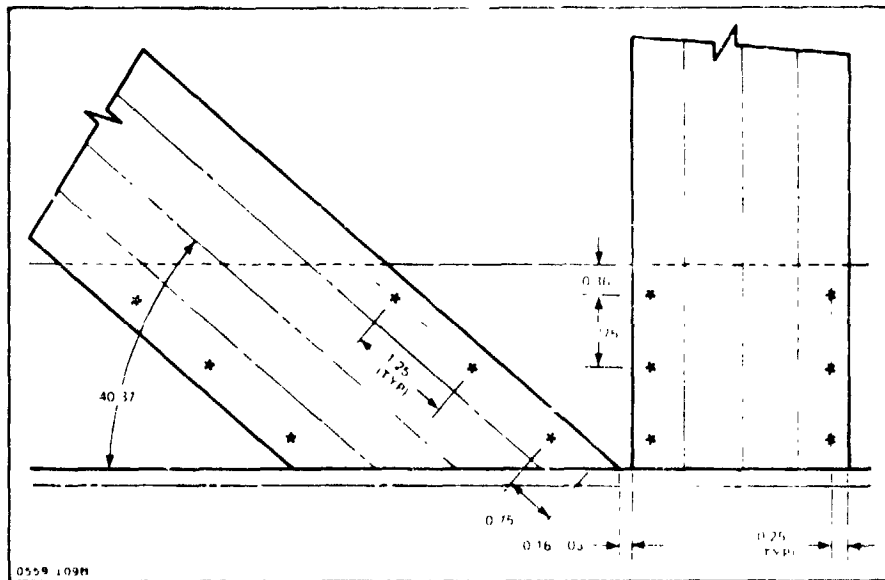
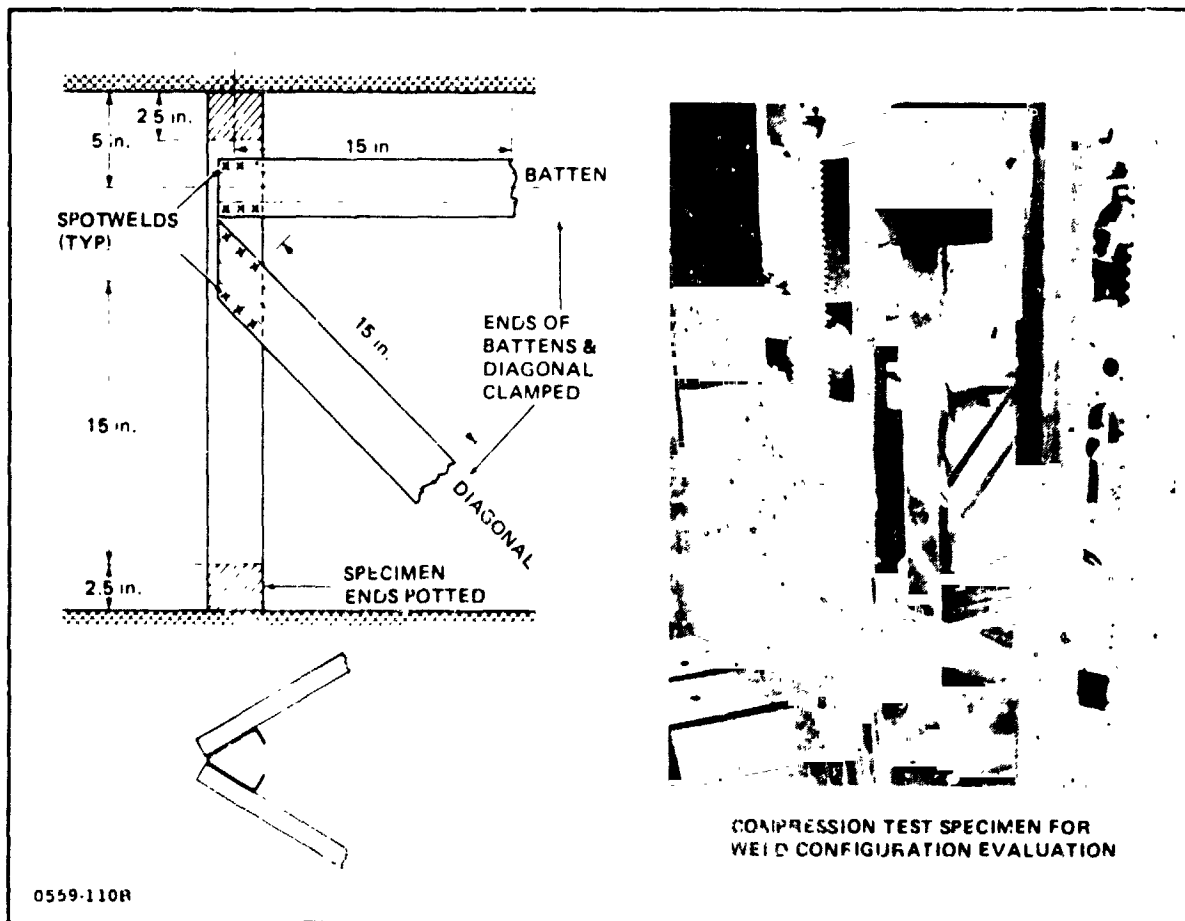
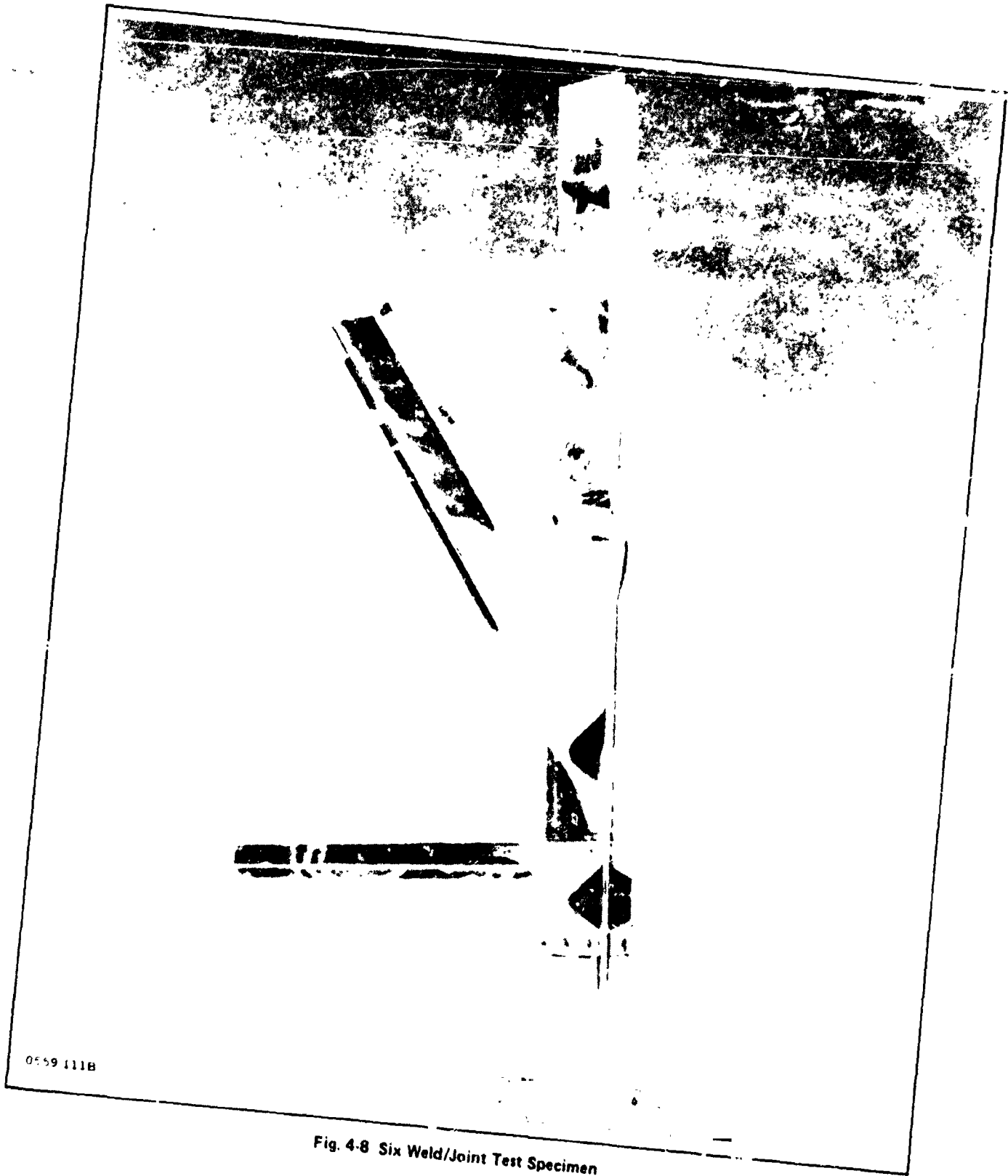


Fig. 4-6 Spotweld Configuration No. 3: 6 Weld/Junct, Minimum Spacing



COMPRESSION TEST SPECIMEN FOR WELD CONFIGURATION EVALUATION

Fig. 4-7 Component Test Arrangement



0559 111B

Fig. 4-8 Six Weld/Joint Test Specimen

Metallographic examination of the configuration No. 2 diagonal brace attachment welds (MP-AMPD-MO-77-133) indicated that buckling failure did not have a detrimental effect on the integrity of the spotweld.

4.1.3.2 Conclusions - Based upon both the successful static compression tests and metallographic examination, the SFDS should use configuration No. 2 for truss fabrication and realize the previously stated advantages.

4.2 QUALITY ASSURANCE

The general objective of quality control in this program was to assure the quality and success of the end product produced by the Space Fabrication Demonstration System. To achieve this goal, the design, construction, and testing of the beam builder was monitored throughout the program.

4.2.1 Beam Builder

Individual components of the beam builder were inspected prior to assembly so as to assure conformance to design drawings and specification requirements. These components were selected because of their critical dimensions and structural importance.

4.2.1.1 Box Beam Weldments, RDM 447-2082-1 - A total of 58 weldments on box beams No. 1, 2, and 3 were magnetic particle inspected. No relevant indications were found on box beams No. 2 and 3. One weld on box beam No. 1 exhibited lack of fusion and some visual cluster porosity. This was considered acceptable for the ground test unit.

4.2.1.2 Bulkhead Plate, RDM 447-2067-1 - The tolerance requirements for the alignment holes were checked at the seller for each plate and found to within blueprint requirement (± 0.0015 in.). The greatest tolerance error found in the holes was only 0.003 in., accounting for the excellent alignment obtained during subsequent assembly.

4.2.1.3 Bulkhead Installation Tool, RDM 447-2083 - The installation tool was dimensionally inspected for conformance to print requirements. The -15 and -13 bushings were within tolerances as were the other major tolerances.

4.2.1.4 Yoder Rolling Mill - Acceptance of the cap member roller mill was accomplished by source inspection of the mill at the seller in Cleveland, Ohio. The acceptance was based upon the satisfactory manufacture of the end product cap member by each of the mills. The first seller inspection revealed the cap members manufactured and witnessed by quality control were not within engineering drawing requirements. After readjusting the mill, a second source inspection of the seller showed the cap manufacture was of high

quality with respect to dimensional requirements and overall geometry. The cap from Machine No. 1 had a slight negative bow of 0.062 in. in 8 ft which could be eliminated with light hand pressure. All other bow conditions from both machines were less than 0.10 in. and also could be eliminated with light hand pressure. Oil canning and flange waviness were minimal (less than 0.010 in. and infrequent.) The breakaway and running torque for both machines were found to be within acceptable limits. Based on the two seller surveillance visits and other supporting data, the machines were found to be acceptable.

4.2.1.5 Beam Builder Alignment Movements - As the various sections of the beam builder were assembled, print tolerances were verified to assure proper functioning of the completed structure. Some of the measurements verified by quality control are as follows:

4.2.1.5.1 Facility Structure:

- Base pads were level to within 0.005 in. and within 0.030 in. with respect to the floor
- Bulkhead No. 1 was perpendicular to the base within 0.005 in.
- Bulkhead No. 2 was level with respect to Bulkhead No. 1 within 0.001 in. and parallel to Bulkhead No. 1 within 0.005 in.
- Bulkhead No. 3 was level with respect to Bulkhead No. 2 within 0.002 in. and parallel to Bulkhead No. 2 within 0.005 in.

4.2.1.5.2 Rolling Mill - Alignments for machine pads on the box beam with respect to 1-in. reference holes were as follows:

- Box beam No. 1: within 0.004 in.
- Box beam No. 2: within 0.005 in.
- Box beam No. 3: within 0.004 in.

Alignment of the machine groove in the rolling mill base plate with respect to the box beam were as follows:

- Box beam No. 1: within 0.003 in.
- Box beam No. 2: within 0.002 in.
- Box beam No. 3: within 0.004 in.

4.2.2 Beam

Because the production or manufacturing of a beam which would meet certain rigid dimensional and structural requirements was paramount to the success of the Space

Fabrication Demonstration System, a major quality emphasis was placed on the end product to meet these specifications. Consequently, a series of material receiving inspection and in-process tests were conducted on the beam materials and sections of the beam itself.

4.2.2.1 Beam Material Receiving Inspection Tests - Coil Aluminum Sheet - The material used for the cap was 2024-T3 aluminum purchased to QQA - 250/4. Table 4-3 shows the results of tests conducted for several coils of aluminum sheet. They were all satisfactory. Table 4-4 shows an actual chemical analysis taken from one of the rolls and establishes the validity of the material chemistry.

Table 4-3 Mechanical Properties of 2024-T3 0.016-in. Aluminum Sheet

ROLL NO.	SPECIMEN NO.	ELONGATION %	ULTIMATE (psi)	YIELD (psi)
		REQD 12.0 MIN	REQD 64,000 MIN	REQD 42,000 MIN
518657	1A	15.5	66,600	44,300
	1B	17.0	66,300	43,800
	1C	15.5	66,600	44,100
	2A	16.0	65,700	43,600
	2B	16.0	66,100	43,100
	2C	15.5	66,600	43,500
518662	1	16.3	69,300	46,700
	2	17.0	69,800	46,500
	3	17.5	69,000	46,800
	4	15.9	69,400	46,700
518663	1	16.3	69,100	*
	2	17.9	70,000	46,300
	3	17.1	69,600	46,900
	4	16.4	69,100	44,400
518664	1	16	69,600	47,400
	2	15.5	69,600	47,400
	3	16	70,300	48,000
	4	15	70,300	48,000
*SPECIMEN SLIPPED IN FIXTURE				
0559-112B				

Table 4-4 Actual Chemical Analysis of 2024-T3 Aluminum Coil Sheet per QQA-250/4

ELEMENT	% MIN.	% MAX.	% ACTUAL
SILICON	-	0.50	0.09
IRON	-	0.50	0.28
COPPER	3.8	4.90	4.13
MANGANESE	0.30	0.90	0.05
MAGNESIUM	1.2	1.80	1.34
ZINC	-	0.05	0.14
TITANIUM	-	0.05	0.03
VANADIUM	-	0.05	0.016
ZIRCONIUM	-	0.05	0.01
0559-113B			

4.2.2.2 Beam Spotweld Tests - In order to investigate the quality of the beam spotwelds, several welds taken randomly from a manufactured beam were metallurgically micro-sectioned and examined. The weld quality was of commercial standards as required by specification. It was judged that the spotwelds were of sufficient quality to meet the test requirements of the beam.

4.2.2.3 Beam Dimensional Inspection:

4.2.2.3.1 6-m Hand Fabricated Beam:

- Cap - The dimensions of the caps were within drawing tolerances and did not exhibit any flange waviness or oil canning in excess of 0.015 in. The bend radii were found to be free of cracks
- Brace Members - The dimensions for the height and flange measurements of the braces selected were satisfactory, through the overall width and central angle were slightly out of tolerance due to hand shearing of the ends
- Vertical Brace Spacing - The vertical brace spacing were slightly out of tolerance due to the hand shearing of the braces previously mentioned
- Cap Member Spacing - The cap member spacing and cap member alignment were within drawing tolerances.

4.2.2.3.2 6-m Machine Fabricated Beam:

- Cap - The cap member (Fig. 4-3) dimensions were found to meet engineering structural requirements, though measurement of the two base angles was complicated by the rounded configuration of the base flats; Table 4-5 shows five angular measurements along the three cap members manufactured by the beam builder

Table 4-5 Angular Measurements of Cap Member Manufactured by Beam Builder

ANGLE	REQUIREMENT	CAP A	CAP B	CAP C
A ₁	60° ± 45'	61° 55'	60° 15'	60° 30'
A ₂	60° ± 45'	60° 45'	59° 45'	61° 15'
A ₃	60° ± 45'	60° 45'	60° 35'	60° 45'
A ₄	60° ± 45'	60° 20'	60° 25'	60° 30'
A ₅	60° ± 45'	60° 50'	60° 30'	61°
0559-114B				

- Brace Members - Brace width dimensions were improved due to the elimination of the hand cutting operation used on the hand fabricated beam
- Vertical Brace Spacing - The vertical brace spacing improved on the machine fabricated beam to within 0.045 in. of print requirements
- Cap Member Spacing - The cap spacing dimensions were good on the machine fabricated beam with measurements varying to within ± 0.070 in. of print requirements
- Length Measurements - Part of the beam builder acceptance criteria included the conformance of a 4-Bay Beam, a 10-Bay Beam, and three End Caps to the critical length dimensions required by the print. The results of these measurements are listed in Table 4-6. All measurements were taken along the length of the three caps for each beam and all were acceptable, see Fig. 4-9.

Table 4-6 Length Dimensions of Beams & Caps

ITEM REQD	RESULTS		
	A	B	C
4-BAY BEAM	27' 30/32"	27' 29/32'	27' 29/32'
10-BAY BEAM	50' 24/16'	50' 23/16'	50' 23/16'
CAP MEMBERS	70' 23/32'	70' 22/32'	70' 22/32'
0559-115B			

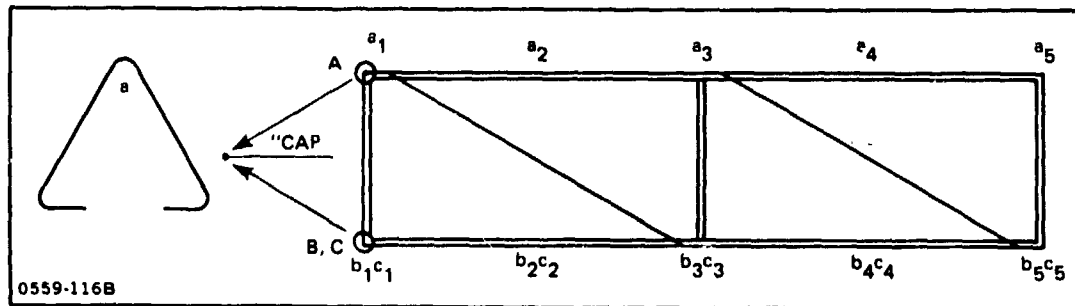


Fig. 4-9 Cap Member Dimension Locations

4.3 STRUCTURAL TESTS

This subsection summarizes the tests carried out to verify the 1-m x 40-m beam structural design concept. Various tests were conducted at different periods in the development phase to resolve particular problem areas. Following is a summary of tests; further details are provided in the following sections and in the references.

- Two 0.56-m (22-in.) cap specimens were compression tested in a universal testing machine. The objective of these tests was to verify the use of three spotwelds per leg on the batten, and diagonal, to cap attachment. One specimen had four spotwelds, the other three. Cap ends were potted and machined parallel. Two batten segments about 0.3-m long were spotwelded to the cap; also one diagonal segment about 0.3-m long was also spotwelded to only one side of the cap. The opposite ends of the battens and the diagonal were clamped. The test purpose was to determine whether local buckling of the cap flat sides would peel the spotwelding on the three-spot specimen compared to the four-spot specimen. The results showed there was no spotweld failure and all specimens failed at approximately the same load. The additional data obtained from this test was that, because the specimen was so short and had lateral members attached, the failure mode appears to be local compression crippling rather than torsion thus providing additional data on the section characteristics. Failing load for the three-spotweld specimen was 3456 N (777 lb), average.
- Two 1.2-m cap specimens were tested in the universal test machine. The cap section was an early smaller cross section of the later design and the material was 0.041-cm clad 2024-T3. The failure loads were 2357 N (530 lb) and 2291 N (515 lb).
- Four 1.5-m roll formed cap specimens were compression tested in a universal test machine. The cross section was the final selected design with a thickness of 0.041-cm bare aluminum alloy 2024-T3. The first two specimens failed at 2246 N (505 lb) each; the difference between the two test specimens was a transducer tension force applied to the flanges of one specimen at mid-length. The other had no transducers. The remaining set of two specimens failed at 2211 N and 2166 N. These specimens were also roll formed but had appreciable waviness in all the free edge flanges.
- Test of 1-m x 6-m (4-bay) beam hand assembled. A 1-m x 6-m (4-bay) beam was tested under compression load to obtain the ultimate strength of the cap/batten/diagonal combination. The beam was hand assembled and spotwelded from roll formed parts made of bare 2024-T3 aluminum alloy. Test objective was to establish a baseline for strength capability of machine made part. Failure load was 6703 N, which is 21% above ultimate design load.
- Test of 1-m x 6-m specimen fabricated by beam builder for comparison with above test specimen; failure was at 6112 N, 10% above ultimate design load.

- Test of 1-m x 4.5-m beam which was hand fabricated from 2024-T3 alclad aluminum. Specimen was early design which was later modified.

4.3.1 Compression Test of 0.56-m (22-in.) Cap Specimens

Paragraph 4.1.3 presents the results of the compression test program conducted on three specimens represented by Fig. 4-10. One of the test specimens incorporated eight spotwelds per brace attachment to the cap; the other two used three spotwelds per brace. The test objective was to determine whether local buckling in the cap flat sections would peel the welds as the compression load increased. Brace ends were clamped in order to induce local peel forces in the spotwelds. The three specimens were fabricated from 0.040-cm 2024-T3 clad aluminum. Each load in each specimen was cycled 15 times between zero and 1334 N, then to failure.

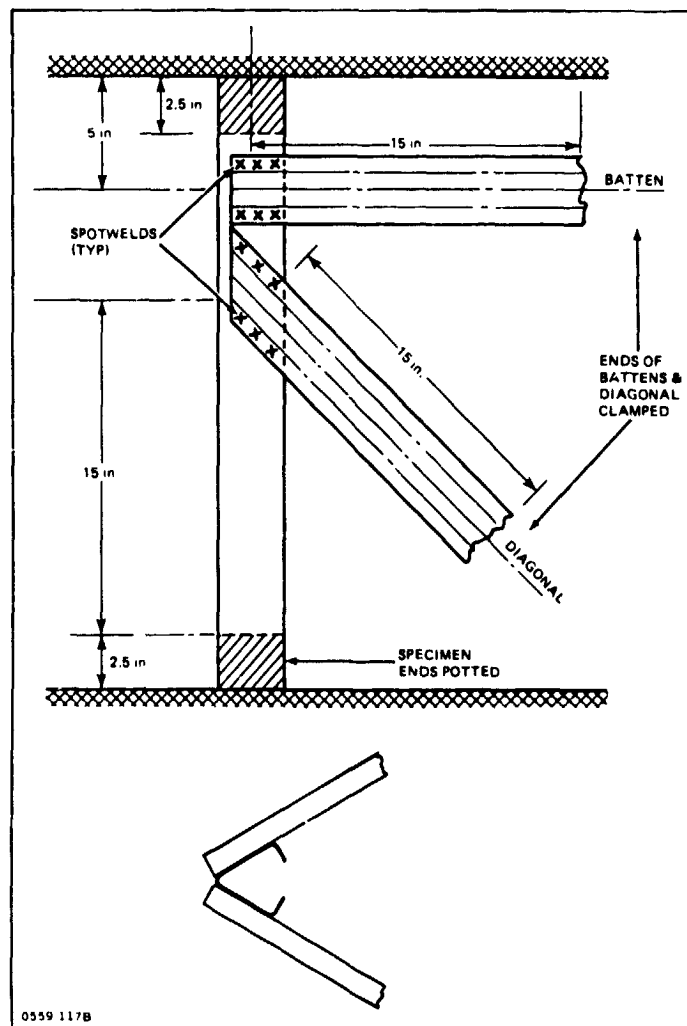


Fig. 4-10 Compression Test Specimen Comparison Failure Load Six or Eight Spotwelds per Brace

The results of the test are given in Paragraph 4.1.3.

Based on the test results and metallographic examination of the welds, the design incorporated the six-spotweld configuration.

4.3.2 Compression Test of Two 1.22-m (48-in.) Cap Specimens

The first triangular cap element 1.22-m (48 in.) long tested in the universal testing machine on 18 November 1976 sustained 2357 N (530 lb) compression load before total failure in a combination of torsion bending buckling mode at about mid-span. The initial local buckling waves were observed at 1379 N (310 lb).

The second triangular cap element identical to the specimen above was also tested in the universal testing machine and carried a 2291 N (515 lb) compression load before total failure in a combined torsion/bending buckling mode at about 1/4 of its span. The initial local buckling waves were observed at 1200 N (270 lb). The load was then dropped to zero and the buckles disappeared.

4.3.3 Compression Test of 1.5-m (59-in.) Cap Specimens

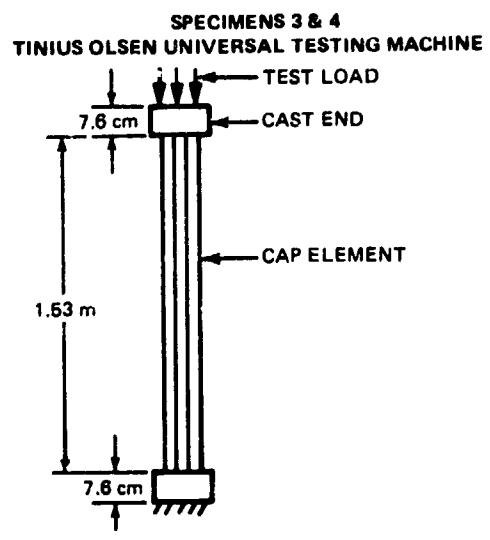
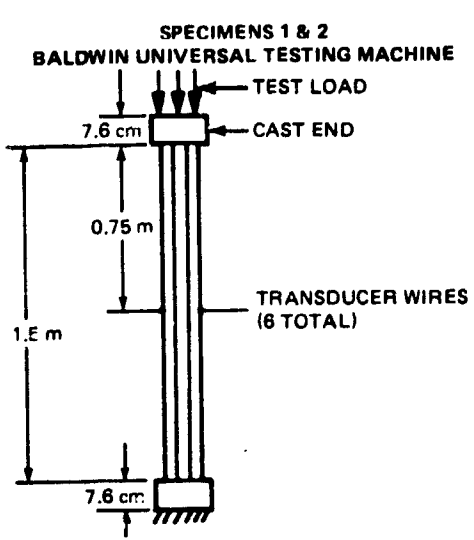
Two sets of compression tests on individual 1.5-m (0.016-in.) thick cap specimens were run in universal testing machines. The first two specimen tests were carried out to determine the effects of deflection measuring transducers located on the flanges at mid-span; one specimen included transducers which applied 16 to 18 oz lateral forces to each flanges; the other specimen had no transducers attached.

Each specimen was roll formed with the ends molded into an epoxy compound and machined flat for loading in the Baldwin Universal Test Machine. Both specimens failed at 2246 N (505 lb) (Fig. 4-11).

The second set of tests were carried out on two 1.5-m (0.016-in.) thick caps in a Tinius Olsen Universal Test Machine to determine the effect of load capability of build-in flange ripples caused during the roll forming process in the Yoder rolling mill. The worst flange leg deviation from straightness was approximately 0.075 in.; all flanges exhibited some degree of misalignment. As shown in the test log the specimens failed at 2211 N (499 lb) and 2166 N (487 lb).

4.3.4 Test of 1-m x 6-m (4-Bay) Beam, Hand Assembled

A structural test of a 1-m x 6-m long specimen (four 1.5-m bays) was tested on May 5, 1978 under an axial compression load applied by an hydraulic cylinder and tension rod interconnector loading fixtures at each end of the specimen. The test specimen



TEST SETUP

TEST DATA LOG

1. COMP. TEST OF SFDS CAP ELEMENT WITHOUT X-DUCERS

RUN NO.	TEST LOAD (lb)	REMARKS
1	50	
2	100	
3	200	
4	250	
5	300	
6	350	
7	400	
8	425	
9	450	
10	475	
11	500	505 BUCKLED, LOAD DROPPED OFF, WOULD NOT HOLD ANYMORE.

3. COMP. TEST OF SFDS CAP ELEMENT NO. 3

RUN NO.	TEST LOAD (lb)	REMARKS
1	0	
2	50	
3	100	
4	200	
5	250	
6	310 LIMIT	
7	50	
8	350	
9	400	425 lb HEARD NOISE
10	430 ULT	
11	450	
12	475	
13	499 FAILED	SPEC BUCKLED

2. COMP. TEST OF SFDS CAP ELEMENT WITH X-DUCERS

RUN NO.	TEST LOAD (lb)	REMARKS
1	50	
2	100	
3	200	
4	250	
5	300	
6	350	
7	400	
8	425	
9	450	
10	475	
11	500	505 BUCKLED, UNLOADED
12	525	
13	550	

4. COMP TEST OF SFDS CAP ELEMENT NO. 4

RUN NO.	TEST LOAD (lb)	REMARKS
1	0	
2	50	
3	100	
4	200	
5	250	
6	310 LIMIT	
7	350	
8	400	
9	430 ULT	
10	450	451 lb HEARD NOISE
11	475	483 lb HEARD NOISE
12	487 FAILED	SPEC BUCKLED

AVG BUCKLING LOAD = $\frac{499 + 487}{2} = 493$

% DEVIATION = $\frac{505 - 493}{505} = \frac{12}{505} = -2.37\%$

0559-118B

Fig. 4-11 Compression Tests of SFDS Cap Elements

represented the four bays at the center section of the SSPS 40-m beam for which the design load is combined bending and axial load; the maximum compression cap load is 1846 N (415 lb) ultimate and the two tension cap loads are +138 N each. Because it was not feasible to test the full 40-m specimen, the test simulation (Fig. 4-12) was designed to apply the 1927 N compression load equally to each cap for a total beam load of 5782 N (1300 lb) ultimate. This assumption is obviously conservative.

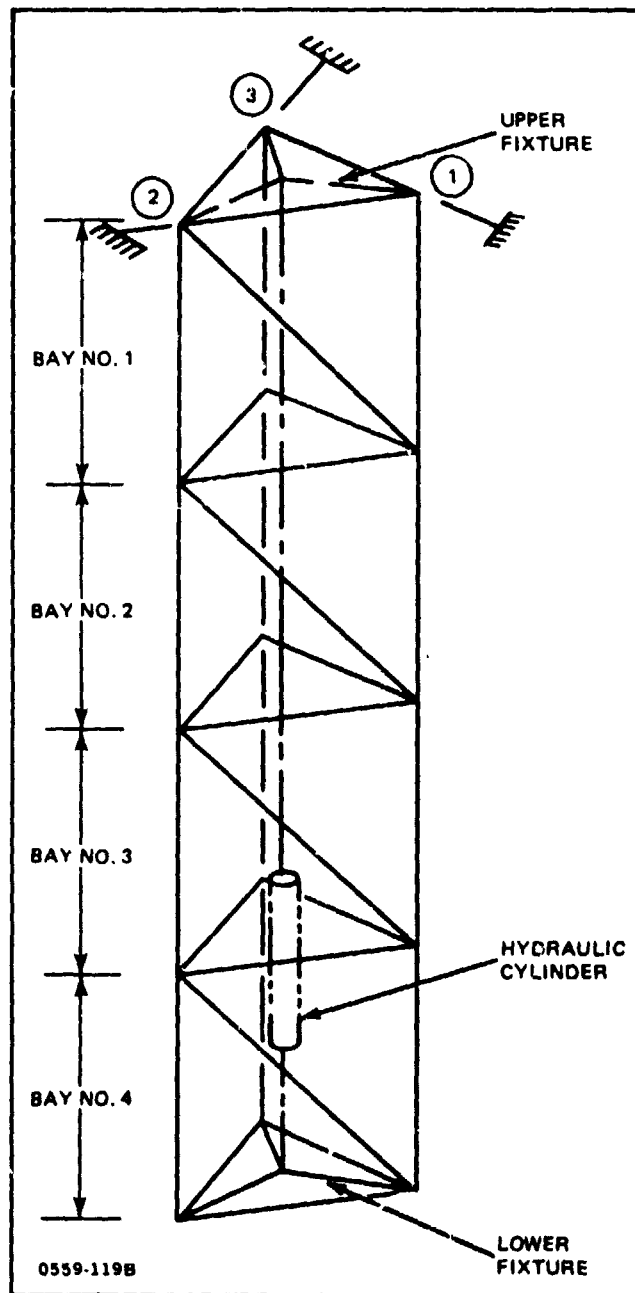


Fig. 4-12 6-m Compression Test Specimen

The structure failed at a total load of 6703 N (1507 lb); the failure mode was cap torsion/flexure instability in Bay III with an average load per cap of 2233 N (502 lb) compression.

Figure 4-12 illustrates the test specimen and the load application technique including the end fixtures and the three instrumented links installed at the upper fixture to measure induced horizontal loads for a pure compression condition. In addition the links simulate the loads carried in the torsion carrying end attachment for the ends of the basic 40-m beam for the design case of 2558 N (575 lb) total end force; this torsion was estimated from the measured test data at an applied end load of 2558 N. Cap ends were potted with approximately 3 in. of HYCEL compound and machined flat to preclude local cap crushing during loading. Typical instrumentation, both strain and deflection gages, were included and locations are given in Fig. 4-13.

In order to keep instrumentation costs within acceptable limits, the total number of installed strain gages was 154 and deflection gages, 67; their distribution is given in Table 4-7.

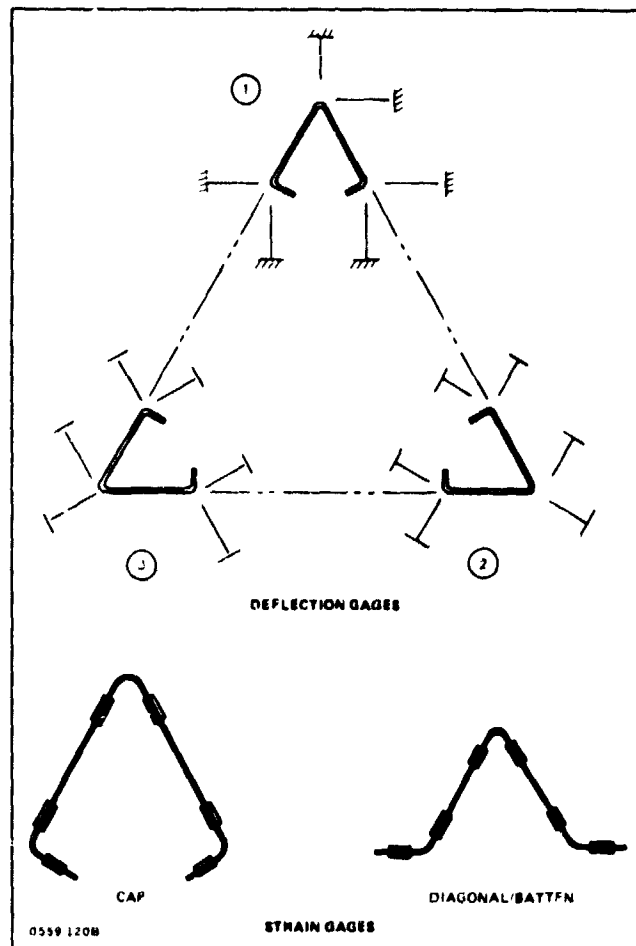


Fig. 4-13 Typical instrumentation

Table 4-7 Test Specimen Instrumentation (Sheet 1 of 2)

ELEMENT BAY	STATIONS IN BAY	NO. OF GAGES PER MEMBER	NO. OF MEMBERS	TOTAL NO. OF GAGES
1	2	12	3	72
CAPS 2	1	6	2	12
AXIAL GAGES 3	1	4	1	4
4	1	4	1	4
			SUBTOTAL	92
DIAGONALS 1	1	12	2	24
2	1	2	1	2
AXIAL GAGES 3	1	2	1	2
4	-	-	-	-
			SUBTOTAL	28
BATTENS 1/2	1	8	2	16
AXIAL GAGES 2/3				
3/4				
			SUBTOTAL	16

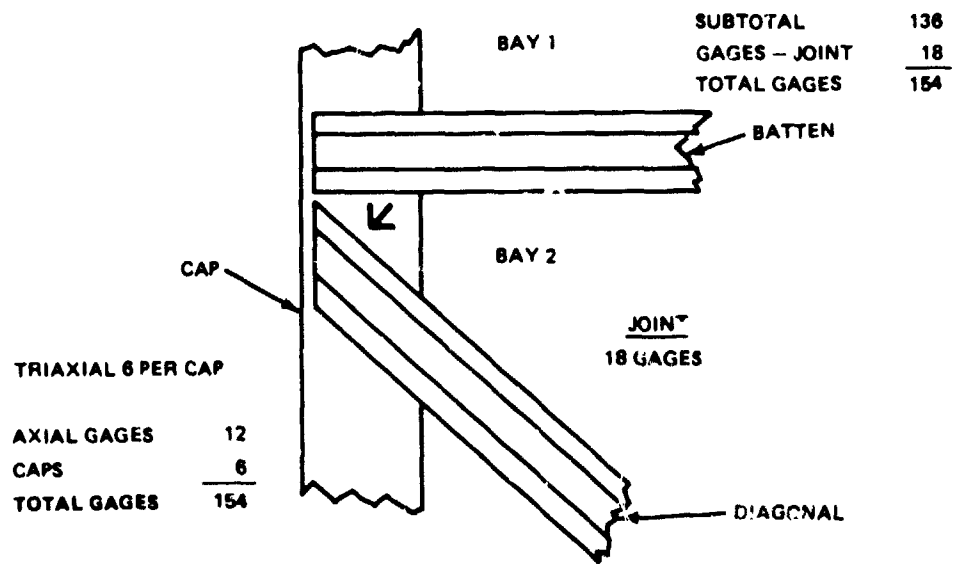


Table 4-7 Test Specimen Instrumentation (Sheet 2 of 2)

NUMBER & LOCATION OF DEFLECTION GAGE	
LOCATION	NO. OF GAGES
UPPER FIXTURE	7
BAY 1, TWO STATIONS	2 X 18
BAY 2, ONE STATION (MID)	18
BAY 3, ONE STATION, ONE CAP ONLY	6
TOTAL	67

0559-1218

The hand-assembled truss was subjected to a compressive load in accordance with the test log appearing on Table 4-8. The load was applied incrementally up to 110% of design ultimate load. Instrumentation readings were recorded at each load level. During the excursion from 110% to 120%, the truss failed as a result of buckling of the No. 1 cap in Bay 3. The load link indicated a load of 6503 N (1462 lb) at failure. Adding the fixture tare weight of 200 N (45 lb) to this value gives a failing load of 6703 N (1507 lb) or 16% of design ultimate based on an ultimate test load of 5782 N (1300 lb). There were no indications of any spotweld failures prior to buckling of the cap.

Table 4-8 Test Log - Manually Assembled Beam

RUN NO.	TEST LOAD		REMARKS	PHOTO NO.
	% BASE	(lb)		
1	0		LOAD LINK & JACK DISCONNECTED (psi)	X
2	10	85	30	
3	20	215	110	
4	30	345	180	
5	40	475	240	X
6	50	605	305	
7	60	735	370	X
8	71	885	445 (LIMIT LOAD)	X
9	2	30	LOAD LINK & JACK CONNECTED (psi)	X
10	20	215	110	
11	40	475	240	
12	60	735	370	
13	71	885	445 (LIMIT LOAD)	X
14	80	995	550	X
15	90	1125	565	X
16	100	1255	630 (ULTIMATE LOAD)	X
17	110	1385	695	X
18	120	1515	760	X
19	130	1645	825	X
20	140	1775	890	X
21	150	1905	955	X
	0% (POST FAILURE)			X
0559-122B				

Review of the displacement gage data indicates that the hand-assembled truss compressed 0.38-in. nominally at ultimate load. The maximum lateral displacement at ultimate load was 1.35 in. on the cap that subsequently failed. Lateral displacements were generally small up to limit load.

Review of the strain gage data indicates that local buckling of cap No. 1 is apparent at a load of 20%. Buckling in cap No. 2 is evident at 50% and in cap No. 3 at 60%. Load

in the one diagonal instrumented was low up to 90% of ultimate load. Changes in batten loads became significant at 60%. The maximum strain the lateral restraint at ultimate load was 179 μ in./in.

Measured data are shown in Ref. 2-16, Section 2; these include the strains, stresses and deflections of all instrumentation for limit and ultimate loads. Also included are data measurements versus percent of applied load for typical points on the structure. Figures 4-14 and 4-15 show the plots of measured stresses versus developed length of the cap cross section in bay No. 1 for 1300 lb and limit loads, respectively. While the curves are drawn connecting points across the corner locations, these extrapolations are only for

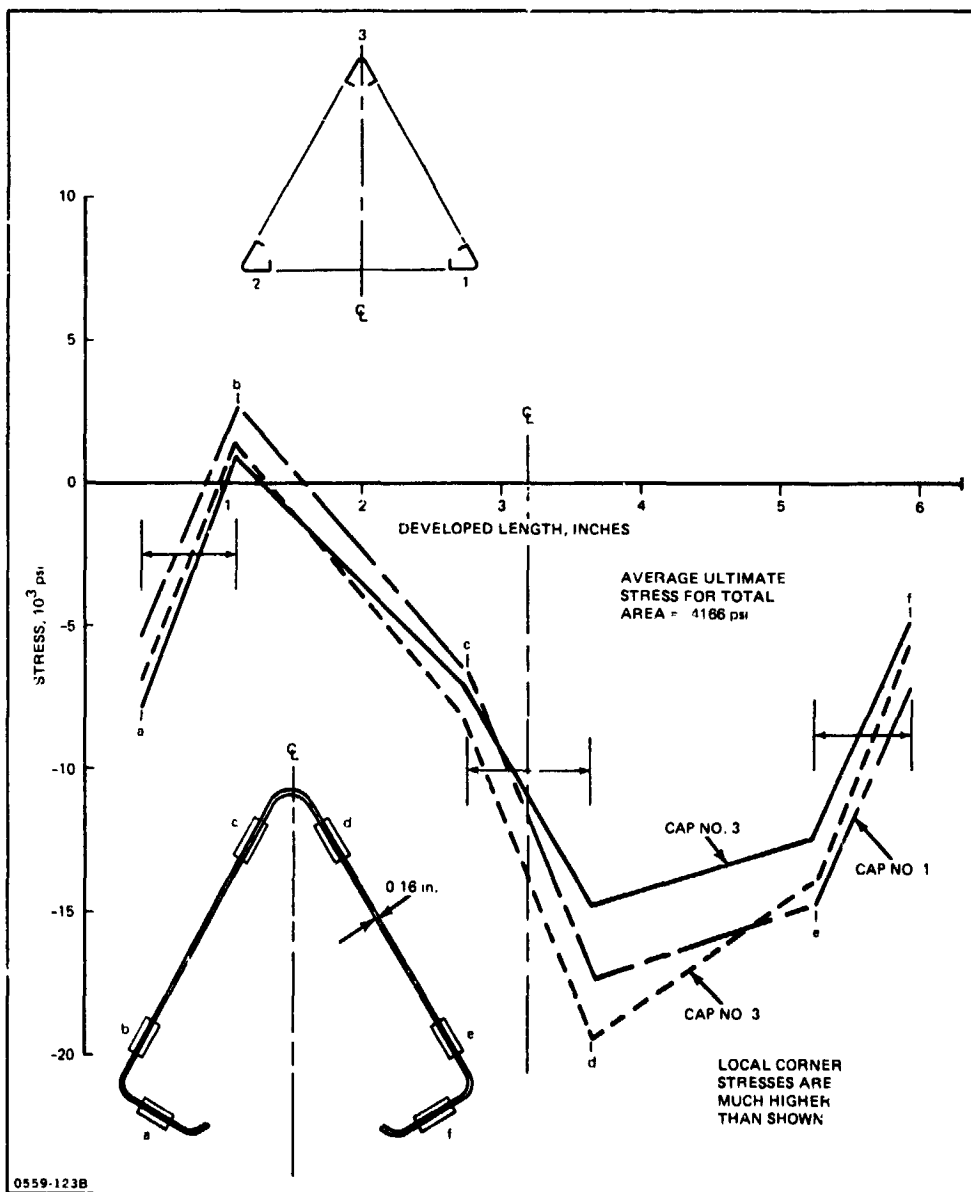


Fig. 4-14 Cap Stresses Bay No. 1 versus Developed Flat Pattern of Cap at 1300 Pounds

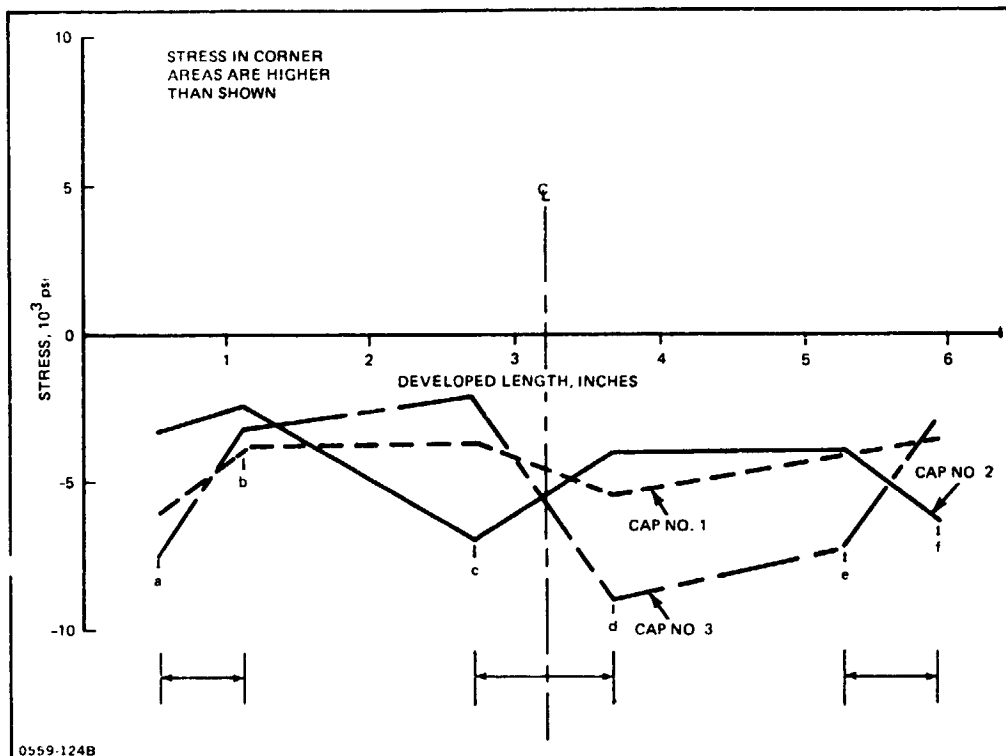


Fig. 4-15 Cap Stresses Bay No. 1 versus Developed Flat Pattern of Cap at 930 Pounds

identification because the local corner stresses are much higher, particularly on the center-line. The curve at ultimate indicates a high degree of torsional strain as do the deflection data. Figures 4-16 and 4-17 show similar data for the diagonals in bay No. 1. The data for the battens between bay No. 1 and bay No. 2 are given in Fig. 4-18.

The average ultimate stress for the cap members is $-2.87 \times 10^7 \text{ N/m}^2$ (-4166 psi); this figure does not represent the peak stress levels which are higher than those measured because the local buckling of the flat sides reduces the effective area appreciably. The peak compression stress measured at point d of cap No. 3 is $-13.4 \times 10^7 \text{ N/m}^2$ (-19500 psi), Fig. 4-14. Figure 4-15 shows the stresses at 4130 N (930 lb) applied load.

Loads data in the diagonal members in bay No. 1 were estimated for the externally applied load conditions on the 6-m beam at 4130 N (930 lb) and at 5782 N (1300 lb). The diagonal member load is 64.9 N (14.6 lb) at limit and 98 N (22 lb) ultimate compression. Stresses in the diagonals and battens are shown in Fig. 4-16, 4-17, and 4-18.

Because the horizontal component in the diagonal is related to the forces measured by the horizontal load links attached to the upper fixture, a comparison was made between the load link forces and the component of diagonal forces. The load values based on the link strains show some difference between each link; however, when the three loads are

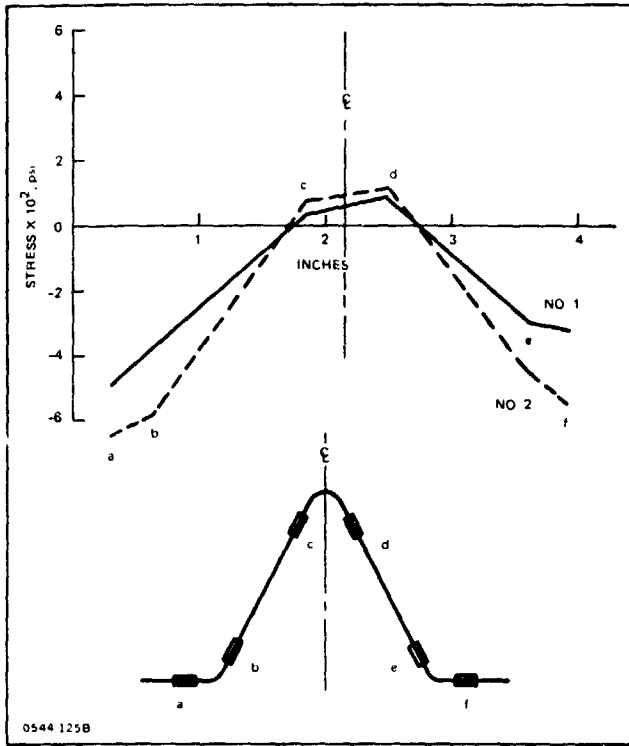


Fig. 4-16 Stresses in Diagonals in Bay No. 1 at Limit Load

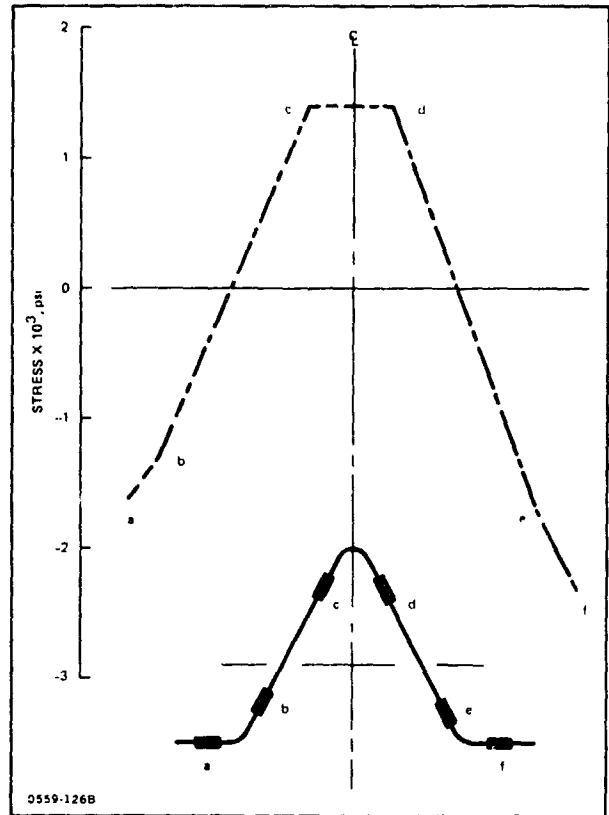
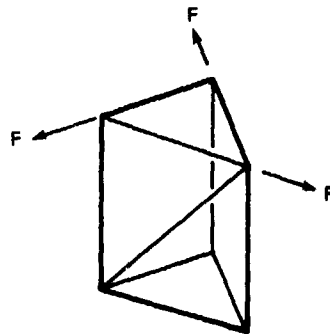


Fig. 4-17 Stresses in Diagonal in Bay No. 1 at Ultimate Load

averaged the horizontal components are 34.7 N (7.8 lb) limit and 70 N (15.7 lb) ultimate. The horizontal components for the upper bay diagonals give 40 N (9 lb) limit and 60 N (13.4 lb) ultimate.

In order to estimate the induced end torsion caused by axial compression on the 40-m beam, the horizontal components at the beam end are reduced by ratio of the actual 40-m beam end load of 2558 N (575 lb) to the test load of 5782 N (1300 lb) assuming linearity.



$$F = 60 \left(\frac{575}{1300} \right) = 26.5 \text{ N (5.96 lb) ULTIMATE} \\ \text{OR } 17.7 \text{ N (4 lb) LIMIT}$$

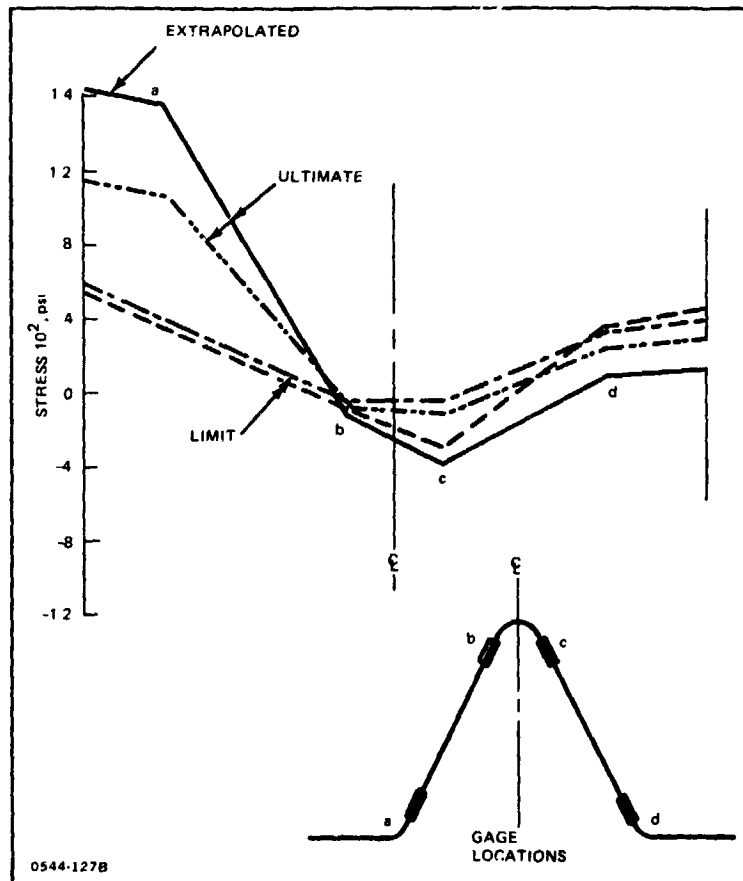


Fig. 4-18 Stresses in Battens versus Developed Flat Pattern at Bottom of Bay No. 1

The induced end torsion is 17.5 N m (155 in.-lb) limit. This low level torsion load does not present a problem for the end truss attachment design. The torsions between 40-m beam segments are self-equilibrating in the end fitting.

4.3.5 Test of 1-m x 6-m (4-Bay) Beam Fabricated by Beam Builder

This section incorporates the test data of truss specimen that was assembled by the Beam Builder. The test was conducted on August 17, 1978. The test specimen was a 4-bay aluminum truss similar to the hand-assembled specimen covered in Subsection 4.3. It was instrumented with 24 strain gages and 25 displacement transducers. Truss set up for the test was accomplished in the same manner as the hand-assembled specimen. Load was applied incrementally up to ultimate load (100%). One cap of the truss buckled resulting in failure of the truss when the load was being increased to 110% of ultimate. The measurement of the applied load plus the tare weight of the upper fixture indicates that failure occurred at 6111 N (1374 lb) or 106% of design ultimate load. Spotwelds (total of two)

joining the diagonals to the caps at the bottom of bay No. 2 and the bottom of bay No. 3 failed below limit load (71% of ultimate). Noises noted during the test indicates that additional spotweld failures occurred during the load excursion from limit load to failure.

The truss fabricated by the Beam Builder was identical to the hand-made truss in material, dimensions and spotwelding with one exception. The caps on the Beam Builder made truss extended 4-1/2 in. beyond the edges of the batten at the top and bottom. The caps on the hand-made truss were cut flush with the edges of the batten at the top and bottom.

It was noted, upon receipt of the truss at Grumman's Plant 5 after fabrication, that two of three in-line spotwelds at the Batten/cap No. 1 joint on the one end were separated. After installation of the truss in the test fixture, it was determined that the third weld at this joint had failed. The joint was clamped using two C-clamps prior to the application of test loads.

It was also noted that cap No. 1 of the machine-made truss was more irregular in shape (ripples in the extrusion) than caps No. 2 and 3.

Table 4-9 Test Log - Automatically Fabricated Beam

RUN NO.	TEST LOAD		REMARKS	PHOTO NO.
	% BASE	(lb)		
1	0		LOAD LINK & JACK DISCONNECTED (psi)	X
2	10	85	30	
3	20	215	110	
4	30	345	180	
5	40	475	240	X
6	50	605	305	
7	60	735	370	X
8	71	885	445 (LIMIT LOAD)	X
9	2	30	LOAD LINK & JACK CONNECTED (psi)	
10	20	215	110	
11	40	475	240	
12	60	735	370	
13	71	885	445 (LIMIT LOAD)	X
14	80	995	550	X
15	90	1125	565	X
16	100	1255	630 (ULTIMATE LOAD)	X
17	110	1385	695	X
18	120	1515	760	X
19	130	1645	825	X
20	140	1775	890	X
21	150	1905	955	X
	0% (POST FAILURE)			X

0559-129B

The truss fabricated automatically by the Beam Builder was subjected to a compressive load in accordance with the Test Log appearing on Table 4-9. The load was applied incrementally up to limit load (71% of ultimate) and returned to approximately zero. Two spotwelds (one at the diagonal/cap No. 1 joint at bottom of Bay No. 2 and the other at the diagonal/cap No. 1 joint at bottom of Bay No. 3) were determined to have failed. These areas were clamped using C-clamps prior to the final run to failure. The truss was loaded incrementally to ultimate load (100%). When the load was being increased to 110%, the truss failed as a result of buckling of the No. 2 cap in bay No. 3. The load link indicated a load of 5911 N (1329 lb) at failure. This load plus the fixture tare weight of 200 N (45 lb) yields a failing load of 6112 N (1374 lb) or 106% of design ultimate based on an ultimate load of 5782 N (1300 lb). During the final run to failure, numerous noises indicating the failure of spotwelds were heard at the higher loads (limit to failure).

Review of the displacement gage data indicates that the truss fabricated by the Beam Builder compressed 0.5 in. nominally at ultimate load. The maximum lateral displacement at ultimate load was 2.84 in. on cap. No. 3. Lateral displacements were generally small up to 60%. At limit load (71%), the largest lateral displacement was 0.53 in. in cap No. 2, the cap that eventually buckled at failure. Lateral displacements on cap No. 1 were generally smaller than the displacements of cap No. 2 and 3 throughout the test.

4.3.6 Test of 1-m x 4.5-m (3-Bay) Beam Hand Fabricated

A compression test of a 1-m x 4.5-m beam (three 1.5-m bays) was tested on 19 November 1976 using the same fixtures to apply load as described in Paragraphs 4.3.4 and 4.3.5 except that there were no horizontal restraints at the upper fixture. The upper end of the specimen had no lateral or torsional restraint. All parts were made by brake forming and rivetted at all joints. The material was 2024-T3 clad aluminum with a thickness of 0.041 cm. (0.016 in.). The specimen failed at 5604 N (1260 lb); the failure mode was torsion/flexure buckling of the cap in the upper bay.

5 - CONCLUSIONS & RECOMMENDATIONS

5.1 CONCLUSIONS

The Automatic Beam Builder was developed, fabricated, and demonstrated within the established contract cost and schedule constraints. The ABB demonstrated the feasibility of:

- Producing lightweight (0.85 lb/ft) beams automatically within the required rate of 1 to 5 ft of completed beam per min
- Producing structurally sound beams with an axial design load of 5538 N based on the Grumman photovoltaic Satellite Solar Power System design reference structure.

Flight test demonstration of the aluminum ABB's operational capability in the space environment should be the next major milestone. This should be preceded by a balanced analysis and ground test program to develop the flight demonstration unit and establish the data base required for the flight test program.

5.2 RECOMMENDATIONS

The following recommendations will lead to an orderly and cost effective flight demonstration program:

- ABB analysis and design effort to redesign the primary and secondary structure for launch loads and lightweight considerations
- Loads and dynamics analysis to provide the overall dynamic model and verify the quasi-static loads of primary structure plus dynamic model of the various subsystems to verify launch, boost, and random vibration loads
- Design of launch locks to insure post launch operational capability of Yoder mill assembly, cross brace magazine, carriage assembly and weld clamp assembly
- System analysis and preliminary design to select and tailor flight test instrumentation, i.e., accelerometers, temperature sensors, strain gages, lightweight high frequency shakers, and electro-optical systems to measure beam straightness
- A coordinated ground test program including thermal vacuum tests, ground vibration surveys, and water tank neutral buoyancy tests to provide preliminary verification of the analysis and establish baseline data for the flight tests.